



**This electronic thesis or dissertation has been  
downloaded from Explore Bristol Research,  
<http://research-information.bristol.ac.uk>**

*Author:*

**Palacios, Ensor R**

*Title:*

**Contribution of cerebellar sensorimotor representations to behaviour**

**General rights**

Access to the thesis is subject to the Creative Commons Attribution - NonCommercial-No Derivatives 4.0 International Public License. A copy of this may be found at <https://creativecommons.org/licenses/by-nc-nd/4.0/legalcode>. This license sets out your rights and the restrictions that apply to your access to the thesis so it is important you read this before proceeding.

**Take down policy**

Some pages of this thesis may have been removed for copyright restrictions prior to having it been deposited in Explore Bristol Research. However, if you have discovered material within the thesis that you consider to be unlawful e.g. breaches of copyright (either yours or that of a third party) or any other law, including but not limited to those relating to patent, trademark, confidentiality, data protection, obscenity, defamation, libel, then please contact [collections-metadata@bristol.ac.uk](mailto:collections-metadata@bristol.ac.uk) and include the following information in your message:

- Your contact details
- Bibliographic details for the item, including a URL
- An outline nature of the complaint

Your claim will be investigated and, where appropriate, the item in question will be removed from public view as soon as possible.



**This electronic thesis or dissertation has been  
downloaded from Explore Bristol Research,  
<http://research-information.bristol.ac.uk>**

*Author:*

**Palacios, Ensor R**

*Title:*

**Contribution of cerebellar sensorimotor representations to behaviour**

**General rights**

Access to the thesis is subject to the Creative Commons Attribution - NonCommercial-No Derivatives 4.0 International Public License. A copy of this may be found at <https://creativecommons.org/licenses/by-nc-nd/4.0/legalcode>. This license sets out your rights and the restrictions that apply to your access to the thesis so it is important you read this before proceeding.

**Take down policy**

Some pages of this thesis may have been removed for copyright restrictions prior to having it been deposited in Explore Bristol Research. However, if you have discovered material within the thesis that you consider to be unlawful e.g. breaches of copyright (either yours or that of a third party) or any other law, including but not limited to those relating to patent, trademark, confidentiality, data protection, obscenity, defamation, libel, then please contact [collections-metadata@bristol.ac.uk](mailto:collections-metadata@bristol.ac.uk) and include the following information in your message:

- Your contact details
- Bibliographic details for the item, including a URL
- An outline nature of the complaint

Your claim will be investigated and, where appropriate, the item in question will be removed from public view as soon as possible.

# Contribution of cerebellar sensorimotor representations to behaviour

Enzor Rafael Palacios



A dissertation submitted to the University of Bristol in accordance to the requirement for award of the degree of PhD in the Faculty of Life Science

School of Physiology, Pharmacology and Neuroscience

September 2023

word count: 21895





# Dedication and Acknowledgment

I would like to dedicate this work to three people: my mother, Maria Cristina Danza, my father, Rafael Palacios, and my girlfriend, Chloe Slaney, who make me happy.

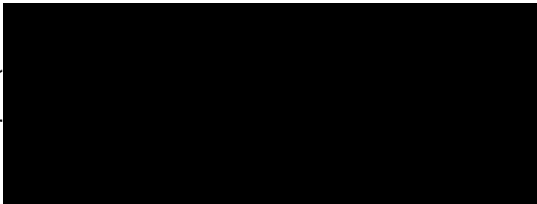
I would like to thank for their mentoring my two supervisors, Conor Houghton and Paul Chadderton, as well as Karl Friston. I would also like to thank for their support all the members of the lab, including Simon Bright, Daniela Franchini, Elisabeth Meyer and Marie Tolken.



# Declaration

I declare that the work in this dissertation was carried out in accordance with the requirements of the University's Regulations and Code of Practice for Research Degree Programmes and that it has not been submitted for any other academic award. Except where indicated by specific reference in the text, the work is the candidate's own work. Work done in collaboration with, or with the assistance of, others, is indicated as such. Any views expressed in the dissertation are those of the author.

SIGNED:

A large black rectangular redaction box covers the signature area. To the left of the box, a small white curly bracket is drawn, indicating the redacted content.

DATE: 06/09/2023



# Abstract

The cerebellum is important for behavioural control. It is not necessary for the generation of behaviour, but it is critical for its fluency and coordination. Its computations are often explained in terms of an estimation process, which allows to predict, and therefore refine, behavioural dynamics. At its simplest, this estimation process allows to integrate sensory and motor information, in order to refine actions (based on incoming sensory information), and predict sensations (based on actions). However, it is still unclear (i) how cerebellar state estimation bidirectionally interacts with brain-wide neuronal dynamics, and (ii) how this estimation process may be adapted to different behavioural contexts.

Here we addressed these two questions using computational and experimental techniques. The computational work investigated cerebellar computations, and how they contribute to whole-brain dynamics - here approximated by a simple set of differential equations. In essence, we sustain that behavioural coordination is a fundamental cerebellar function, explaining its pervasive role in behavioural control, and described a general model of cerebellar state estimation that enables to coordinate different behavioural variables or domains.

The experimental work investigated how the cerebellar cortex represents sensorimotor information, and how these representations change as a function of the state of the network, which could reflect different behavioural contexts. In particular, we recorded both population activity in the lateral cerebellar cortex and whisking behaviour in mice. To change the state of the network, we manipulated the level of inhibition, by reducing the activity of a population of inhibitory neurons, the Golgi cells. Our results suggests that Golgi cell inhibition may be an important mechanism through which sensorimotor representations in the cerebellum are tuned, which in turn has an impact on downstream behavioural control.

In summary, we combined computational and experimental techniques to gain insights into how neuronal dynamics in the cerebellum may be linked to and inform theories of cerebellar computations and functioning, and how these dynamics may contribute to behavioural control.



# Contents

<b>1</b>	<b>General Introduction</b>	<b>1</b>
1.1	Introduction . . . . .	1
1.2	The cerebellum . . . . .	3
1.2.1	Cerebellar organisation . . . . .	3
1.2.2	Cerebellar physiology . . . . .	8
1.2.3	Cerebellar computations . . . . .	10
1.3	Aims and overview . . . . .	15
<b>2</b>	<b>Cerebellar state estimation supports behavioural coordination</b>	<b>17</b>
2.1	Introduction . . . . .	17
2.1.1	Cerebellar state estimation supports efficient coordination of behavioural domains . . . . .	17
2.1.2	The free energy principle . . . . .	19
2.1.3	FEP and the cerebellum . . . . .	20
2.1.4	Aim and overview . . . . .	20
2.2	Materials and methods . . . . .	22
2.2.1	Neuronal dynamics as inference . . . . .	22
2.2.2	State space models . . . . .	23
2.2.3	Recognition dynamics . . . . .	24
2.2.4	Action-perception cycle . . . . .	26
2.3	Results . . . . .	27

2.3.1	Cerebellar contribution to neuronal inference . . . . .	27
2.3.2	The cerebellum: internal model and neuronal dynamics . . . . .	27
2.3.3	Simulation of motor coordination . . . . .	32
2.4	Discussion . . . . .	43
<b>3</b>	<b>Cerebellar cortical representations of whisking behaviour in mice</b>	<b>49</b>
3.1	Introduction . . . . .	49
3.1.1	The whisker system model . . . . .	49
3.1.2	Cerebellar representations of the whisker system . . . . .	50
3.1.3	Golgi cell computations . . . . .	51
3.1.4	Aim and overview . . . . .	53
3.2	Materials and Methods . . . . .	55
3.2.1	Surgical operations . . . . .	55
3.2.2	Recording procedure . . . . .	56
3.2.3	Electrophysiological analysis . . . . .	57
3.2.4	Behavioural analysis . . . . .	57
3.2.5	Histology . . . . .	60
3.2.6	Golgi cell manipulation . . . . .	61
3.2.7	Unit encoding of setpoint . . . . .	61
3.2.8	Tuning curve analysis . . . . .	61
3.2.9	PCA analysis, whisking-pc cross correlation, and pc loadings . . . . .	64
3.2.10	Setpoint decoding . . . . .	64
3.2.11	Statistical analysis for the CNO manipulation . . . . .	65
3.2.12	Analysis of pre- and post-drop neuronal and whisking data . . . . .	67
3.2.13	Comparison of the pre- and post-drop standard deviations (std's) of the units' activity absolute peaks. . . . .	67
3.2.14	Comparison of the pre- and post-drop linear fits of the initial whisking protraction phase. . . . .	68
3.3	Results . . . . .	71
3.3.1	Whisking representations . . . . .	71



---

3.3.2	Golgi cell manipulation . . . . .	87
3.3.3	Contribution of Golgi cells to whisker representations . . . . .	93
3.3.4	Discussion . . . . .	101
3.4	Covid statement . . . . .	107
<b>4</b>	<b>General discussion</b>	<b>109</b>
4.1	Computational modelling of the cerebellum . . . . .	109
4.2	Cerebellar representations of whisking behaviour . . . . .	111
<b>5</b>	<b>References</b>	<b>115</b>



# List of Figures

1.1	Cerebellar circuitry . . . . .	5
1.2	Models for motor control . . . . .	14
2.1	Cerebellar and extra-cerebellar hierarchical model . . . . .	28
2.2	Mapping elements of the model to cerebellar circuitry . . . . .	31
2.3	Whisker-respiration coordination . . . . .	33
2.4	Cerebellar contribution to whisking-respiration coordination (1) . . . . .	37
2.5	Cerebellar contribution to whisking-respiration coordination (2) . . . . .	38
2.6	Cerebellar contribution to whisking-respiration coordination (3) . . . . .	39
2.7	Cerebellar state estimation . . . . .	40

2.8	[Cerebellar-dependent coordination of limb and tail movements during locomotion] <b>Cerebellar-dependent coordination of limb and tail movements during locomotion.</b> Left (‘With cerebellar contextualisa- tion’): average vertical displacement of the front right, front left, hind right and hind left limbs as well as of the tail during locomotion across 14 strides. Shaded area denotes the standard deviation. In the presence of cerebellar expectations of inter-limb coordination, the front right and front left limbs are phase locked with the hind left and hind right limbs, respectively, and the two pairs of limbs have opposite phase. This results in the pairwise coordination of limb vertical displacement. At the same time, tail movements, which are modelled as a passive consequence of limb dynamics, symmetrically follows the dynamics of the two pairs of limbs. Right (‘Without cerebellar contextualisation’): in the absence of cerebellar control of limb dynamics there is no front-hind limb coordination, as each limb moves out of phase compared to the others, and tail movements become asymmetric. . . . .	42
3.1	Chemogenetic manipulation . . . . .	54
3.2	Exemplar unit . . . . .	58
3.3	DLC whisker tracing . . . . .	59
3.4	NeuroPixels trace . . . . .	60
3.5	DREADDs expression . . . . .	62
3.6	DREADDs and NeuroPixels trace . . . . .	63
3.7	Neuronal and whisker activity . . . . .	72
3.8	Single unit encoding of whisking setpoint . . . . .	73
3.9	Tuning curves from one recording . . . . .	74
3.10	Example of unit tuning curves . . . . .	75
3.11	Tuning curve heterogeneity . . . . .	76
3.12	Tuning curve clustering . . . . .	77
3.13	Tuning curve subgroups are associated to different whisking encoding patterns . . . . .	78
3.14	Extraction of the first 3 principal components . . . . .	79
3.15	Projected population activity . . . . .	80

3.16	Neuronal activity-angle cross-correlation . . . . .	81
3.17	Cross-correlation peaks . . . . .	82
3.18	Variance explained by the first 3 principal components . . . . .	83
3.19	Principal component loads . . . . .	85
3.20	Setpoint decoding . . . . .	86
3.21	Muscimol reduces population spike count . . . . .	88
3.22	Spike count dynamics (bin width 1 minute) . . . . .	89
3.23	Spike count dynamics (bin width 5 minute) . . . . .	90
3.24	Statistical analysis of CNO application . . . . .	91
3.25	Inverse Gamma variance contrasts . . . . .	92
3.26	Comparison of average whisking and neuronal activity pre- and post-drop. . . . .	94
3.27	Comparison of the std of absolute peaks in neuronal activity pre- and post-drop . . . . .	95
3.28	Difference between conditions in post-pre contrasts of std of absolute peaks in neuronal activity . . . . .	96
3.29	Time window for linear fit of whisking protraction . . . . .	97
3.30	Comparison of whisking protraction linear fits pre- and post-drop . . . . .	98
3.31	Pre- and post-drop cross-correlation peaks . . . . .	99
3.32	Pre- and post-drop cross-correlation cumulative sums . . . . .	100



# List of Tables

3.1	Neuronal and behavioural data . . . . .	70
-----	---	----





# Chapter 1: General Introduction

## 1.1 Introduction

The nervous system is the part of an animal's body that controls behaviour, namely, the repertoire of actions with which an animal interfaces with its environment. Behaviour is the product of external conditions, stimuli and constraints, as well as somatic drivers and needs, such as homeostatic ones. The interaction between these different internal and external factors is often complex and difficult to predict; nevertheless, the nervous system is constantly producing functional behaviour, capable of accommodating and reconciling different somatic and external states.

Over evolutionary time, the nervous system has become more complex and compartmentalised, with the appearance of specialised structures processing information related to different aspects of the environment. This evolutionary trajectory can be seen as reflecting the increased richness of both the world animals live in and their behaviour. For example, animals have become receptive to different properties of their surrounding, such as light, sound and chemicals, and have developed different ways to interface with it, such as by means of limbs, vibrissae, and vocalisation. Importantly, this richness also concerns the interactions between the different external and somatic variables involved in behaviour: for example, locomotion relies on the integration of different types of information, including proprioceptive, visual, vestibular and auditory information, which are not independent to one another. Consequently, the nervous system must have also evolved a way to both efficiently and accurately account for these interactions.

The cerebellum, a prominent structure of the nervous system, may play a particularly relevant

role in this account. Historically, the cerebellum has mostly been linked to basic motor control, but its more general function has been very difficult to define. This uncertainty stems from the heterogeneous involvement of the cerebellum in a variety of behavioural aspects, which might have made it difficult to pinpoint its overall role in behaviour. One possibility, that could explain this heterogeneity, is that the cerebellum has evolved to bind together and coordinate the different variables involved in behaviour, such as the body position, visual cues and position with respect to gravity in the case of locomotion.

This thesis aims to elucidate the cerebellar contribution to general behaviour, by means of both theoretical and experimental work. The theoretical work, in particular, addresses how neuronal representations about behaviourally relevant variables within the cerebellum may be used by it to promote or enforce behavioural coordination by interacting with extra-cerebellar regions. The experimental work, on the other hand, addresses how cerebellar neuronal dynamics represent or encode behaviour, by focusing on representations of whisking activity in mice.

## 1.2 The cerebellum

The cerebellum is an evolutionary old brain region, appearing in all vertebrates with a structure well preserved across species [24, 13]. It constitutes the ceiling of the brainstem, with which it comprises the rhombencephalon (hindbrain), the most primitive of the three subdivisions of the central nervous system; the other being the mesencephalon (midbrain) and prosencephalon (forebrain). Through the brainstem, the cerebellum connects to many other brain regions, including cortical and subcortical areas [208, 209, 111, 34, 113, 227]. Although often multi-synaptic in nature, this pervasive connectivity underpins the remarkable involvement of the cerebellum in a wide range of behavioural functions, encompassing simple reflexes as well as more complex functions, such as emotional processing, language, and social interactions [129, 206, 11]. Accordingly, whilst the majority work on the cerebellum implicates its role in motor control, there is growing evidence for its role in a wide range of behavioural functions; a role that matches the degree of evolution and complexity of cognitive abilities underlying behaviour (please see [95] for an example in birds).

The architecture of the cerebellum stands in stark contrast to its functional heterogeneity. In fact, its neuronal organisation is relatively simple and stereotypical, comprising a small pool of cell types and presenting little variation throughout its regions; although there is also a growing amount of evidence highlighting regional genetic, cellular and structural specificities [32]. This uniform architecture hints at a single, fundamental computation performed by the cerebellum, which might be adapted from place to place depending particular input received and information manipulated [4]. Accordingly, the appreciation of this archetypal neuronal organisation can provide important insights onto cerebellar computation. In what follows, I will therefore give a description of its general structure.

### 1.2.1 Cerebellar architecture

The cerebellum consists of two main parts: the cortex and the nuclei (please see Figure 1.1). The cortex is characterised by a clear organisation in three layers [178], namely, the input or granular layer, the molecular layer, and the Purkinje cell layer. There are also three nuclei

in each cerebellar hemisphere: from lateral to medial, these are the dentate, interpositus, and fastigial nucleus. The internal organisation of each nucleus, once considered homogeneous, has only recently started to be elucidated [128]. In contrast, the organisation of the the cerebellar cortex, at least in its basic elements, has been known for a long time [58, 98], and will be the focus of this section.

Within the cerebellar cortex, the granular layer constitutes the first stage of information processing, where extra-cerebellar input conveyed by mossy fibres arrive. The mossy fibre pathway, originating mainly from brainstem nuclei and the spinal cord [205], is the most conspicuous cerebellar input pathway, carrying information from most brain regions [171, 23, 231]. In the granular layer, each mossy fibre ramifies to generate several excitatory (glutamatergic) contacts with the two neuronal populations located in this layer, the granule cells and the Golgi cells. granule cells are small, tightly packed excitatory neurons, constituting, by number, more than half the neurons in the entire nervous system. On the other hand, their inhibitory counterpart, Golgi cells, are big and sparsely distributed interneurons.

Contact between mossy fibres and these two neuronal populations occur within specialised structures called glomeruli, consisting of a glial sheath that encases pre- and post-synaptic structures, and forms an isolated microenvironment where neurotransmitters can more easily diffuse [53, 166, 196]. Importantly each glomerulus is centered around a single, extensive mossy fibre presynaptic structure, but contains dendrites from tens of granule cells, as well as Golgi cell dendrites and axonal terminals [123, 46]. Because of this divergent mossy fibre-granule cell synaptic organisation, together with the fact that granule cells greatly outnumber mossy fibres, this stage of information processing is deemed to favour an expansion of extra-cerebellar neuronal representations in the granule cell population [140].

Neural representations in granule cells depend on the dynamic excitation-inhibition balance set within glomeruli. Because granule cells are not recurrently connected, excitation in this layer is feedforward, arising mainly from incoming mossy fibres. In contrast, Golgi cells can produce both feedforward and feedback inhibition, depending on whether their activity is driven by mossy fibre or granule cell excitation, which target the basal and apical portion of the Golgi cell dendritic arborisation, respectively. Overall, inhibition in the granular layer can be quite complex and composite, despite originating from a single neuronal population. In fact, Golgi cells

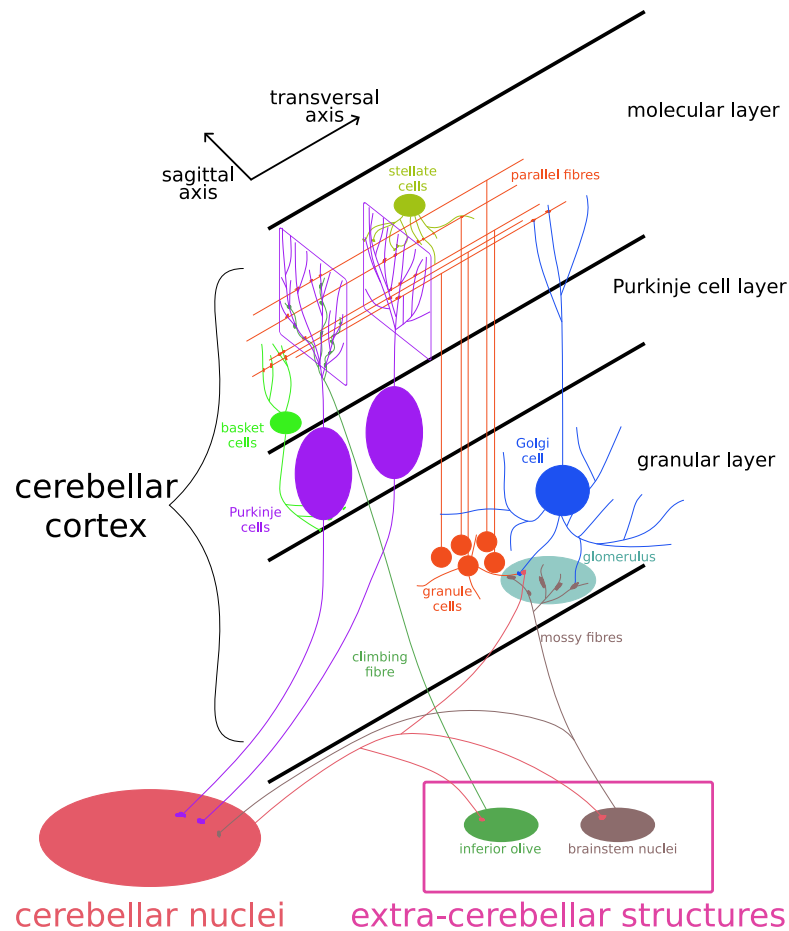


Figure 1.1: **Cerebellar circuitry.** Information enters the cerebellum via mossy fibres and climbing fibres; the former originate primarily from brainstem nuclei and spinal cord, while the latter originate from the inferior olive. Mossy fibres make synaptic contacts with excitatory granule cells and inhibitory Golgi cells within glomeruli in the granular layer, as well as with cerebellar nuclei cells through collaterals. In the glomeruli, the excitation-inhibition balance set by mossy fibres and Golgi cells drives granule cell activity, which travels through parallel fibres to reach the molecular layer. In here, parallel fibres excite both molecular layer interneurons, comprising basket cells and stellate cells, and Purkinje cell dendritic trees. Patterns of excitation and inhibition set by parallel fibres and molecular layer interneurons respectively drive simple spikes in Purkinje cells, whose axons exit the cortex to enter cerebellar nuclei where they form inhibitory synapses. At the same time, climbing fibres ramify within the dendritic tree of single Purkinje cells to evoke complex spikes, which drive plasticity in local synapses and interact with simple spike generation. Finally, axons exiting the cerebellar nuclei transmitted information back to extra-cerebellar structures, origin of both mossy fibres and climbing fibres, as well as to the cerebellar cortex through collaterals.

are reciprocally coupled through chemical and electrical synapses, which enables coordination, in terms of both synchronisation and desynchronisation, of inhibition across the granular layer [55, 225, 235]. Moreover, at the synaptic level, GABA released from Golgi cells operates on different types of receptors, each with its characteristic ligand affinity and spatial distribution [53, 41, 43]. As a result, Golgi cell inhibition can operate at different temporal and spatial scales within glomeruli, and appears capable of finely controlling and sharpening representations in the granular layer [174].

From the granular layer, information is relayed by granule cells to neurons whose dendrites are located in the molecular layer. The axons of granule cells, upon ascending into the molecular layer, bifurcate into fibres which run in parallel to each other along the transverse axis for as long as a few millimetres [98, 165]. Along their course, parallel fibres make synaptic contacts with Golgi cell, Purkinje cell and molecular layer interneuron dendrites. Molecular layer interneuron is a label indicating two broad classes of small interneurons, whose soma and dendrites reside in the molecular layer: the basket cells and the stellate cells [132]. These neuronal populations form an intricate network of interconnected cells, which ultimately control Purkinje cell activity. Basket cells and stellate cells differ in both their physiology and morphology, like the part of Purkinje cells they target, with stellate cell inhibiting the dendritic arbor, and basket cells preferentially inhibiting the soma. This in turn has important consequences on how they modulate Purkinje cell activity [20], namely, by controlling how incoming information is either integrated or transmitted.

As for Purkinje cells, these are the sole output neuron of the cerebellar cortex, where feedforward molecular layer interneuron inhibition and parallel fibre excitation converge. These neurons are intrinsically active, firing small and short action potentials, the simple spikes, at a rate of around 30 Hz *in vitro* [99]; by firing at a constant rate, which is modulated by molecular layer interneuron and parallel fibre input, Purkinje cells can represent information with both increases and reductions in activity. The Purkinje cell soma is located in the Purkinje cell layer, the third and last stage of information processing within the cerebellar cortex, whereas their dendrites develop in the molecular layer, branching in a stereotypical fan-like shape [178, 98]. These complex dendritic arborisations look thin in the parasagittal plane but are wide in the transversal plane, lying in parallel one next to each others, and orthogonally to the direction of parallel fibres: as such, each parallel fibre can make one or two contacts with each Purkinje cell dendrite, but

connects with hundreds of them [115]. This particular synaptic organisation, in contrast to the divergent connectivity found in the granular layer, seems to favour integration of information at the level of single Purkinje cells or subgroups of them.

Purkinje cells are also the target of climbing fibres, which constitute the second main stream of information entering the cerebellum. Climbing fibres are axonal projections originating from the inferior olive [49], a bilateral medullary structure whose function is tightly associated with the cerebellum [153, 2, 117]. In fact, cerebellar and extra-cerebellar input converge within the inferior olive, and comparison between the two is thought to give rise to prediction errors that are transmitted by climbing fibres directly to Purkinje cells. These signals are critical for associative learning in the cerebellum, triggering important plastic changes in the synapses located in the Purkinje cell dendritic trees. Specifically, each Purkinje cell is innervated by a single climbing fibre; however, because a climbing fibre can form up to 100 strong synapses on each Purkinje cell [119], each of these connections is powerful, generating characteristic excitatory events known as complex spikes. These action potentials, compared to the brief, small in amplitude simple spikes arising from parallel fibre input, are long-lasting, high in amplitude, and have a complex, non-stereotypical shape [173]; moreover, they occur at a much lower rate of 1 Hz [207]. Importantly, complex spikes interact with simple spikes to produce depression in synaptic connections, therefore changing the connectivity structure within the molecular layer.

From the Purkinje cell layer, axonal projections exit the cerebellar cortex and enter the cerebellar nuclei, where they form inhibitory synapses with local neurons [119]. Notably, cerebellar nuclei also receive extra-cerebellar input via mossy fibre collaterals [204]; therefore, cerebellar nuclei networks are in the position to compare incoming extra-cerebellar information with information processed by the cerebellar cortex [19]. Eventually, cerebellar nuclei neuronal representations of behaviourally relevant states are sent to extra-cerebellar regions [119] – closing the loop – where they drive, modulate or correct neuronal dynamics therein.

Finally, it is important to remark that the above canonical description of the cerebellar microcircuit is incomplete and it does not consider several key aspects. In particular, cerebellar information processing is often described as feedforward; however, many connections, together with additional cell types that are often overlooked, contribute to feedback, recurrent loops within the cerebellum itself. In particular, within the granular layer exist two neuronal populations that

are important in shaping neuronal dynamics in the granular layer. Lugaro cells, located just beneath the Purkinje cell layer, have dendrites that span both the transversal and sagittal plane, receive inhibitory input from tens of Purkinje cells, and inhibit both molecular layer interneurons and Golgi cells; hence implementing long-range feedback loops within the cerebellar cortex [139, 52]. On the other hand, unipolar brush cells are excitatory neurons positioned at the bottom of the granular layer that receive and amplify excitatory mossy fibre input [164, 195]. Notably, mossy fibres can either have extra-cerebellar origin or come from cerebellar nuclei, carrying feedback input to the cerebellar cortex [110]. Finally, feedback loops within the cerebellum are also implemented via long-range inhibitory connections from cerebellar nuclei to the granular layer, targeting Golgi cells [3], and by Purkinje cell collaterals targeting both cortical interneurons [237] and granule cells [93].

### 1.2.2 Cerebellar physiology

The stereotypical cerebellar architecture described above has been an attractive working ground when trying to bridge the gap between structure and functions of neuronal networks. In fact, a wealth of studies have addressed how the cerebellar network encodes behaviourally relevant variables, how changes in its structure are reflected in changes in neuronal representations, and how its neuronal code contributes to functional behaviour, namely, behaviour where sensory, motor, and cognitive components of it are seamlessly integrated and coordinated.

One exemplary model classically used to investigate cerebellar functions is the oculomotor system. This system is responsible for eye movements and reflexes, including smooth-pursuit, gaze holding, nystagmus, and the vestibulo-ocular reflex, all of which are impaired by cerebellar lesions [203]. For example, smooth tracking of moving targets is impaired after damage to a small cerebellar lobe called the flocculus. In this area, Purkinje cell simple spike rates encode the motion of visual stimuli on the retina [159, 212] as well as eye kinematics [181], with a preference for one direction along either the horizontal or vertical axis. In turn, these neuronal representations, important for fine control of eye movements [145], are carefully adjusted by inferior olive-evoked complex spikes, which trigger synaptic changes at the parallel fibre-Purkinje cell synapse to modulate the tuning and strength of simple spikes [242].



Plasticity at the parallel fibre-Purkinje cell synapse has been used as a paradigm for learning in the brain and has been extensively studied. The most famous plasticity mechanism at this site is long-term depression (LTD) [118]. LTD consists in the protracted strength reduction of the parallel fibre-Purkinje cell connection, triggered by the repeated co-occurrence of simple spikes and complex spikes [116]. LTD underlies many forms of associative learning, such as that occurring during eyelid conditioning, where a conditioned stimulus such as airpuff becomes associated with an unconditioned stimulus to produce a conditioned blinking response [155].

Because LTD relies on complex spikes, these events have often been considered a teaching or error signal for the parallel fibre-Purkinje cell synapse, possibly instantiating a form of supervised learning [190]. This view invests the inferior olive, the origin of climbing fibres evoking complex spikes, with the key role of instructor for learning in the cerebellum. However, this framework is mostly applicable to simple behavioural paradigms where there is a clear error signal, like in conditioning and adaptation paradigms [189, 170]. In more complex scenarios, instead, climbing fibres have been found to transmit a wide range of stimuli, including reward-like and predictive input [101, 136], with a graded code [83] that is modulated by numerous mechanisms, involving pre- and post-synaptic activity, inhibition and other network signals [26, 154, 28, 133, 243]. This heterogeneity in climbing fibre signalling thus indicates that LTD is not limited to error correction, but contributes to more general associative learning involving the olivo-cerebellar system.

In parallel, many mechanisms other than classical LTD also exist that support learning throughout the cerebellum [97, 85]. For example, in contrast to LTD, LTP (long term potentiation) at the parallel fibre-Purkinje cell synapse leads to increased connectivity strength, and is not associative, requiring only sustained presynaptic activity [198, 144]. On the other hand, other sites of synaptic plasticity involve molecular layer interneurons, neurons in the granular layer and cerebellar nuclei neurons [97, 85, 39]. Moreover, properties of synaptic plasticity mechanism differ across cerebellar regions, adapted to the specific characteristics of the behaviour encoded [215]. Overall, the ubiquity and diversity of learning mechanisms in the cerebellum highlights the ability of this structure to learn associations between behaviourally relevant variables in a variety of contexts.

As a consequence, investigation of cerebellar functions is now more and more often conducted

using more complex behavioural paradigms, also thanks to advances in recording techniques, such as multichannel and optical recording [136, 92]. These studies have highlighted how the cerebellum, at every stage of information processing, accurately represents all kinds of variables involved in behaviour, including autonomic states, task-contingencies (e.g., reward signals) and general motor activation [89, 228, 136, 191, 94, 140]. This means that neuronal representations in the cerebellum recapitulate with fidelity those found in other brain regions, such as the motor cortex, and do so in a learning-dependent manner [229]. These precise cerebellar representations of task parameters are then used to fine tune a range of behavioural dynamics across task contingencies, such as timed motor initiation [25], kinematics of reaching movements [224], and even accumulation of evidence for decision making [50]. Altogether, these findings may suggest that the cerebellum is capable of holding and refining internal models supporting all aspects of behaviour.

The ability of the cerebellum to integrate multiple sensory, motor and cognitive domains may be at the core of its contribution to functional behaviour. At its simplest, this integration involves sensory and motor information, of which the whisker system in mice offers a paradigmatic example [223]. Neuronal activity in the cerebellum, and in particular in the lateral portion of its cortex [37, 38], has been described to encode whisking dynamics, and its output is known to play a key role in the control of whisker behaviour [149, 184, 21, 191]. However, many questions remain open, such as how whisking-related information processing in the cerebellum may be adapted to different behavioural contexts; these contexts may require to focus on particular behavioural interactions instead of others, such as when exploring a place, when rapidly moving, or when interacting with conspecifics. Investigating how cerebellar control of whisking activity may be sensitive to the behavioural context is therefore crucial to understand its role in behaviour.

### 1.2.3 Theories of cerebellar computations

Information processing within the cerebellum is often associated with a unique, fundamental computation, which is adapted from place to place to the specific properties and requirements of the behaviours encoded and supported. Accordingly, it is increasingly recognised that cellular, molecular and network specificities across cerebellar regions may underlie a compartmentalisation

of information processing [33]. For example, a coarse cerebellar subdivision can be found across the longitudinal (medio-lateral) axis, with the lateral, paravermal and vermal cerebellar cortex connecting respectively to the dentate, interpositus and fastigial nuclei [124]. This macroscopic connectivity pattern is thought to reflect the level of cognitive complexity of the behaviours each region is involved in, with the lateral cerebellum and dentate nucleus associated with higher level processes. A more fine-grained subdivision is instead based on the cerebellar organisation in modules, each defined by specific connectivity patterns involving circumscribed regions of the inferior olive, sagittally oriented subpopulations of Purkinje cells, and subregions within each cerebellar nuclei [5]. Further functional compartmentalisation of the cerebellar-olivary system have also been put forward, for example by calling upon the existence of parasagittal microzones and micromodules [5], or based on molecular patterning (e.g., zebirin stripes [18]). To date, however, the exact mapping between the variously defined cerebellar structure and functions is still an open question.

Beyond regional specificities, the cerebellar architecture has been an inspiration for many models and theories. In particular, its organisation in well-defined cortical layers and nuclei has suggested a decomposition of information processing into different canonical stages; although feedback loops within the cerebellum hints that these stages are highly interconnected and possibly not completely separated. In brief, these stages include an expansion of extra-cerebellar representation in the granular layer, the associative encoding of variables in the Purkinje cell population, and some sort of comparison between or integration of extra-cerebellar and cerebellar cortical representations in the cerebellar nuclei. Notably, this decomposition is already present in classical, Marr-Albus models [153, 2], whereby the cerebellum operates as a perceptron or classifier. In these models, the role of the cerebellum is to learn the association between mossy fibre input and specific motor responses; this is achieved by first expanding mossy fibre input patterns in the granular layer to increase their discriminability, and then learning to associate each input pattern with an appropriate Purkinje cell response, via changes in the synaptic structure instructed by inferior olive teaching signals.

Following the work from Marr and Albus, adaptive filter models advanced the original idea of a static pattern classifier by conceiving the cerebellar cortex as a filter, capable of transforming time-varying mossy fibre input into a sequence of Purkinje cell output [81]. Similar to the Marr-

Albus model, in adaptive filters Purkinje cell activity evolves to minimise its correlation with teaching signals conveyed by climbing fibres. The biological implementation of the adaptive filter and analogous reservoir computing models again relies on two sequential processes, taking place in the granular layer and Purkinje cells, respectively [241, 47, 193]. These are (i) an analysis step, expanding the original time-varying input in a sufficiently complete set of outlasting signals or basis functions; and (ii) a synthesis step, where the newly created signals are recombined into the output time-series. Thus, in analogy to an augmented representational space in classical pattern separation, adaptive filters presume a temporal expansion of mossy fibre activity in the granular layer.

In contrast to the perceptron and adaptive filter models, other theories have instead focused on the cerebellar computation from the perspective of the entire network of brain regions subserving motor control (Fig 1.2, top), of which the cerebellum is one component. In many of these theories [122, 158, 239, 54, 67, 12], the cerebellum plays the role of an internal or forward model, namely, a model that is used to predict the sensory feedbacks – both from the body and the external world – generated by one’s action. Briefly, in motor control there is a body whose actions are directed by motor commands, and these commands are issued by an inverse model, which attempts to minimise an arbitrary cost function, or alternatively maximise a reward function. Then, within this closed loop made of desired states, motor commands and sensory feedbacks, forward models play a key role for online refinement of actions, by enabling the adjustment of motor commands previous to and during execution of movements, anticipating and short-circuiting sensory feedback. Notably, there is a large body of empirical results that is congruent with the idea that the cerebellum implements forward models [147, 168, 10, 201, 31, 217]. Moreover, this idea can be extended to other, more cognitively-involved functions [186, 121, 143], which makes it a theory for the ubiquitous cerebellar involvement in behaviour.

The hypothesis of the cerebellum as a forward model is closely related to, and can be incorporated within, a more general theory of neuronal computations, which views neuronal dynamics *tout court* as an inference process (Fig 1.2, bottom). This theory has its roots in Helmholtz’s definition of perception as inference [102], and has been extensively developed within the theoretical framework of the Free Energy Principle (FEP) [71]. The FEP, and its corollary theory, active inference [78, 44], asserts that both perception and action are the product of an inference process,

which is based on an underlying internal or generative model of how sensory input or observations are generated. Crucially, in this framework, the need for a distinction between different types of internal models encoded in the various brain regions (e.g., forward or inverse) dissolves [72], as well as the qualitative distinction between sensory predictions and motor commands [1]: here, the biophysical structure of the whole brain encodes a deep or hierarchical, modular generative model, and motor commands reduce to predictions about proprioceptive sensations that are easily realised at the level of motor reflex arcs. Consequently, the FEP shifts the question from whether the cerebellum implements forward models for the sake of state predictions, to which type of generative model does it encode, and how does its model integrate within the overall whole-brain hierarchical model [74]. Notably, this perspective may help to understand the observed ubiquitous cerebellar involvement in a range of behaviours aspects, including the more cognitive ones.

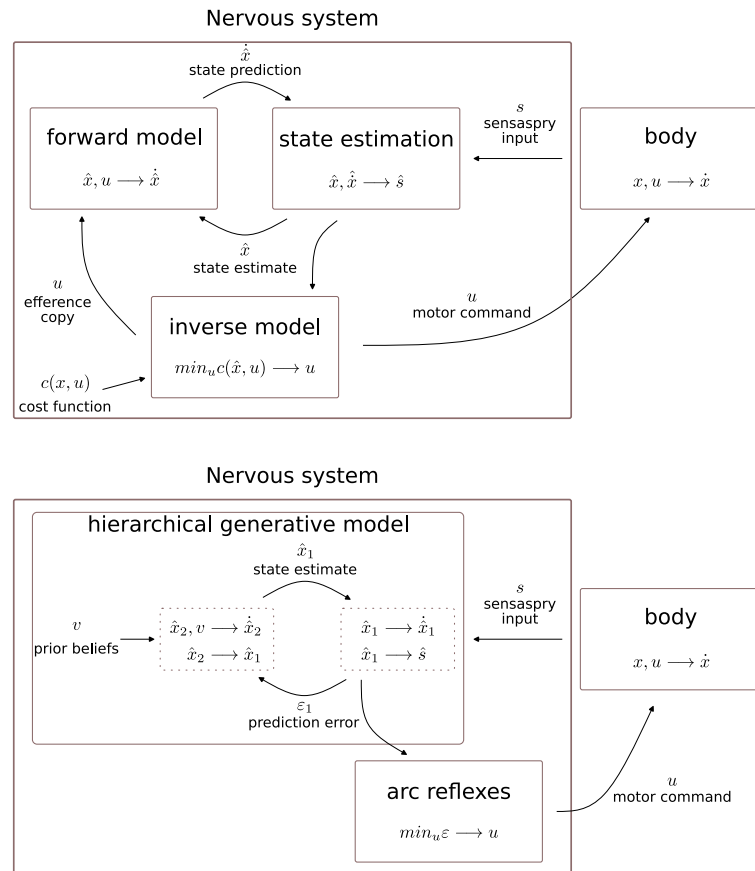


Figure 1.2: **Models for motor control.** Top: diagram of motor control based on separate models. Here, the body changes its states  $x$  based on the current state and motor command  $u$  (the mapping is shown as an arrow from  $x, u$  to  $\dot{x}$ ). The command  $u$  is generated by an inverse model, designed to minimise a cost function  $c$  by selecting an appropriate  $u$  based on current estimated state  $\hat{x}$ ; the choice of  $c$  is arbitrary and context-dependent. Estimation of  $x$  is based on sensory input  $s$  and predictions  $\hat{\dot{x}}$ ; these predictions, generated by a forward model, implement a closed loop that enables compensation of sensory delays. Cerebellar functions are often associated with the implementation of a forward model, which predicts changes in states  $\hat{x}$  based on the current estimate  $\hat{x}$  and efference copy  $u$  from the inverse model. Bottom: motor control based on hierarchical generative models. The entire brain instantiates a hierarchical model of how hidden causes  $x$  change over time and how they produce  $s$  (or states at the lower level). State estimation rests on neuronal message passing involving estimates  $\hat{x}$  and prediction errors  $\varepsilon$ , scoring the difference between real and predicted sensory states ( $s - \hat{s}$ ). Notably, estimation also depends on prior beliefs  $v$ , which here substitute the cost function  $c$ . These beliefs are characteristic of the particular system in question (e.g., a fish), and bias state estimation towards states that are most expected (e.g., being in the water). Realisation of expected states ultimately occurs at the level of spinal arc reflexes, implementing a simple, hardwired inverse model of how muscle contraction leads to minimisation of proprioceptive  $\varepsilon$ . In this framework, the cerebellum is part of the overall hierarchical model, and the question then becomes how does it fit within the latter.

### 1.3 Aims and overview of the thesis

The work presented in this thesis aims at elucidate the cerebellar contribution to behaviour by means of both theoretical and experimental work.

The theoretical part of the work investigates how cerebellar computations contribute to whole-brain dynamics. This contribution is based on the link between cerebellar internal models and extra-cerebellar dynamics; however, the exact nature of this link is still unclear. Here, we address this issue, and propose the idea that the key function of the cerebellum is to support behavioural coordination by controlling extra-cerebellar neuronal dynamics, underlying discrete behavioural domains, via its own estimates about those dynamics. Specifically, we propose that the cerebellar internal model learns and continuously infers interactions between behaviourally relevant states, where these interactions express how dynamics of distinct but connected behavioural variables should jointly unfold over time. The ensuing cerebellar estimates can then be used to constrain extra-cerebellar dynamics, so to realise coordination expected by the cerebellar model. In other words, learned expectations held by the cerebellar internal model about behavioural coordination drives general coordination of extra-cerebellar neuronal dynamics underlying behavioural production.

The experimental part of the work investigates instead how whisking behaviour is encoded within the lateral cerebellar cortex, and how this encoding affects behaviour. Whisking is a key aspect of the rodent behavioural repertoire, supporting many different motor and cognitive domains [134, 51, 238, 7, 210, 232]. Whisking activity is well represented in the lateral cerebellar cortex [37, 38], and the cerebellum in turns plays a central role in the control of whisking behaviour [184, 191]. However, it is not known whether and how neuronal representations in the cerebellar cortex change based on the state of the network – which may be reflecting different behavioural states – and how these changes may affect behaviour itself. The state of the cerebellar cortical network is affected by several factors, including the level of inhibition, which is under the control of different mechanisms such as neuromodulation [174]. Thus, we investigate how neuronal representations of whisking, and whisking behaviour itself, may change under different levels of inhibition in the cerebellar cortex.

In more detail, we recorded both (i) population activity throughout the cortex, with Neu-

ropixels I probes, and (ii) unilateral whisker position, with a high-speed camera, in head-fixed mice. Importantly, recording was carried out both in the intact network and during manipulation (reduction) of the Golgi cell activity, a primary source of inhibition in the cerebellar cortex. This setup allowed us to study how whisking-related information is represented by the cerebellar cortical network, and how these representations change when perturbing the state of the network.

The rest of the thesis is organised as follows: we first describe the results of the theoretical work, which comprise a description of a cerebellar internal model capable to infer how behavioural domains couple together; these results also include simulations of behavioural coupling in the context of whisking-respiration coordination in rodents. Next, we continue by presenting the experimental work: we first describe the whisking representations in the intact cerebellar cortical network; then, we describe how these representations change when manipulating Golgi cell inhibition, and in particular when reducing it. Briefly, neurons in the lateral cerebellum appear to accurately represent whisking behaviour, and in particular upcoming whisking, both at a single cell and population level. On the other hand, manipulation of the network's state, while not affecting the quality of neuronal representations, impacts both neuronal and whisking activity. In particular, reducing Golgi cell activity appears to decrease temporal variability of neuronal activity locked to whisking behaviour, while making whisking activity more variable over time.



# Chapter 2: Cerebellar state estimation supports behavioural coordination

This chapter is based on the paper ‘Cerebellar state estimation enables resilient coupling across behavioural domains’ [175], for which I conceived the idea, wrote the manuscript in its entirety, made the figures and wrote their captions. In particular, the exposition follows the same structure of the paper, and the figures and results are the same.

## 2.1 Introduction

### 2.1.1 Cerebellar state estimation supports efficient coordination of behavioural domains

Behaviour is the result of complex interactions between multiple internal states and external conditions. The cerebellum is involved in all behavioural aspects, from the most simple, like reflex execution [61], to more complex and cognitively demanding ones: these include for example emotional control [213, 210], social interactions [129], language [6] and mental representations [156, 199]. However, the exact cerebellar contribution to all these behavioural aspects remains unclear.

Many cerebellar theories assume that its network implements internal probabilistic models

for the estimation of hidden states, and that these estimates are used to correct or finesse computations in other brain regions involved in behaviour [180, 158, 239]. These theories are built upon many empirical findings, showing that neuronal dynamics in the cerebellum reflect a state estimation process [147, 168, 10, 201, 220, 217]. Nevertheless, it remains unknown the precise nature of the link between cerebellar internal models and neuronal dynamics in other brain regions.

Some key cerebellar features are particularly important when looking to understand its function. First, the cerebellum has a relatively simple network architecture, possibly indicating it performs a specific universal or fundamental computation [4]. Second, its inter- and intra-regional connectivity seem to favour sensorimotor and multimodal integration [208, 209, 111, 34, 113, 227]. Third, the cerebellum is well known to express associations between behaviourally relevant states through plastic changes in its connectivity structure [42]. Taken together, these features speak to a high-level, general role of the cerebellum in providing extra-cerebellar regions with precise estimates of how various states interact during behaviour. That is, because functional behaviour requires dynamic coordination of external and somatic states, here we sustain the idea that the chief cerebellar function is to contribute to behaviour by learning and executing interactions or context sensitivity among hidden states.

In more detail, here we pursue the idea that the cerebellar-dependent contextualisation of states' dynamics on one another is based on generative or internal models encoding expectations about state interactions. These expectations are acquired through learning, and shape cerebellar estimates that are then used to constrain and modulate neuronal dynamics in extra-cerebellar structures. This description of cerebellar function is in line with prominent theories of the cerebellum as a Smith predictor, a forward model, a model predictive control or as an implementation of predictive coding [54, 179, 222, 201, 67, 137, 185, 74] – all of which involve a state prediction and estimation process. In this work, we will use a formalism that generalises these theories, the free energy principle (FEP), which I will introduce below.

### 2.1.2 The free energy principle

At its core, the FEP is a theory of self-organisation [187], an ubiquitous process that at its simplest describes the spontaneous emergence of ordered patterns in a system from interactions among its components. This definition can be extended to describe biological systems, as systems embedded in an environment that are able to maintain a functional coupling with – and therefore a separation from – it. As such the FEP has been used to describe biological self-organisation at various temporal and spatial scales, including morphogenesis [70, 176], neuronal dynamics [130, 177, 114], cognitive functions [76, 62, 77, 160] and social organisation [163, 68].

In essence, the FEP is a variational principle used to describe the dynamics of internal states of a system, where these dynamics are predicated to minimise a quantity called variational free energy ( $F$ ).  $F$  is an upper bound on the surprisal (negative log probability) of sensory exchanges of the system with its environment; intuitively, higher surprisal is associated with sensory input or observations that are uncharacteristic of the system in question. The time average of surprisal is entropy, corresponding to the level of dispersion of sensory input towards an undefined, death-like state. Therefore, by minimising  $F$ , a system is able to bound entropy production; namely, it self-organises to counteract the intrinsic tendency to decay.

The key aspect of the FEP is that it uses an information theoretic quantity,  $F$ , which is based on a probabilistic model of how observations are generated, to describe the physical process underlying biological self-organisation. In details, it offers a dual perspective on a system, by linking the physical dynamics of that system with its dynamics in an encoding space: in particular, in a space of probabilities, where each point corresponds to a conditional probability distribution encoded by the system's states, over external states generating observations. Consequently, a self-organising system, capable of maintain itself over time, is necessarily a good probabilistic model of its environment, and is able to predict its sensory exchange with it. Applying the FEP to the brain and behaviour, the nervous system can be understood as a probabilistic model of how hidden states, both somatic and environmental, generate sensory states or observations, and the action-perception cycle in which a system engages can be described in terms of Bayesian inference: this is known as active inference [71].

### 2.1.3 FEP and the cerebellum

The use of the FEP to explain brain functioning requires us to identify the generative model whose structure and ensuing inference process can be mapped onto the neuronal architecture and dynamics. The cerebellar model is an integral part of the overarching hierarchical model that is the nervous system, and here we place it at a high level in this hierarchy. This choice is motivated by the fact that the cerebellum receives and reciprocates input from most brain regions, and that cerebellar lesions do not abolish the production of behaviour *per se*, but instead have an impact on its fluency, precision and coordination. All this speaks to a role of the cerebellum in contextualising concurrent, lower-level inference processes throughout the brain responsible for behavioural production.

In more detail, this means that the cerebellum infers the context of behaviourally relevant hidden states, rather than hidden states *per se*. Cerebellar state estimation infers the behavioural context, including states' interactions, from ascending information from extra-cerebellar brain regions, and returns control parameters that contextualise (i.e., coordinate) inference in those regions. Crucially, this contextualisation relies on linear or weakly nonlinear cerebellar models, in contrast to extra-cerebellar inference processes, which are based on arbitrarily complex, highly nonlinear models, giving rise to cyclic patterns and nested sequences [130, 131, 73].

### 2.1.4 Aim and overview

This work aims at developing a theoretical understanding of a fundamental cerebellar function, namely, its ability to finesse and coordinate behaviour. To this end, we model cerebellar computations as a linear state estimation process that is capable of approximating nonlinear extra-cerebellar dynamics. The key aspect of this model is that it contains expectations about states' interactions, which in turn bias cerebellar state estimation towards coordination. These estimates are then used to coordinate discrete behavioural domains, by constraining (i.e., contextualising) neuronal dynamics in one brain region based on concurrent dynamics in other brain regions, and *vice versa*.

We develop this idea by first presenting a general cerebellar model supporting state estimation of hidden states and their interactions. We then trace a mapping between components of

the model and elements of the cerebellar circuit, to illustrate how this mapping may account for various aspects on the network dynamics. Finally, we present the results of simulations, showcasing cerebellar-based coordination in the context of whisking-respiration synchronisation in rodents, as well as limb and tail coordination during locomotion, for which the cerebellum has been shown to play a role [151, 191]. Importantly, this simple behavioural setting evinces the fundamental cerebellar contribution to coordinated behaviour, which can be generalised to all sorts of behavioural paradigms.

## 2.2 Materials and methods

### 2.2.1 Neuronal dynamics as inference

Bayesian inference is concerned with seeking the posterior distribution over unknown states  $\vartheta$ , given observations  $y$  and a model  $m$  that defines the joint probability distribution between  $\vartheta$  and  $y$ :

$$m = p(\vartheta, y). \quad (2.1)$$

The posterior distribution can be written as:

$$p(\vartheta|y, m) = \frac{p(y|\vartheta, m)p(\vartheta|m)}{p(y|m)}. \quad (2.2)$$

Equation 2.2 is often intractable because the marginal likelihood at the denominator,  $p(y|m)$ , also known as model evidence, involves an expensive integration over all possible values of  $\vartheta$ . Alternatively, one can use variational Bayes, a procedure that seeks to optimise an arbitrarily defined probability density over environmental states, known as variational or recognition density,  $q(\vartheta)$ , to best approximates the true posterior  $p(\vartheta|y)$ . The FEP suggests that the brain performs approximate Bayesian inference. In particular, variational Bayes is based on the minimisation of the Kullback-Liebler (KL) divergence between  $q(\vartheta)$  and  $p(\vartheta|y)$ , which can be expressed in terms of variational free energy ( $F$ ) [22], using Bayes law in Equation 2.2, and dropping reference to  $m$  hereafter for clarity:

$$\begin{aligned} D_{kl}(q(\vartheta)|p(\vartheta|y)) &= \int q(\vartheta) \log \frac{q(\vartheta)}{p(\vartheta|y)} d\vartheta \\ &= F + \log p(y) \end{aligned} \quad (2.3)$$

where

$$F(q(\vartheta), y) = \int q(\vartheta) \log \frac{q(\vartheta)}{p(\vartheta, y)} d\vartheta. \quad (2.4)$$

Notice that  $F$  and  $q(\vartheta)$  depend on the generative model  $m$ , as  $p(\vartheta, y)$  does. From Equation 2.3, changing  $q(\vartheta)$  to minimise  $F$  automatically reduces  $D_{kl}$ , because  $\log p(y)$  does not depend on  $q(\vartheta)$ . Thus, approximate Bayesian inference rests on  $F$  minimisation, which makes  $q(\vartheta)$  approach  $p(\vartheta|y)$ . Moreover,  $F$  minimisation also maximises model evidence, because  $F$  is an upper bound

of the negative log marginal likelihood:

$$-\log p(y) \leq F. \quad (2.5)$$

The brain is thought to parameterise the sufficient statistics of  $q(\vartheta)$ . The question is then what form does  $q(\vartheta)$  take. A common approach is to use the Laplace approximation, under which  $q(\vartheta)$  takes the form of a Gaussian distribution, which is fully defined by its mean or expectation  $\mu$  and variance  $\xi$ ,  $q(\vartheta; \mu, \xi)$  [69]. One consequence of adopting this approximation is that beliefs about hidden or latent states are unimodal, and that the curvature of the distribution around its mode (i.e., the variance) is an analytic function of the mode or expectation. This leaves only one parameter,  $\mu$ , to be encoded by the brain in order to minimise  $F$ , and leads to a description of neuronal dynamics in terms of predictive coding or Bayesian filtering [69, 75]. In this case,  $F$  can be defined as[22]:

$$F(\mu_\vartheta, y) = -\log p(\mu_\vartheta, y) \quad (2.6)$$

### 2.2.2 State space models

The exact form of  $F$  is specified by the model  $m$ . In this work, we use a state space model with first-order generalised motion (bold face refers to vectors) [69]:

$$\begin{aligned} \mathbf{y} &= g(\mathbf{x}) + Z & Z &\sim \text{Normal}(0, \Sigma_z) \\ \frac{d\mathbf{x}}{dt} &= \mathbf{x}' = f(\mathbf{x}, \mathbf{v}) + W & W &\sim \text{Normal}(0, \Sigma_w) \\ \mathbf{v} &= V & V &\sim \text{Normal}(0, \Sigma_v). \end{aligned} \quad (2.7)$$

In this model, observations  $\mathbf{y}$  are generated by two hidden or latent states,  $\mathbf{v}$  and  $\mathbf{x}$ :  $\mathbf{v}$  plays the role of a control or input variable, entering the equation of motion for  $\mathbf{x}$ , whereas  $\mathbf{x}$  is the state of the system. This model is stochastic, including the noise terms  $Z$  and  $W$ , which affect the mapping  $g$  from  $\mathbf{x}$  to  $\mathbf{y}$  and equations of motion for  $\mathbf{x}$ , respectively. In this hierarchical model,  $V$  is a noise term with high variance, which makes the prior over  $\mathbf{v}$  noninformative. Under this

model,  $F$  can then be written as the sum of different components (omitting some terms for clarity):

$$\begin{aligned} F(\boldsymbol{\mu}, \mathbf{y}) &= -\log p(\boldsymbol{\mu}, \mathbf{y}) = -\log p(\boldsymbol{\mu}_x, \boldsymbol{\mu}_v, \mathbf{y}) \\ &= -\log p(\mathbf{y}|\boldsymbol{\mu}_x) - \log p(\boldsymbol{\mu}_x|\boldsymbol{\mu}_v) - \log p(\boldsymbol{\mu}_v) \end{aligned} \quad (2.8)$$

where, using Equation 2.7, each component corresponds to:

$$\begin{aligned} \log p(\mathbf{y}|\boldsymbol{\mu}_x) &= -\frac{1}{2}(\mathbf{y} - g(\boldsymbol{\mu}_x))^T \Sigma_z^{-1}(\mathbf{y} - g(\boldsymbol{\mu}_x)) - \frac{1}{2} \log |\Sigma_z| \\ \log p(\boldsymbol{\mu}_x|\boldsymbol{\mu}_v) &= -\frac{1}{2}(\boldsymbol{\mu}'_x - f(\boldsymbol{\mu}_x, \boldsymbol{\mu}_v))^T \Sigma_w^{-1}(\boldsymbol{\mu}'_x - f(\boldsymbol{\mu}_x, \boldsymbol{\mu}_v)) - \frac{1}{2} \log |\Sigma_w| \\ \log p(\boldsymbol{\mu}_v) &= -\frac{1}{2} \boldsymbol{\mu}_v^T \Sigma_v^{-1} \boldsymbol{\mu}_v - \frac{1}{2} \log |\Sigma_v|. \end{aligned} \quad (2.9)$$

This in turn allows us to write  $F$  as:

$$F(\boldsymbol{\mu}_\theta, \mathbf{y}) = \frac{1}{2} \boldsymbol{\varepsilon}_y^T \Pi_z \boldsymbol{\varepsilon}_y - \frac{1}{2} \log |\Pi_z| + \frac{1}{2} \boldsymbol{\varepsilon}_x^T \Pi_w \boldsymbol{\varepsilon}_x - \frac{1}{2} \log |\Pi_w| + \frac{1}{2} \boldsymbol{\varepsilon}_v^T \Pi_v \boldsymbol{\varepsilon}_v - \frac{1}{2} \log |\Pi_v| \quad (2.10)$$

where we have substituted the covariance matrix with the precision matrix ( $\Pi = \Sigma^{-1}$ ) and used the prediction error terms,  $\boldsymbol{\varepsilon}$ :

$$\begin{aligned} \boldsymbol{\varepsilon}_y &= \mathbf{y} - g(\boldsymbol{\mu}_x) \\ \boldsymbol{\varepsilon}_x &= \boldsymbol{\mu}'_x - f(\boldsymbol{\mu}_x, \boldsymbol{\mu}_v) \\ \boldsymbol{\varepsilon}_v &= \boldsymbol{\mu}_v \end{aligned} \quad (2.11)$$

where

$$\begin{aligned} g(\boldsymbol{\mu}_x) &= \theta_g \boldsymbol{\mu}_x \\ f(\boldsymbol{\mu}_x, \boldsymbol{\mu}_v) &= -\boldsymbol{\mu}_x + \theta_f \boldsymbol{\mu}_v. \end{aligned} \quad (2.12)$$

### 2.2.3 Recognition dynamics

Equation 2.10, Equation 2.11 and Equation 2.12 are used to specify gradient descent of  $F$ , with learning rate  $\kappa$ , which can be used to specify the recognition dynamics, namely, the temporal evolution of expectations about beliefs encoded by the brain:

$$\dot{\boldsymbol{\mu}} = \boldsymbol{\mu}' - \kappa_\mu \frac{dF(\boldsymbol{\mu}, \mathbf{y})}{d\boldsymbol{\mu}}. \quad (2.13)$$



Notably, this gradient scheme assumes that the brain encodes the dynamics of these expectations, in addition to their instantaneous value. Because of this, belief updates,  $\dot{\boldsymbol{\mu}}$ , depends on both the  $F$  gradient (second term in the equation), and the expected motion of those beliefs,  $\boldsymbol{\mu}'$ . Therefore,  $\dot{\boldsymbol{\mu}}$  and  $\boldsymbol{\mu}'$  equate only when  $F$  is minimised [69].

We can now specify the recognition dynamics for the hidden states and causes in the state space model,  $\boldsymbol{x}$ ,  $\boldsymbol{x}'$ ,  $\boldsymbol{v}$ :

$$\begin{aligned}\dot{\boldsymbol{\mu}}_x &= \boldsymbol{\mu}'_x - \kappa_x \frac{F(\boldsymbol{\mu}, \boldsymbol{y})}{d\boldsymbol{\mu}_x} \\ \dot{\boldsymbol{\mu}}'_x &= -\kappa_{x'} \frac{F(\boldsymbol{\mu}, \boldsymbol{y})}{d\boldsymbol{\mu}'_x} \\ \dot{\boldsymbol{\mu}}_v &= -\kappa_v \frac{F(\boldsymbol{\mu}, \boldsymbol{y})}{d\boldsymbol{\mu}_v}\end{aligned}\tag{2.14}$$

where the middle equation in 2.14 is the change in the expected motion of beliefs. Notice that the expected motion  $\boldsymbol{\mu}'_x$  only appears in the recognition dynamics of  $\boldsymbol{\mu}_x$ , as  $v$  does not have any dynamics, and the model does not include generalised motions of order higher than one, and thus there is no  $\boldsymbol{\mu}''_x = d\boldsymbol{\mu}'_x/dt$ .

Finally, using the definition of  $F$  in equation 2.10, we can expand the partial derivatives in Equation 2.14:

$$\begin{aligned}\frac{F(\boldsymbol{\mu}, \boldsymbol{y})}{d\boldsymbol{\mu}_x} &= \frac{1}{2} \left( \frac{d(\boldsymbol{\mu}_y - \theta_g \boldsymbol{\mu}_x)^T}{d\boldsymbol{\mu}_x} 2\Pi_z \boldsymbol{\varepsilon}_y \right) + \frac{1}{2} \left( \frac{d(\boldsymbol{\mu}_{x'} - (-\boldsymbol{\mu}_x + \theta_f \boldsymbol{\mu}_v))^T}{d\boldsymbol{\mu}_x} 2\Pi_w \boldsymbol{\varepsilon}_x \right) \\ &= -\theta_g^T \Pi_z \boldsymbol{\varepsilon}_y + \Pi_w \boldsymbol{\varepsilon}_x \\ \frac{F(\boldsymbol{\mu}, \boldsymbol{y})}{d\boldsymbol{\mu}_{x'}} &= \frac{1}{2} \left( \frac{d(\boldsymbol{\mu}_{x'} - (-\boldsymbol{\mu}_x + \theta_f \boldsymbol{\mu}_v))^T}{d\boldsymbol{\mu}_{x'}} 2\Pi_w \boldsymbol{\varepsilon}_x \right) = \Pi_w \boldsymbol{\varepsilon}_x \\ \frac{F(\boldsymbol{\mu}, \boldsymbol{y})}{d\boldsymbol{\mu}_v} &= \frac{1}{2} \left( \frac{d(\boldsymbol{\mu}_{x'} - (-\boldsymbol{\mu}_x + \theta_f \boldsymbol{\mu}_v))^T}{d\boldsymbol{\mu}_v} 2\Pi_w \boldsymbol{\varepsilon}_x \right) + \frac{1}{2} \left( \frac{d(\boldsymbol{\mu}_v)^T}{d\boldsymbol{\mu}_v} 2\Pi_v \boldsymbol{\varepsilon}_v \right) = -\theta_f^T \Pi_w \boldsymbol{\varepsilon}_x + \Pi_v \boldsymbol{\varepsilon}_v\end{aligned}\tag{2.15}$$

where we used the matrix differentiation property

$$\frac{d\boldsymbol{x}^T A \boldsymbol{x}}{d\boldsymbol{z}} = 2 \frac{d\boldsymbol{x}}{d\boldsymbol{z}} A \boldsymbol{x}\tag{2.16}$$

for symmetric  $A$ .

### 2.2.4 Action-perception cycle

In active inference, Equation 2.13, describes how a system minimises  $F$  by perceiving its environment, namely, by changing beliefs about hidden states that best explain its observations. As an alternative, a system can minimise  $F$  by changing those observations, making them comply with what it expects based on its beliefs about the world. This account of action can be specified with a gradient descent on  $F$ :

$$\begin{aligned} \dot{a} &= -\kappa_a \frac{dF(\boldsymbol{\mu}, \mathbf{y})}{da} \\ \frac{dF(\boldsymbol{\mu}, \mathbf{y})}{da} &= \frac{d\mathbf{y}}{da} \frac{dF(\boldsymbol{\mu}, \mathbf{y})}{d\mathbf{y}} \end{aligned} \tag{2.17}$$

where action  $a$  changes observations  $\mathbf{y}$  so that to minimise  $F$ . Importantly, in this formulation of active inference,  $a$  is not part of the  $m$ , and therefore does not enter the definition of  $F$ . Instead, the brain is assumed to possess an *inverse model* specifying how  $a$  (e.g., muscle contraction) modifies  $y$  (sensory input from muscle spindles). Notably, this model is hardwired at the level of peripheral reflex arcs, and realises predictions about proprioceptive states that are the end product of a cascade of belief propagation involving the whole brain hierarchy [72]. In this work, however, the cerebellar model does not use action to couple back to extra-cerebellar structures, so we do not concern ourselves with  $a$  explicitly.

## 2.3 Results

### 2.3.1 Cerebellar contribution to neuronal inference

How well the brain minimises  $F$  depends on the ability of its generative model to reflect real environmental dynamics, while making them comply with what it expects; a process also known as self-evidencing [106]. From this perspective, lesion models of the cerebellum suggest that its computations benefit behaviour by improving state estimation or inference in other brain regions, rather than performing inference processes that directly underlie perception or the production of behaviour. This can be achieved by the cerebellum via the contextualising extra-cerebellar inference, where the context for one brain region is given by the concomitant dynamics in another brain region, and *vice versa*.

Contextualisation of discrete brain dynamics is critical for proper behaviour, simply because fluent behaviour is coordinated, which implies that the underlying brain dynamics are as well. Cerebellar inference may offer a key contribution to behavioural coordination, by efficiently learning and enforcing coordinated interactions between extra-cerebellar dynamics. This contribution may be particularly relevant for the execution of habitual behaviour [185], where cognitively effortful mental processes are replaced by automated responses.

The cerebellum may therefore integrate information from extra-cerebellar regions, which can generate complex dynamics, based on simple models approximating those dynamics and their interactions. The resulting cerebellar estimates could then serve to refine and optimise those dynamics, realising the necessary coordination among discrete behavioural domains. Such cerebellar-extra-cerebellar communication implies that the cerebellum occupies a high level in the brain hierarchy, from where it could integrate and contextualise information, as illustrated in Figure 2.1. We now turn to describe the nature of the cerebellar model that might underlie behavioural coordination.

### 2.3.2 The cerebellum: internal model and neuronal dynamics

The cerebellum is characterised by a relatively simple architecture, repeated throughout its regions. This suggests that the cerebellum implements a simple and general model, capable of

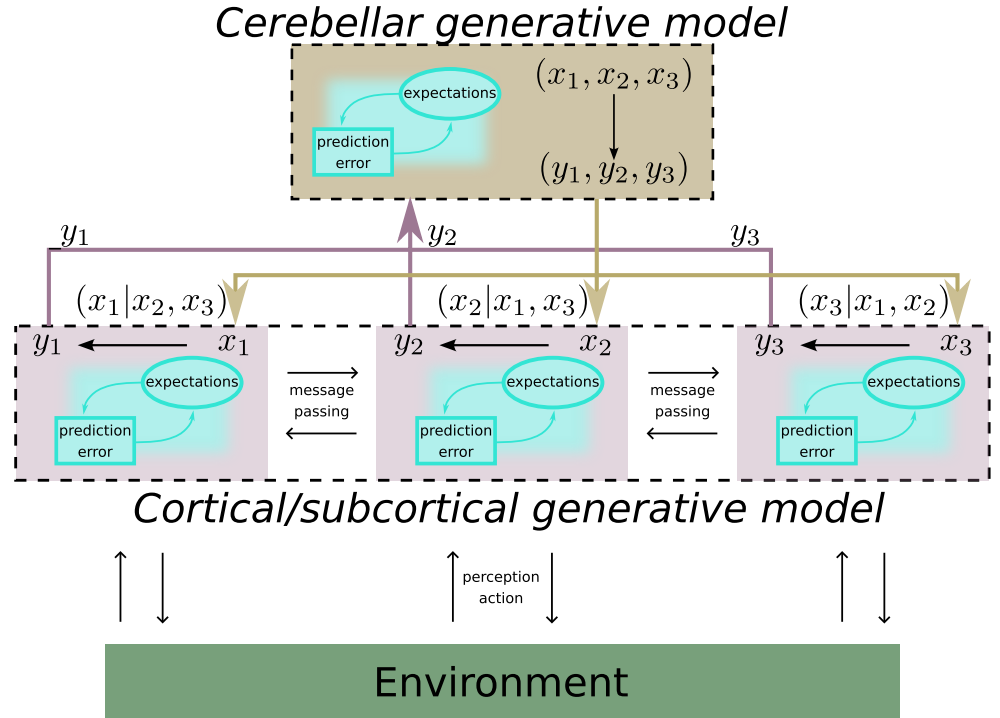


Figure 2.1: **Cerebellar and extra-cerebellar hierarchical model.** In this work, the brain is assumed to instantiate modular generative model (black arrows within pink boxes), reflecting the existence of hidden states ( $x$ 's) generating separate streams of observations ( $y$ 's). Neuronal message passing within and between (potentially hierarchical) modules drives updating of encoded expectations based on unexplained information, namely, prediction errors. At the same time, the cerebellum receives global information – the same prediction errors exchanged by extra-cerebellar structures – and integrates it based on a simple generative model that incorporates interactions between different streams of information (black line from all  $x$ 's to all  $y$ 's). Cerebellar estimates of  $x$ , conditioned on other  $x$ 's, are then returned to extra-cerebellar brain regions to realise expected coordination among  $x$ 's.

approximating different types of behavioural dynamics. In the following, we will describe the model and recognition dynamics presented in the methods, but here rehearsed in the context of cerebellar inference. Here we use a stochastic state space model, where observations  $\mathbf{y}$ , ascending from the periphery or extra-cerebellar structures, are generated by hidden states  $\mathbf{x}$  and causes  $\mathbf{v}$ . (Bold face refers to vectors.) The noise terms  $Z$ ,  $W$  and  $V$  are normally distributed with covariance  $\Sigma_z$ ,  $\Sigma_w$  and  $\Sigma_v$ . In our model,  $\mathbf{x}$  correspond to behaviourally relevant states, whereas  $\mathbf{v}$  are control or contextual states capturing interactions among hidden states. Specifically,  $\mathbf{v}$  enter

the equations of motion  $f$  of  $\mathbf{x}$ , while  $\mathbf{x}$  are mapped through  $g$  onto  $\mathbf{y}$ ;  $\mathbf{v}$  is instead unconstrained ( $\Sigma_V$  has large variance terms):

$$\begin{aligned} \mathbf{y} &= g(\mathbf{x}) + Z & Z &\sim \text{Normal}(0, \Sigma_z) \\ \frac{d\mathbf{x}}{dt} = \mathbf{x}' &= f(\mathbf{x}, \mathbf{v}) + W & W &\sim \text{Normal}(0, \Sigma_w) \\ \mathbf{v} &= V & V &\sim \text{Normal}(0, \Sigma_v) \end{aligned} \quad (2.18)$$

Because the model includes equations of motion for  $\mathbf{x}$ , the cerebellum is able to infer states' dynamics from  $\mathbf{y}$ . Moreover, the mapping  $g$  from  $\mathbf{x}$  to  $\mathbf{y}$  and equations of motion  $f$  for  $\mathbf{x}$  can be linear, in accordance with experimental findings showing linear encoding of behavioural variables [37, 38]. When considering only expected states and causes (Laplace approximation), the mapping and equations of motion can be written as:

$$\begin{aligned} g(\boldsymbol{\mu}_x) &= \theta_g \boldsymbol{\mu}_x \\ f(\boldsymbol{\mu}_x, \boldsymbol{\mu}_v) &= -\boldsymbol{\mu}_x + \theta_f \boldsymbol{\mu}_v \end{aligned} \quad (2.19)$$

These equations specify the *implicit* cerebellar generative model, whose inversion equations, namely the equations describing the inference of  $\boldsymbol{\mu}_x$  and  $\boldsymbol{\mu}_v$  from  $\mathbf{y}$ , can be associated with neuronal dynamics. In particular, inference is about expected values that best explain observations:

$$\dot{\boldsymbol{\mu}}_x = \boldsymbol{\mu}'_x + \kappa_x (\theta_g^T \Pi_z \boldsymbol{\varepsilon}_y - \Pi_w \boldsymbol{\varepsilon}_x) \quad (2.20a)$$

$$\dot{\boldsymbol{\mu}}'_x = -\kappa_{x'} \Pi_w \boldsymbol{\varepsilon}_x \quad (2.20b)$$

$$\dot{\boldsymbol{\mu}}_v = \kappa_v (\theta_f^T \Pi_w \boldsymbol{\varepsilon}_x - \Pi_v \boldsymbol{\varepsilon}_v) \quad (2.20c)$$

where the  $\kappa$ 's and  $\boldsymbol{\varepsilon}$ 's correspond to learning rates and prediction errors, respectively:

$$\begin{aligned} \boldsymbol{\varepsilon}_y &= \mathbf{y} - g(\boldsymbol{\mu}_x) \\ \boldsymbol{\varepsilon}_x &= \boldsymbol{\mu}'_x - f(\boldsymbol{\mu}_x, \boldsymbol{\mu}_v) \\ \boldsymbol{\varepsilon}_v &= \boldsymbol{\mu}_v. \end{aligned} \quad (2.21)$$

All variables and parameters in Equation 2.20 and Equation 2.21 can be mapped onto element of the cerebellar circuitry (see Fig 2.2). In particular,  $\mathbf{y}$  and  $\mathbf{v}$  can be associated with mossy fibre and Purkinje cell population activity, respectively, while both hidden states  $\boldsymbol{\mu}_x$  and velocities  $\boldsymbol{\mu}_{x'}$  are represented by the granule cell population activity, meaning that granule cell encode the trajectory of hidden states, similarly to the coefficients of a Taylor expansion. This temporal encoding is specified in Equation (2.20a), in which  $\dot{\boldsymbol{\mu}}_x$ , changes in expected values of hidden states, are a function of the expected velocity,  $\boldsymbol{\mu}_{x'}$ . In the biophysical network, this relationship is determined by the effects on current state estimation of the recent neuronal history [97, 214]. Notably,  $\dot{\boldsymbol{\mu}}_x$  is also dependent of prediction error terms  $\theta_g^T \Pi_z \boldsymbol{\varepsilon}_y$  and  $\Pi_w \boldsymbol{\varepsilon}_x$ .

The term  $\theta_g^T \Pi_z \boldsymbol{\varepsilon}_y$  corresponds to the unexplained information originating from the comparison between observations  $\mathbf{y}$ , carried by mossy fibre, and predictions  $g(\boldsymbol{\mu}_x)$ , carried by Golgi cell feedback inhibition. This comparison occurs in the glomeruli, which contain dendrites and axonal terminals from granule cells, Golgi cells and mossy fibre, and whose connectivity with granule cells is captured by  $\theta_g^T$ . Additionally,  $\boldsymbol{\varepsilon}_y$  is weighted by the precision matrix  $\theta_g^T \Pi_z$  implemented by Golgi cell inhibition [174], which controls the response of the network to mossy fibre excitatory drive based on the precision of incoming information.

On the other hand,  $\Pi_w \boldsymbol{\varepsilon}_x$  is associated with feedback from Purkinje cell activity, encoding  $\boldsymbol{\mu}_v$ . This feedback can be both direct and indirect: in the first case implemented by **Pjc** modulation of cerebellar cortical interneurons [237] and **grc** [93]; in the second case implemented through recurrent inputs from cerebellar nuclei (**cn**) [110, 3], whose activity is a function of both mossy fibre collaterals and Purkinje cell inhibition.

Next, Equation 2.20b describes changes in the encoded velocities,  $\dot{\boldsymbol{\mu}}_{x'}$ : these changes are driven by the prediction error term  $\boldsymbol{\varepsilon}_x$ , incorporating predictions  $f$  that, in absence of mossy fibre input, sparsify granule cell activity, by attracting  $\boldsymbol{\mu}_x$  toward zero. Notably, as in the case of  $\dot{\boldsymbol{\mu}}_x$ ,  $\dot{\boldsymbol{\mu}}_{x'}$  depends on  $\boldsymbol{\mu}_v$  via  $f$ , and therefore relies on the same feedback mechanisms involving Purkinje cells and cerebellar nuclei.

The last step of information processing in the cerebellar cortex involves  $\boldsymbol{\mu}_v$  (Purkinje cell activity), whose dynamics are described by  $\dot{\boldsymbol{\mu}}_v$ , Equation. 2.20c. Updates are dictated by  $\boldsymbol{\mu}_x$  and  $\boldsymbol{\mu}_{x'}$ , entering  $\boldsymbol{\varepsilon}_x$  via  $f$ , the parallel fibre connectivity matrix defined by  $\theta_f^T$ , which in our model is the connectivity matrix encoding cerebellar expectations about interactions among  $x$ 's.

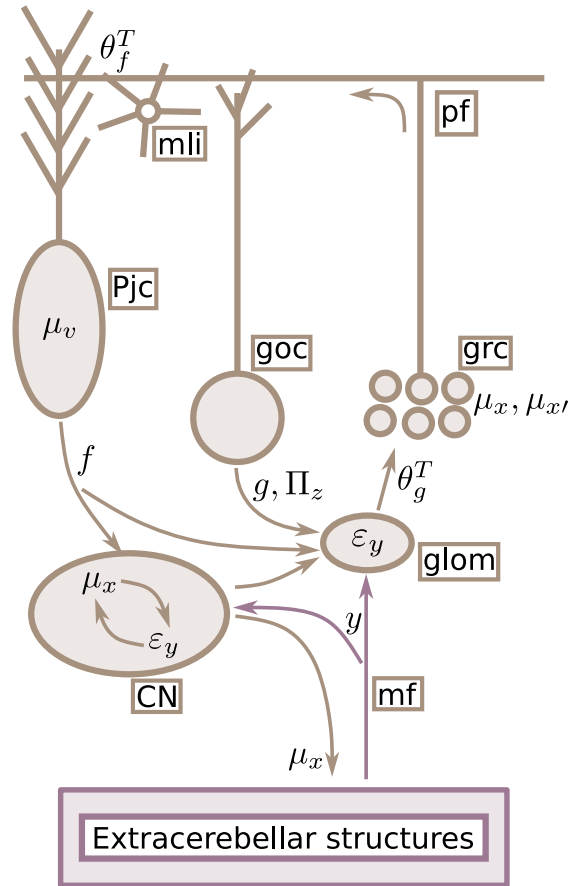


Figure 2.2: **Mapping elements of the model to cerebellar circuitry.** Neuronal elements are distinguished from elements of the model by brown boxes. Mossy fibres carry information  $y$  from extra-cerebellar structures to both cerebellar nuclei and the cerebellar cortex, driving prediction errors  $\epsilon_y$  within them. In the cortex,  $\epsilon_y$  can be associated to the excitation-inhibition balance within glomeruli, which drives Golgi cell and granule cell activity, while being set by Golgi cells, cerebellar nuclei and Purkinje cell feedback activity. Computationally, this feedback consists in predictions generated by the mapping  $g$  (from Golgi cells) and equations of motion  $f$  (from cerebellar nuclei and Purkinje cells), and aims at minimising prediction errors  $\epsilon_y$ . At the same time, Golgi cells also control the precision  $\Pi_z$  of prediction errors. Residual  $\epsilon_y$  are carried by parallel fibres to the molecular layer, where they drive molecular layer interneuron and Purkinje cell activity, encoding  $\mu_v$ , based on the connectivity matrix  $\theta_f^T$ . This connectivity matrix encodes learned expectations about hidden states' interactions, and biases  $\mu_x$  through (direct and indirect) feedback connections. Hidden states  $\mu_x$  are also encoded by cerebellar nuclei, whose extra-cerebellar projections carry cerebellar state estimates to extra-cerebellar structures, where they constrain inference therein. Mossy fibres **mf**; Purkinje cells **Pjc**; granule cells **grc**; Golgi cells **Goc**; glomeruli **glom**; cerebellar nuclei **cn**; molecular layer interneurons **mli**.

Finally, the cerebellum couples back to extra-cerebellar regions via cerebellar nuclei, whose activity replicates the encoding of  $\mu_x$ , as they are assumed to receive the same information as the cerebellar cortex via mossy fibre collaterals.

### 2.3.3 Simulation of motor coordination

I now describe the results of two sets of simulations showcasing the contribution of cerebellar state estimation to motor coordination. This coordination relies on expectations held by the cerebellum about interactions between different behavioural dynamics. A plausible mechanism through which these expectations may be acquired and encoded is synaptic plasticity at the level of the parallel fibre connectivity matrix ( $\theta_g^T$ ), as shown in studies of behavioural conditioning [40] and adaptation during eye movements [242]. Through these expectations, the cerebellum is then able to provide extra-cerebellar structures with top-down empirical prior or constraints promoting coordination.

In particular, the first set of simulations is concerned with the synchronisation of whisking and respiration in mice, for which the cerebellum has been found to be important [191] (Figure 2.3). This synchronisation is a key aspect of rodent’s behaviour, as it underwrites functions such as exploration of the environment, as well as the coordination of many other motor domains, such as locomotion, eye movements and head positioning [65, 138, 232, 15]. The dynamics of these behaviours is the result of an intricate network of brain structures, encompassing among others brainstem pattern generators and premotor cortical areas, all of which are modulated by cerebellar outputs [9, 14, 191, 216, 90].

These simulations start from the specification of a cerebellar generative model and a generative process, the latter encoded by extra-cerebellar regions (e.g., central pattern generators) driving dynamics of whisking and respiration. Importantly, extra-cerebellar regions also reflect an inference process, in this case concerned with latent states (e.g. amplitude and phase) associated with whisking and inspiration-respiration cycles. According to active inference, extra-cerebellar inference drives motor behaviour, by generating proprioceptive predictions that are realised at the level of motor reflex arcs [72]; however, in this work we do not explicitly simulate extra-cerebellar inference, but approximate it with a stochastic process. Therefore, by acting on the



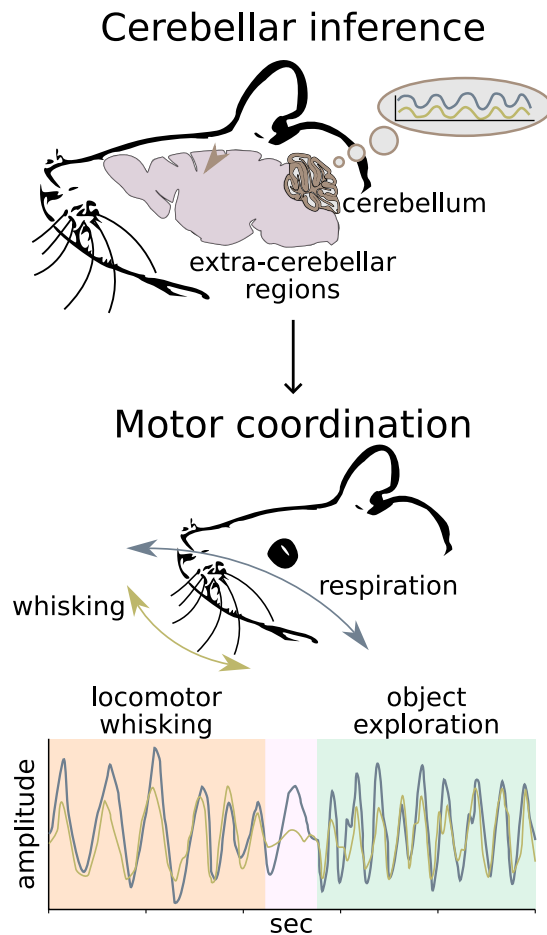


Figure 2.3: **Whisker-respiration coordination.** The cerebellum is engaged in an inference process that involves reciprocal message passing with extra-cerebellar structures (violet-brown cycle). With experience, the cerebellum learns to expect how brain dynamics interact or coordinate with each others, and efficiently generates estimates that incorporate these expectations. In the context of whisking (gold line) and respiration (grey line), cerebellar estimates constraint their dynamics to evolve in synchrony. This contextualisation can be adapted to different behavioural regimes, here exemplified by a regime of locomotor whisking, with low whisking and respiration rates (orange background), and a regime of object exploration, with high whisking and respiration rates (green background), separated by a brief period with no whisking (pink background).

generative process, the cerebellum implicitly controls whisking and respiratory behaviour.

The generative process consists in a Kuramoto system, whose output variables  $w$  and  $r$  can

be associated respectively with the somatic states of whisker position and expansion of the rib cage. The Kuramoto model specifies the whisker and respiration phases:

$$\begin{aligned} r &= \sin \phi_r \\ w &= \alpha \sin \phi_w. \end{aligned} \tag{2.22}$$

whose rate of change is set by intrinsic angular velocities,  $\omega_w$  and  $\omega_r$ , and perturbed by independent Gaussian noise  $Q_w$  and  $Q_r$  and offset  $\omega_0$ . On the other hand, the  $\alpha$ ,  $\omega_w$  and  $\omega_r$  terms are state dependent, and are changed throughout the simulation time in order to stop or restart whisking, by setting  $\alpha$  to 0 or 1, and to increase or decrease the frequency of whisking and respiration, by modifying  $\omega_w$  and  $\omega_r$ :

$$\begin{aligned} \frac{d\phi_w}{dt} &= \omega_w + k \sin(x_w - \phi_w) + Q_w & Q_w &\sim \text{Normal}(0, \sigma_w) \\ \frac{d\phi_r}{dt} &= \omega_r + k \sin(x_r - \phi_r) + Q_r & Q_r &\sim \text{Normal}(0, \sigma_r) \\ \omega_r &= \omega_w + \omega_0. \end{aligned} \tag{2.23}$$

The choice of using the Kuramoto system is due to the fact that it incorporates a coupling term, which in standard formulations couples the sine of two or more oscillators. In the present work, instead, these terms,  $k \sin(x_w - \phi_w)$  and  $k \sin(x_r - \phi_r)$ , couple the phase of whisking and respiration to the corresponding cerebellar hidden states,  $x_w$  and  $x_r$ ; that is, there is no explicit or direct coupling between the two oscillators other than that afforded by cerebellar expectations about how  $x_w$  and  $x_r$  interact with each others. This coupling is therefore dependent on the cerebellar generative model, which takes the same form of the state space model in Equation 2.18:

$$\begin{aligned} \mathbf{y} &= g(\mathbf{x}) + Z & Z &\sim \text{Normal}(0, \Sigma_z) \\ \frac{d\mathbf{x}}{dt} &= \mathbf{x}' = f(\mathbf{x}, \mathbf{v}) + W & W &\sim \text{Normal}(0, \Sigma_w) \\ \mathbf{v} &= V & V &\sim \text{Normal}(0, \Sigma_v). \end{aligned} \tag{2.24}$$

where  $\mathbf{y}$ ,  $\mathbf{x}$  and  $\mathbf{v}$  are now associated with whisking and respiration somatic states:

$$\mathbf{y} = \begin{bmatrix} w \\ r \end{bmatrix}, \quad \mathbf{x} = \begin{bmatrix} x_w \\ x_r \end{bmatrix}, \quad \mathbf{v} = \begin{bmatrix} v_w \\ v_r \end{bmatrix}. \quad (2.25)$$

The cerebellar generative model recapitulates inference in extra-cerebellar regions. Thus, observations  $\mathbf{y}$  are associated with peripheral input engendered from the dynamics of somatic states  $w$  and  $r$  returned by the generative process. In the cerebellum,  $\mathbf{y}$  is predicted from the mapping  $g$  involving hidden states  $x_w$  and  $x_r$ . These hidden states represent somatic states  $w$  and  $r$ , and have dynamics controlled by hidden causes  $v_w$  and  $v_r$ , whose estimates are biased by expectations about hidden states' interactions, encoded in the parallel fibre connectivity matrix  $\theta_f$ :

$$\begin{aligned} g(\mathbf{x}) &= \theta_g \mathbf{x} & \theta_g &= \begin{bmatrix} 1 & 0 \\ 0 & 1 \end{bmatrix} \\ f(\mathbf{x}, \mathbf{v}) &= -\mathbf{x} + \theta_f \mathbf{v} & \theta_f &= \begin{bmatrix} 1 & 1 \\ 1 & 1 \end{bmatrix}. \end{aligned} \quad (2.26)$$

In the present model, learning the connectivity matrix  $\theta_f$  is a prerequisite for the cerebellar state estimation to drive fluent and coordinated behaviour; this step is critical, and presumably relies on the continuous adaptation of the parallel fibre connectivity matrix based on climbing fibre input.

From Equation 2.24, Equation 2.25 and Equation 2.26, one can then specify the inversion dynamics (Equation 2.20 and Equation 2.21) that are associate with (average) neuronal dynamics in the cerebellum.

Please notice the difference between the generative process and model: both describe how the same somatic states related to whisking and respiration evolve over time, but the way they describe these dynamics is different. Extra-cerebellar structures implement a nonlinear (Kuramoto) model to describe those dynamics, whereas the cerebellum uses a linear description, in line with its simple architecture and linear encoding of behaviourally relevant variables [37, 109, 190]. Therefore, the cerebellum is able to synthesize extra-cerebellar dynamics and, importantly, their interactions, with a simpler model. This approximation works because the cerebellum infers

the context and not the content of behaviour, and may underlie the cerebellar role in finessing behaviour and reducing its cognitive load during habitual behaviour [185].

The results of the simulation are shown in Fig 2.4, Fig 2.5 and Fig 2.6, one for each simulation condition used (explained below). In all three cases, whisking and respiration have dynamics which change based on the behavioural state of the *in silico* mouse, which is done to exemplify cerebellar-dependent coordination in different regimes of behaviour. These states consist in a period of locomotor whisking, during which the animal displays low rates of whisking and respiration, an intermediate period with whisking amplitude decaying to 0, and a final period of object exploration, during which whisking and respiration have high basal rates.

For all three figures (Fig 2.4, Fig 2.5 and Fig 2.6), the top half shows the output of the generative (extra-cerebellar) process in simulations where the cerebellum holds expectations about whisking-respiration coordination, encoded by an all-one  $\theta_f$  matrix (see Equation 2.25); this condition is labeled ‘With cerebellar contextualisation’. The bottom half shows instead the output of the generative process when  $\theta_f$  is a diagonal matrix, that is, the cerebellum does not expect interactions between whisking and respiration; this condition is labeled ‘Without cerebellar contextualisation’.

Each of the three figures is associated with a different simulation condition. In Fig 2.4, whisking and respiration oscillatory rates have offset  $\omega_0 \neq 0$ ; in Fig 2.5, the two variables have the same intrinsic velocity, but evolution of their phase is subject to independent Gaussian noise; in Fig 2.6, there is neither offset nor noise, but an external perturbation is applied to whisker dynamics, abruptly changing its phase.

The level of behavioural synchronisation in all figures is displayed in three ways. The left panels show the amplitude or displacement from a reference or resting point of  $w$  and  $r$  in the time domain. The middle panels show the time evolution of the  $w$  and  $r$  difference. The right panels show whisking and respiration variables in their joint state space, together with the synchronisation manifold (dotted black line).

In all cases, when the cerebellum expects synchronised dynamics between whisking and respiration, it is able to overcome chaotic forces, and realises behavioural coordination. This is because cerebellar estimates, biased towards synchrony, enter the coupling terms in the generative process,  $k \sin(x_w - \phi_w)$  and  $k \sin(x_r - \phi_r)$ , where they act as constraints for  $w$  and  $r$

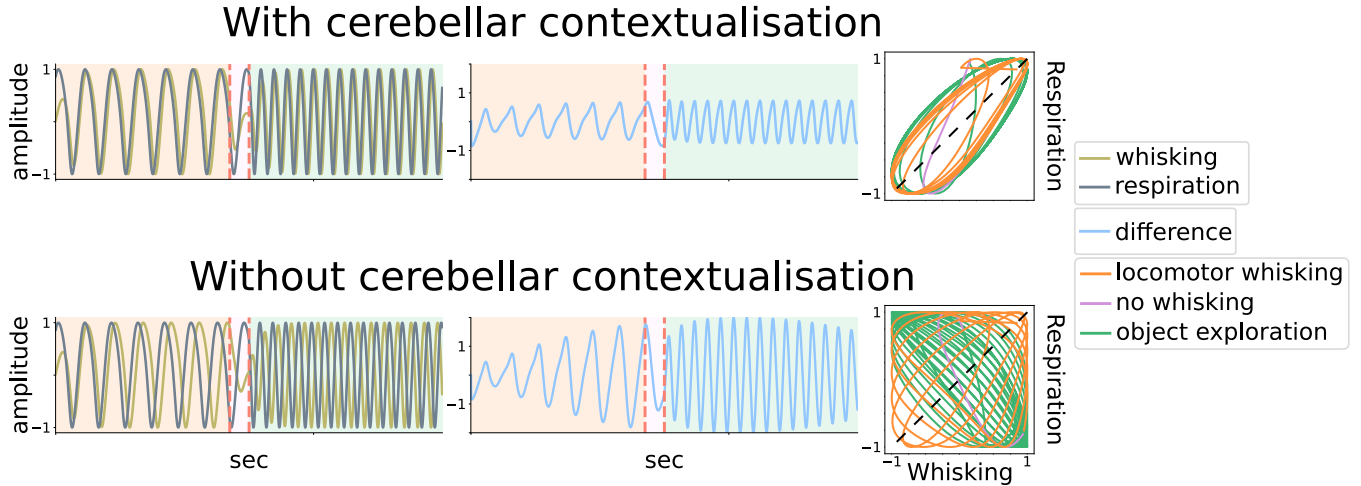


Figure 2.4: **Cerebellar contribution to whisking-respiration coordination (1)** In these simulations, whisking and respiration oscillatory rates have offset  $\omega_0 \neq 0$ . Vertical dotted red lines demark the transition from one behavioural state (i.e. fast, slow whisking/breathing and no whisking) to another. Top half (‘With cerebellar contextualisation’): the cerebellum is endowed with expectations about whisking-respiration coordination, and consequently it is able to realise these expectations – despite offset  $\omega_0$  – by biasing extra-cerebellar states (whisking  $w$  and respiration  $r$ ) accordingly. This coordination is shown in the left panel, displaying the evolution of the two variables over time; in the middle panel, displaying the evolution of their difference; and in the right panel, displaying their evolution in the joint state-space (straight line corresponds to synchronisation manifold). In this and other figures, behavioural modes, namely, locomotion, object exploration and intermediate state, are color-coded using orange, green and pink for the background (left and middle panel) or lines (right panel). Bottom half (‘Without cerebellar contextualisation’): now the cerebellum has no prior beliefs that whisking and respiration should evolve jointly. As such the two variables (left) and their difference (middle) diverge over time, while circulating far from the synchronisation line in state-space (right).

phase dynamics. On the other hand, with a naïf cerebellum (i.e., no expectations in place), these constraints are effectively absent, because cerebellar estimates limit themselves to follow desynchronised dynamics. The bias on cerebellar state estimation can be better appreciated by comparing inference in the presence or absence of cn outputs, namely, when the cerebellum can or cannot realise expected synchrony (Fig. 2.7).

As a second example – dealing with whole-body dynamics – we simulate the coordination of limbs and tail during locomotion. Locomotion relies on coordination between many body parts,

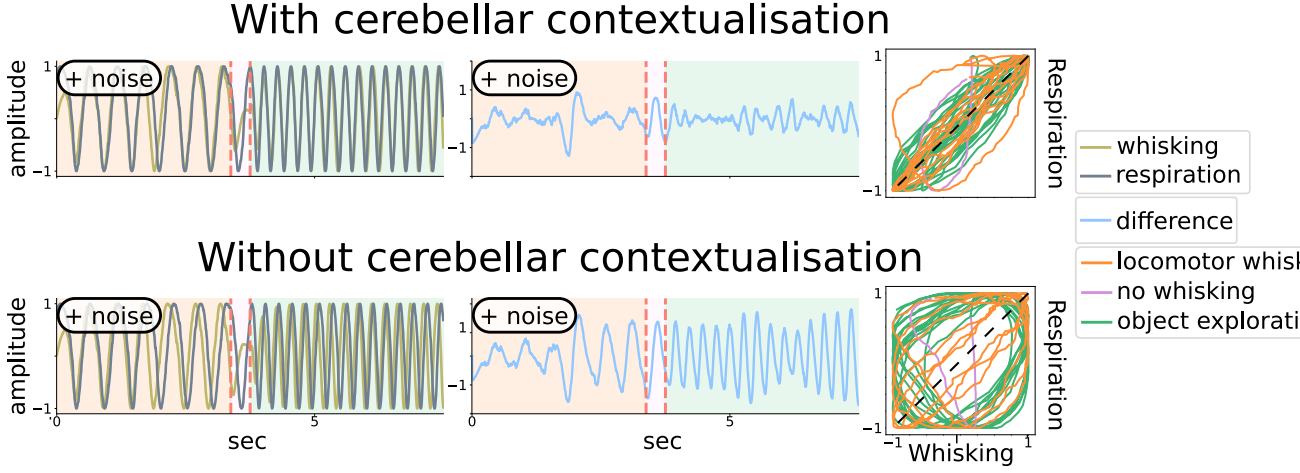


Figure 2.5: **Cerebellar contribution to whisking-respiration coordination (2)**. The figure layout is the same as for Fig 2.4, but now whisking and respiration have (same) angular velocities that are perturbed by independent Gaussian noise. Again, the presence or absence of cerebellar expectations about behavioural synchrony determines whether whisking and respiration stay coupled (top) or not (bottom).

which in turn depends on an intact cerebellar cortex [151]: in mutant mice with a cerebellar deficit, for instance, pairwise coordination of front and hind limbs on opposite sides is lost, together with symmetric tail dynamics. Here, we model extra-cerebellar neuronal dynamics driving the vertical movement of limbs during the stride cycle:

$$\begin{aligned}
 l_{fr} &= \sin \phi_{fr} \\
 l_{fl} &= \sin \phi_{fl} \\
 l_{hr} &= \sin \phi_{hr} \\
 l_{hl} &= \sin \phi_{hl}.
 \end{aligned}
 \tag{2.27}$$

The displacement of the front right ( $l_{fr}$ ), front left ( $l_{fl}$ ), hind right ( $l_{hr}$ ) and hind left ( $l_{hl}$ ) limbs are mapped from their phase  $\phi$  in the stride cycle, whose joint dynamics are described by a

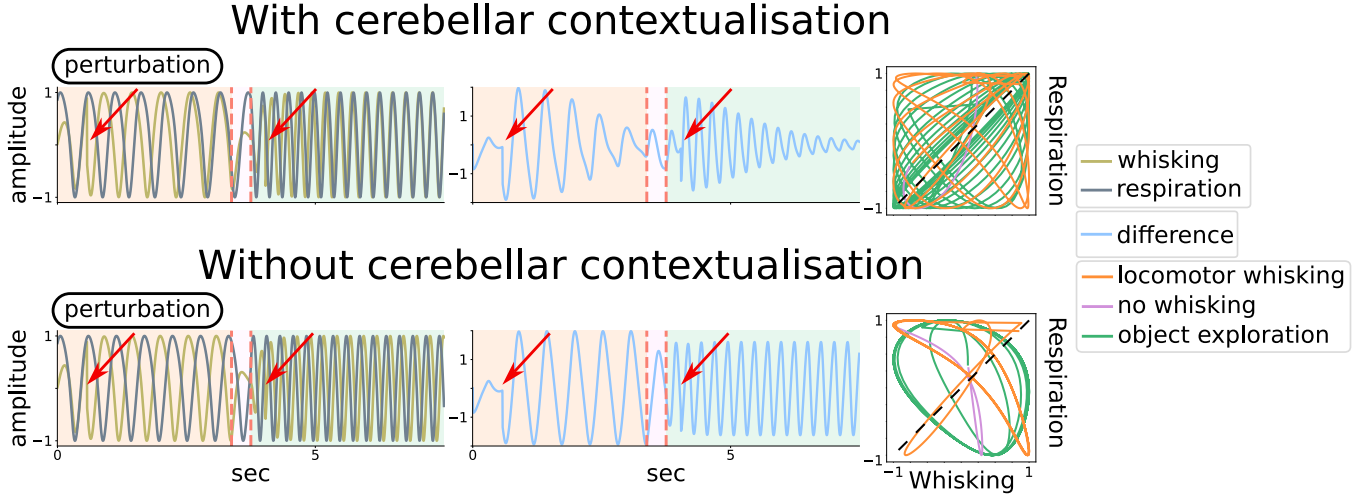


Figure 2.6: **Cerebellar contribution to whisking-respiration coordination (3)**. Same layout as for Fig 2.4 and Fig 2.5, but now the perturbation is external, applied to the whisker system at two distinct time points of the simulation (indicated by red arrows). With cerebellar expectations in place, the two oscillators return synchronised (top); this does not happen in the case of a naïve cerebellar model (bottom).

Kuramoto system, including cerebellar estimates  $x$  about limb position:

$$\begin{aligned}
 \frac{d\phi_{fr}}{dt} &= \omega + k_1 \sin(x_{fr} - \phi_{fr}) + Q_{fr} & Q_{fr} &\sim \text{Normal}(0, \sigma_{fr}) \\
 \frac{d\phi_{fl}}{dt} &= \omega + k_1 \sin(\phi_{fr} - \phi_{fl}) + k_2 \sin(x_{fl} - \phi_{fl}) + Q_{fl} & Q_{fl} &\sim \text{Normal}(0, \sigma_{fl}) \\
 \frac{d\phi_{hr}}{dt} &= \omega + k_1 \sin(\phi_{fr} - \phi_{hr}) + k_2 \sin(x_{hr} - \phi_{hr}) + Q_{hr} & Q_{hr} &\sim \text{Normal}(0, \sigma_{hr}) \\
 \frac{d\phi_{hl}}{dt} &= \omega + k_1 \sin(\phi_{fr} - \phi_{hl}) + k_2 \sin(x_{hl} - \phi_{hl}) + Q_{hl} & Q_{hl} &\sim \text{Normal}(0, \sigma_{hl})
 \end{aligned} \tag{2.28}$$

The generative process imposes a phase shift of  $\pi$ ,  $\frac{3}{2}\pi$  and  $\frac{1}{2}\pi$  to  $l_{fl}$ ,  $l_{hr}$  and  $l_{hl}$  compared to the  $l_{fr}$ , through the coupling terms  $k_2 \sin(\phi_{hr} - \phi)$ . This bias maximises the time during which at least one paw is touching the ground, and characterises locomotion in absence of cerebellar contributions to whole-body coordination in mice; individual limb dynamics, in contrast, are indistinguishable from those described in healthy animals [151] (Fig 2.8, right).

On the other hand, when cerebellar compensatory input,  $k_1 \sin(x - \phi)$ , are present,  $l_{fr}$  and

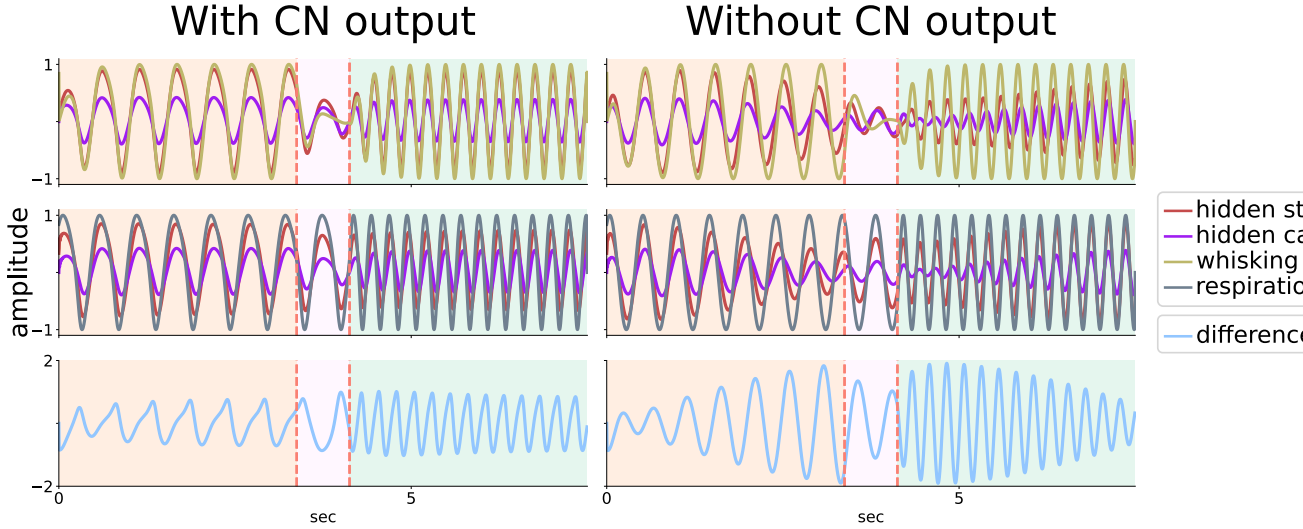


Figure 2.7: **Cerebellar state estimation.** This figure displays the time evolution of variables in the generative model and process related to whisking (top panels) and respiration (middle panels), as well as the difference of somatic states  $w$  and  $r$  (bottom panels). The simulation condition is the same as in Fig. 2.4, where respiration oscillates faster than whisking (offset  $\omega_0 \neq 0$ ). Left: simulations when the cerebellum expects synchronisation and can couple back to extra-cerebellar structures to constrain dynamics therein. In this case, hidden states  $x_w$  and  $x_r$  (red lines) closely match real states  $w$  (gold lines) and  $r$  (grey lines), as the latter are constrained by the former. Also, hidden causes  $v_w$  and  $v_r$  (purple lines) are regular and relatively high in amplitude, reflecting constant synchrony between  $w$  and  $r$ . Right: the cerebellum expects synchrony, but cannot realise it because the output from cerebellar nuclei is turned off. In this case, the cerebellum can only estimate whisking- and respiration-related variables without affecting these behaviours; consequently, the more  $w$  and  $r$  desynchronise, the smaller the amplitude of estimated hidden states and causes. This occurs because of the friction between what the cerebellum observes and what it expects.

$l_{hl}$  are phase-locked, as do  $l_{fl}$  and  $l_{hr}$ , and the two pairs are anti-correlated (Fig 2.8, left). Compensatory input from the cerebellum rest on a generative model (a state space model as in equation 2.7) that holds expectations about inter-limb coordination in the **pp** connectivity



matrix  $\theta_f$ :

$$\begin{aligned}
 g(\mathbf{x}) &= \theta_g \mathbf{x} & \theta_g &= \begin{bmatrix} 1 & 0 & 0 & 0 \\ 0 & 1 & 0 & 0 \\ 0 & 0 & 1 & 0 \\ 0 & 0 & 0 & 1 \end{bmatrix} \\
 f(\mathbf{x}, \mathbf{v}) &= -\mathbf{x} + \theta_f \mathbf{v} & \theta_f &= \begin{bmatrix} 1 & -1 & -1 & 1 \\ -1 & 1 & 1 & -1 \\ -1 & 1 & 1 & -1 \\ 1 & -1 & -1 & 1 \end{bmatrix}.
 \end{aligned} \tag{2.29}$$

where

$$\mathbf{x} = \begin{bmatrix} x_{fr} \\ x_{fl} \\ x_{hr} \\ x_{hl} \end{bmatrix}, \quad \mathbf{v} = \begin{bmatrix} v_{fr} \\ v_{fl} \\ v_{hr} \\ v_{hl} \end{bmatrix}. \tag{2.30}$$

Finally, tail movements can be modelled as a passive consequence of limb dynamics [151]:

$$t = \sin \phi_{fr} + \sin \phi_{fl} \tag{2.31}$$

Notably, in the presence of cerebellar coordination, tail excursions on the vertical axis ( $t$ ) are symmetric with respect to the dynamics of the two pairs of limbs (Fig 2.8), which may improve balance and movement efficiency. Conversely, this symmetry is disrupted in the absence of cerebellar input. In other words, in our model, optimal tail movement during locomotion emerges from the cerebellar control and correction of limb dynamics.

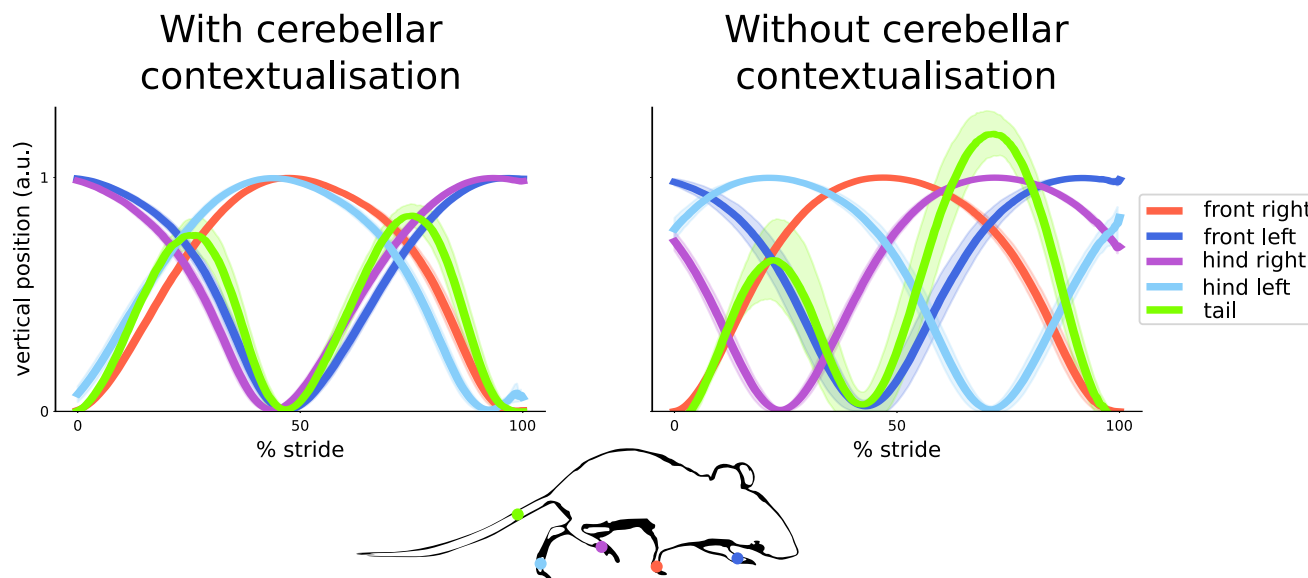


Figure 2.8: [Cerebellar-dependent coordination of limb and tail movements during locomotion] **Cerebellar-dependent coordination of limb and tail movements during locomotion.** Left ('With cerebellar contextualisation'): average vertical displacement of the front right, front left, hind right and hind left limbs as well as of the tail during locomotion across 14 strides. Shaded area denotes the standard deviation. In the presence of cerebellar expectations of inter-limb coordination, the front right and front left limbs are phase locked with the hind left and hind right limbs, respectively, and the two pairs of limbs have opposite phase. This results in the pairwise coordination of limb vertical displacement. At the same time, tail movements, which are modelled as a passive consequence of limb dynamics, symmetrically follows the dynamics of the two pairs of limbs. Right ('Without cerebellar contextualisation'): in the absence of cerebellar control of limb dynamics there is no front-hind limb coordination, as each limb moves out of phase compared to the others, and tail movements become asymmetric.

## 2.4 Discussion

In this work we presented a theoretical treatment of cerebellar computations that addresses its pervasive involvement in behaviour. In particular, we proposed that the key function of the cerebellum is to contextualise behavioural domains, which leads to fluent, coordinated behaviour. The main idea is that the cerebellum contributes to the coordination of discrete behavioural domains by estimating how variables interact with each other. This means that the cerebellar model is concerned with the inference of the time-varying context wherein the dynamics of multiple behavioural variables unfold, and uses the context to constrain these dynamics. Notably, the context is set by all variables that contribute to behaviour at any given time, such as sensory or reward cues informing action execution, motor activity informing predictions about sensory consequences, or the dynamics of one motor system constraining the dynamics of other modalities. The proposed cerebellar-dependent contextualisation of behavioural domains may therefore provide a theoretical ground to empirical findings highlighting the importance of an intact cerebellum for seamless, resilient to perturbations, coordinated behaviour [151, 152].

The present account of cerebellar functions is congruent with the fact that the cerebellum integrates and reciprocates information from most brain regions [208, 209, 111, 34, 113, 227], and that its modular and homogeneous architecture supports a simple neuronal code, fit to efficiently learn and infer associations and reciprocal interactions among sensorimotor states [153, 2, 120]. Accordingly, cerebellar state estimation reflects learned relationships among these variables, and constrains extra-cerebellar dynamics with timed state estimates that are conditioned on other states (Fig 2.1).

The cerebellar-dependent coordination of behaviour may provide a key benefit to computations in other brain regions in terms of efficiency and cognitive load. This is because the cerebellar architecture and neuronal organisation is relatively simple and stereotypical, which in turn hints at a simple cerebellar generative model, underlying linear or weakly nonlinear inference dynamics. As such, cerebellar state estimation, guiding inference in other brain regions through contextual priors, may be critical to finesse and simplify extra-cerebellar computations, especially during habitual, stereotypical behaviours [185].

In practice, our cerebellar model complies with the FEP, a theory of self-organisation used to

explain dynamics of biological systems from first physics principles [71, 79]. Applying the FEP to the brain means that neuronal dynamics can be read as inversion (inferential) dynamics based on a generative model of how observations are generated by hidden (both external or somatic) states in the environment. This in turn contrasts with other theories of the cerebellum, such as adaptive filter models, which also rely on the minimisation of an objective function, but treat the cerebellum as a function approximator, rather than a generative model.

The FEP offers therefore a formal connection linking cerebellar neuronal dynamics and network [4] with internal probabilistic models [239, 120]. In particular, here we have characterised cerebellar computations in terms of Bayesian filtering based on a state space model, in accordance with theories of the cerebellum as a state estimator or Kalman filter [180, 158, 217]. From this perspective, then, the cerebellum may optimise extra-cerebellar dynamics by increasing the efficiency with which they destroy  $F$  gradients (i.e., minimise prediction errors).

To illustrate these ideas, we used a paradigmatic example of behavioural coordination, namely, whisking-respiration phase synchrony in rodents [48], as well as limb and tail coordination during locomotion [151]. In the present simulations, the cerebellar model infers control states enforcing synchrony between these two variables, by constraining extra-cerebellar regions driving behavioural dynamics (Fig. 2.3). Notably, this coordination is dependent on the cerebellar generative model, and in particular on its (previously learned) expectations about whisking-respiration synchrony encoded in the parallel fibre connectivity matrix.

The proposed cerebellar model (Fig 2.2) expresses average patterns of connectivity and neuronal activity in the cerebellum, and is able to explain some important features of this brain structure. First, because the underlying generative model is dynamic, neuronal activity (e.g. in **grc** and **Pjc**) encodes state trajectories: this may explain the coexistence of past and future information encoded in the population activity in the cerebellar cortex [182], and could afford higher temporal precision compared to a neuronal code restricted to represent the instantaneous value of states.

A second important feature of the model is its linearity, reflecting empirical findings of linear encoding of many task-related variables [37, 109, 190]. However, some forms of nonlinear inference are still easily implementable in this model in a biologically plausible manner [17], which may be used in some regions of the cerebellum to deal with temporal offsets in interactions among

variables, such as in the case of delays in classical conditioning paradigms [221, 61].

A third point relates to recurrent and feedback loops within the cerebellar circuitry. This aspect is often neglected by conventional theories, but is becoming more and more prominent, as highlighted by evidence of feedback loops from Purkinje cells and cerebellar nuclei back to granule cells, Golgi cells and other interneurons [139, 52, 110, 3, 237, 93]. Notably, this recurrent internal connectivity is accounted for by the inversion dynamics described here (Eq. 2.20), despite the simplicity of the model used.

On a last note, many lines of study emphasise the probabilistic nature of models encoded by or instantiated in the brain [135, 150, 59, 87]. This is a key aspect for inference processes in the brain, as they need to take in account uncertainty. In the cerebellum, this account may underlie for example the Golgi cell-dependent control of the excitation-inhibition balance in the granule cell population, reflecting the precision or relevance of incoming extra-cerebellar input [174]. This control might be carefully modulated through various mechanisms (e.g., neuromodulation), and in the present model is encoded by the precision matrix  $\Pi_z$  (Equation. 2.20), setting the magnitude of state estimate updates.

Changes in the precision matrix  $\Pi_z$  can have a strong impact on cerebellar state estimation in our model, as they affect the magnitude of prediction errors driving inference. Accordingly, future research should aim at test whether changes in cerebellar computations, resulting from manipulation of Golgi cell-dependent inhibition, are congruent with a change in precision-weighting mechanisms of mossy fibre input. At the same time, it would be interesting to compare these results with those obtained from manipulations of molecular layer interneurons: in our model, these interneurons enable mossy fibre input to bidirectionally impact Purkinje cell activity, via  $\theta_f^T$ ; however, molecular layer interneurons could also control the magnitude of the updates of hidden causes,  $v$ , by setting  $\Pi_w$ . Thus, precision-weighting of ascending input could occur at various levels of the cerebellar cortex hierarchy.

The present model can also be extended significantly in different directions. First, here we have used a minimal model, comprising two idealised oscillators, to showcase cerebellar-dependent coordination of behaviour. However, more realistic simulations are possible, which may include other relevant motor modalities like locomotion, head movement control, or licking [138, 157, 91]. Moreover, the simulation may be expanded to other task conditions, including

perceptual tasks [12] or decision making [86, 50, 200].

Second, a crucial improvement could involve the model itself. In particular, it would be important to include the olivary-climbing fibre system as a second source of input to the cerebellum, paralleling the mossy fibre pathway. This second pathway transmits many different types of information, including sensory, motor and more cognitive input [80, 50, 126, 100, 112]; this again highlights the pervasive cerebellar involvement in behavioural control. In the present model, climbing fibre input would still reflect prediction errors, similarly to parallel fibre input, therefore updating estimates encoded by Purkinje cells. However, the type of information conveyed should be particularly informative of task contingencies (e.g., related to unconditioned stimulus), such as to drive the learning of new interactions or associations among behavioral variables (e.g., the conditioned stimulus and reflex) encoded in the parallel fibre connectivity matrix,  $\theta_f^T$  (see for example [74]). In the present work, prediction errors conveyed by climbing fibre input would then underlie learning of an association between whisking and respiration in the cerebellar cortex.

In addition to the olivary-climbing fibre system, the present model could also include a more detailed description of cerebellar nuclei. Here cerebellar nuclei are replicating hidden states  $x$  encoded in granule cell; this is justified by the fact that cerebellar nuclei receive the same mossy fibre information reaching the cerebellar cortex, but this does not seem the case everywhere in the cerebellum [218]. Alternatively, cerebellar nuclei could encode different hidden states, which would still be related to those encoded by granule cell via Purkinje cell predictions. Moreover, this approximation of cerebellar nuclei activity overlooks differences in information processing between the granular layer and cerebellar nuclei. Thus, future work should aim at expanding the cerebellar model presented here, to give a more detailed account of the role of cerebellar nuclei in cerebellar state estimation.

Finally, our simulations show that, when we remove cerebellar contextualisation, the phase of respiration and whisking, as well as inter-limb phase, decouples. This is to be expected, given the way the generative processes are set up, and serves as a proof of concept for the cerebellar-based coordination of behavioural variables; however, future work should aim to integrate cerebellar contributions to extra-cerebellar dynamics with existing extra-cerebellar inter-areal connectivity, which is also likely to play a role in behavioural coordination. It would be interesting, for example, to investigate how cerebellar-dependent coordination of extra-cerebellar dynamics may be itself

modulated based on the behavioural context: one mechanisms through which this could happen may involve tuning of the impact of cerebellar nuclei outputs onto extra-cerebellar dynamics, based for example on the the intrinsic dynamics of recipient neuronal structures, especially when multi-synaptic connectivity is involved; alternatively, another mechanisms may involve the direct modulation of the state estimation process in the cerebellar cortex by neuromodulatory systems, which are also sensitive to the behavioural context.

In conclusion, we described a model of cerebellar state estimation supporting coordination of different behavioural variables or domains. We sustained that coordinating behaviour is a key function of the cerebellum, and may explain its ubiquitous involvement in behavioural control. The key idea is that coordination is based on the cerebellar capacity to learn and infer how different behavioural states interact with each other, and to use this inference to bias or contextualise inference in extra-cerebellar regions accordingly. We simulated synchronisation of whisking and respiration as well as limb and tail coordination during locomotion in rodents to illustrate how the cerebellum may guide inference processes in extra-cerebellar regions; however, the present work can be generalised to any behavioural context where associations between task-relevant variables is critical for behaviour.





# Chapter 3: Cerebellar cortical representations of whisking behaviour in mice

## 3.1 Introduction

### 3.1.1 The whisker system as a model for sensorimotor integration

Behaviour requires the integration of diverse information to produce and reach desired outcomes. At its simplest, this could involve the integration of sensory and motor information to guide actions (based on incoming sensory information), and predict sensations (based on actions). This cycle is at the core of active perception, namely, the purposeful, sensation-seeking interaction with the world.

The cerebellum is deemed critical for active perception. For example, cerebellar activity is preferentially linked to object exploration rather than movement *per se* [84], and is involved in active sensory acquisition [12]. More generally, the cerebellum is thought to learn internal models that combine and transform sensory and motor information in order to coordinate and refine behaviour; this is in line with evidence about neuronal representations in the cerebellum reflecting both sensory and motor domains [236, 111]. Hence, elucidating how the cerebellum integrates and transforms sensory and motor information is key to understand how it contributes to behaviour.

One system widely used to study behaviour is the whisker system in rodents. This system is key for the rodent behavioural repertoire, supporting object localisation and identification [134, 51], guidance of locomotion [7, 232], development and expression of emotional skills [210] and social behaviour [238]. Notably, the cerebellum plays a central role in controlling whisker behaviour, including refinement of whisking trajectories [184] and coordination with other behavioural rhythms [191]. As such, the whisker system is an optimal model to investigate how the cerebellum transforms sensory and motor information and ultimately contributes to behaviour.

### 3.1.2 Cerebellar representations of the whisker system

In the cerebellar cortex, neuronal activity encoding sensory- and motor-related representations of the whisker system are localised in its lateral portion [184, 21], which includes Crus I, Crus II and the simplex. In these areas, artificially evoked neuronal activity produces changes in whisking parameters [184], while spontaneous activity can either be evoked by passive whisker deflection [226, 36, 57, 108, 188] or precede voluntary whisking [37]. Notably, whisker representations in these areas are multiple, scattered, and intermingled with representations of other sensory surfaces in the perioral region [202], as well as of other sensory modalities (e.g., auditory and visual) and motor systems (e.g., respiration) [113, 191, 103].

This so-called fractured organisation of neuronal representations is unlike that found in brain regions forming somatotopic maps, as in the barrel cortex [240]. This fractured organisation may be particularly functional to support cerebellar-specific integration of sensory and motor modalities, which in turn may play a key role in behavioural coordination. Such organisation is plastic, originating from experience-dependent changes of connectivity patterns taking place at all levels of the cerebellar cortex [85, 42]. Notably, beyond adaptation due to long-term structural changes, neuronal representations in the cerebellum may also be dynamically adjusted at a faster time scale, based on the behavioural context, similar to what happens throughout extra-cerebellar regions [60].

Neuronal correlates of whisking activity are based on a linear code, preferentially representing the low-pass filtered whisker position, called the setpoint [37]. This code is used to build up neuronal representations via sequential information processing across layers of the cerebellar cortex

[38], and relies on synaptic transmission that can be extremely precise [188]. Overall, these linear transformations may be optimal to efficiently integrate whisker dynamics with those of other behaviourally relevant variables, and tuning these transformations to the present behavioural context may be of critical importance for functional behaviour. However, it is still unclear how cerebellar cortical transformations, and therefore its representations of whisking behaviour, may change depending on the state of the network.

### 3.1.3 Role of Golgi cells in cortical computations

A key component of the cerebellar cortex, determining how it integrates and transforms incoming information, is the Golgi cell population. In classical Marr-Albus models, it is assumed that the cerebellum classifies mossy fibre input patterns by associating each with a target Purkinje cell output, and that Golgi cell inhibition promotes associative learning by increasing the discriminability of mossy fibre input, a process known as pattern separation [153, 2]. Pattern separation effectively consists in sparsifying network activity through normalisation and decorrelation: the former scaling neuronal excitability to the global intensity of presynaptic input [27], hence forcing selective encoding of one input pattern at time [153, 2, 16, 146]; the latter ubiquitously decreasing response similarity by reducing correlations in neural activity via threshold effects [29, 30].

Closely related to Marr-Albus theories is the cerebellar adaptive filter model, which extends the original idea of a static pattern classifier to a filter dealing with time-varying input [81, 241, 47, 193]. Here, Golgi cells contribute to the dimensionality expansion of the continuous stream of mossy fibre input to the granular layer in the spatio-temporal domain, by enabling the generation of a fixed set of long-lasting granule cell responses through strong granule cell-Golgi cell and Golgi cell-Golgi cell recurrent connections. Notably, in both adaptive filter and perceptron models, Golgi cells are generally deemed to be relatively insensitive to the structure of incoming information, and their activity is thought either to act in a blanket-like fashion, or to be mostly dominated by recurrent connectivity within the granular layer.

On the other hand, different studies have documented precise Golgi cell representations of task-related variables, such as widespread sensory stimulation, general motor activity, or circumscribed events of whisking and locomotion [107, 94]. Moreover, the temporal structure of input

is also reflected in the Golgi cell activity: due to electrical connections among Golgi cells [55], coincidence or alternatively temporal offset among mossy fibre input can elicit synchronisation or desynchronisation between local Golgi cell networks [235]. Finally, the particular connectivity of the Golgi cell network also supports broader synchronisation, entraining slow fluctuations within the granular layer that are intimately linked with other brain rhythms [169, 192]. Overall, these findings show that Golgi cells are sensitive to the structure of incoming extra-cerebellar information, meaning that their activity is tuned by the spatio-temporal properties of mossy fibre input.

Thus, Golgi cells seem to also contribute more subtly to the encoding of behaviourally-relevant variables. Along these lines, Golgi cell inhibition has been shown to control how granule cells integrate and combine extra-cerebellar information, leading to the dynamic encoding of different input combinations by partially segregated clusters of granule cells [64]. In the simple case of two stimuli, for example, this means that one stimulus can evoke different responses across granule cell subgroups depending on the second stimulus, and that this contextual encoding relies on Golgi cell inhibition. As such, disruption of Golgi cell inhibition can lead to impaired behaviour [233], possibly because the latter relies on integration of information about different behavioural dynamics at the level of the granular layer.

In mice, whisking behaviour is tightly coupled with other physiological rhythms and motor activities [48, 138, 157]. Altering Golgi cell inhibition, therefore, could affect whisking dynamics by changing its coordination with other behavioural variables. Notably, Golgi cell inhibition is finely tuned by numerous mechanisms, including neuromodulatory systems and feedback loops within the cerebellum [52, 110, 3, 237, 167, 63, 141]. This control may change how incoming whisking information is encoded and transformed by the cerebellar cortex [174], depending for example on changes in the behavioural context, which requires a focus on different aspects of behaviour. However, it remains to be tested whether, and how, changing levels of Golgi cell inhibition may impact neuronal representations of whisker behaviour.

The effects of tuning Golgi cell activity on neuronal and behavioural activity depend on how inhibition controls granule cell activity. Experimentally, Golgi cell inhibition has been associated with decreased temporal precision of the granule cell response to mossy fibre input [56]. Interestingly, this is in apparent contrast with the effects of classical feedforward inhibition,

which narrows the temporal window for excitation, thus increasing the temporal precision of the initial response of a network to its input [234, 82, 162]. Golgi cells are also a source of feedforward inhibition, but because they can be activated by distinct mossy fibre pathways than those driving granule cells, their inhibition may precede or be concomitant with the initial period of granule cell excitation. Consequently, Golgi cells can decrease the temporal precision of the initial granule cell response to one stream of mossy fibre input, by delaying this response depending on information from parallel mossy fibre pathways. This control of response timing, in turn, could be one mechanism through which information about different behavioural variables is integrated by the cerebellar cortex [34], and may play a key role in motor initiation [35].

### 3.1.4 Aim and overview

The aim of this project was to study how neuronal activity in the cerebellar cortex represents and contributes to behaviour. In particular, we focused on sensorimotor representations of the whisker system in mice, an ideal model to investigate how the cerebellar cortical transformation of sensorimotor information relates to behavior. Because cerebellar representations may not be fixed, but may adapt to the behavioural context at hand, we investigated how changes in the state of the network may affect cerebellar and consequently whisking dynamics. A key element of this circuit is the Golgi cell population, which regulates the transformation of information in the cerebellar cortex, and whose activity is controlled by many different mechanisms operating at different temporal and spatial scales [174]. We therefore decreased Golgi cell activity in order to change the state of the network and analysed how this change affects neuronal representations in the cerebellar cortex and behaviour.

Once deemed to provide inhibition in a fixed, blanket-like fashion to the granule cell population, Golgi cells are now known to be also sensitive to the temporal and spatial structure of mossy fibre input, which could enable them to control excitation in the granular layer more subtly. Thus, one possibility is that decreasing Golgi cell inhibition may remove a key mechanism for sparse coding, and lead to saturation of network activity and degradation of neuronal representations therein. Alternatively, decreased inhibition may lead to more subtle effects, such as an increase in the temporal precision of the initial timing of neuronal activity. In this case, ef-

fects of our manipulation on whisking behaviour could preferentially affect the onset of whisking activity.

In this study, we recorded both (i) population activity in the lateral cerebellum using NeuroPixels I probes and (ii) whisker position with a high-speed camera in head-fixed mice. Manipulation of the network's state was achieved via reduction of Golgi cell inhibition. In particular, a subset of recordings was performed in animals that selectively expressed inhibitory DREADDs (designer receptors exclusively activated by designer drugs) in Golgi cells; localised expression of DREADDs was achieved via chemogenetic means (Figure 3.1). In these mice, it was possible to reduce inhibition in the granular layer by activating DREADDs with an exogenous drug (Clozapine N-oxide; CNO) applied topically on the recording site. This allowed us to test whether lowering inhibition levels leads to a degradation of whisking-related representations or to more subtle changes of these representations, and how this affects whisking itself.

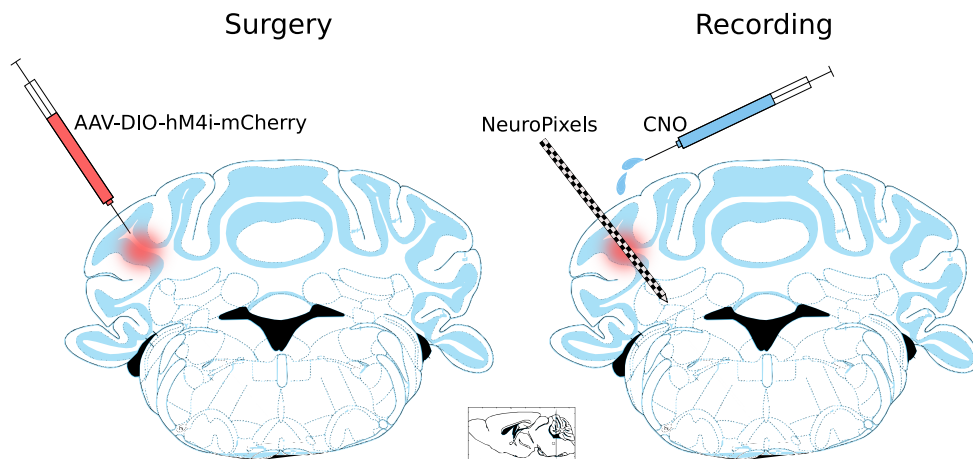


Figure 3.1: Chemogenetic manipulation of Golgi cells. left: we injected cre-dependent adeno-associated-virus AAV-DIO-hM4D(Gi)-mCherry for expression of inhibitory DREADDs (designer receptors exclusively activated by designer drugs) in the lateral cerebellum of C57BL/6-Slc6a5<tm1.1(cre)Ksax> (GlyT2-Cre knockin) mice. Right: during electrophysiological recording, DREADDs were activated by the exogeneous drug clozapine N-oxide (CNO) to reduce the level of Golgi cell inhibition in the network. CNO was applied topically on top of the recording site and allowed to diffuse in the cerebellar cortex.

## 3.2 Materials and Methods

All experimental procedures involving animal were performed in accordance with the United Kingdom Home Office guidelines. All surgical procedures and recordings were performed in mice (both males and females) aged between 3 to 6 months.

### 3.2.1 Surgical operations

To perform recordings under normal and perturbed network conditions, we used both wild-type (C57BL6J) mice and genetically-modified C57BL/6-Slc6a5<sup>tm1.1(cre)Ksak</sup> (GlyT2-Cre knockin) mice, which express Cre-recombinase selectively in Golgi cells in the cerebellum [127].

GlyT2 mice underwent two surgical operations: one to induce Cre-dependent expression of DREADDs in cerebellar Golgi cells via viral injection, and one to prepare the animal for head-fixed extracellular recording. At the beginning of both surgical sessions, anaesthesia was induced with isoflurane (5%) and maintained (1-2%) for no longer than 2 hours. Pedal reflex was monitored to assess the depth of anaesthesia. To induce analgesia, mice were injected subcutaneously with carprofen (Rimadyl, 5 mg/kg), buprenorphine (Vetergesic, 0.1 mg/kg) and lidocaine (2 mg/kg, locally). Surgery was carried out on a stereotaxic frame in aseptic conditions to prevent infections. After the surgical operation, mice were placed in a warmed box (37°) and allowed to recover for as much time as they needed. Signs of neurological impairment and pain were checked during the post-surgery recovery period.

During the first surgical session, a small craniotomy (about 1 mm diameter) was performed over Crus I (from Bregma, -6.36 cm and +2.5 cm in the anterior-posterior and medio-lateral axis, respectively), and AAV-DIO-hM4D(Gi)-mCherry virus for the Cre-dependent expression of DREADDs (500-1000 nl) was injected with a glass pipet at different depths (100 µm separation starting from 600 µm), waiting 2 minutes between pipet retractions. At the end of the operation, skin over the head was sutured.

The second surgical session took place 8 weeks after the first one to allow virus expression. First, neck muscles were gently moved to uncover the cerebellum. Then, a head plate was fixed with superglue on top of bregma. Subsequently, a first craniotomy (1.5 mm diameter)

was performed on the right cerebellar hemisphere, dura was removed and a reference screw was inserted and put in contact with the underlying brain. To secure both head place and the reference screw, dental cement was used to cover the skull, leaving free the area on top of Crus I on the left cerebellar hemisphere. Dental cement was also used to create the recording well. A second craniotomy (about 2 mm diameter) was performed on top of the left Crus I, followed by the durotomy. Finally, a first layer of agarose (1.5% in phosphate buffer saline, PBS) was used to cover the brain, a second layer of Kwik-Seal was used to protect the brain, and a third layer of nail polish was used to fix the quickseal.

Wild-type mice underwent only the second surgical operation, needed to prepare the animal for the recording session. Both wild-type and GlyT2 mice had their whiskers trimmed on the left (recording) side, except for the whiskers C1, C2 and C3 (posterior whiskers on the third row from top).

### 3.2.2 Recording procedure

Animals underwent two recording sessions, the first performed at least 4 hours after recovery from the craniotomy, the second the day after. During both sessions, mice were head-fixed and placed in the recording apparatus. The Kwik-Seal was removed, the surface of the brain cleaned from agarose and kept moist with PBS. In case of dura regeneration, a second durotomy was performed. The probe was fixed to a micromanipulator (Scientifica) via a custom-made 3D printed holder. The probe was coated with (2.5 mg/ml) DiI stain for *ex vivo* probe tracking before insertion at a speed of 2-5  $\mu\text{m/s}$  until about 2.5/3 mm of depth from the surface. Once reached this depth, the probe was retracted for about 100  $\mu\text{m}$  and then left to settle for 10-15 min, allowing the brain to relax. The start of the video and electrophysiological recording were synchronised by a TTL pulse originating from the video software (streampix). A baseline of 10 or 20 min was recorded prior to topical administration of CNO, which consisted in filling the recording well made of dental cement after PBS was dried out. We used a 30  $\mu\text{M}$  concentration for CNO, following [211], who showed that an intracranial injection of 1  $\mu\text{M}$  CNO is already enough to reliably inhibit presynaptic neurotransmitter release within minutes. The recording then continued for the subsequent 40-50 mins, for a total recording time of 1 hour. Video and



neuronal recording were obtained at 299 and 30000 samples/sec, respectively. After recording, the probe was extracted, rinsed with deionised water and left in freshly made 1% tergazyme solution for at least 24 hours. The mice, instead, were either returned to their cage or culled with schedule 1 method before brain extraction, depending on whether they had already undergone one recording session. Before mice were returned to their cage, the surface of the brain exposed was first rinsed with PBS, then covered with agarose, and finally protected with a layer of quickseal that was fixed to the surrounding dental cement with nail polish.

### 3.2.3 Electrophysiological analysis

The open-source software spikeGLX (<https://billkarsh.github.io/SpikeGLX/>) was used to record NeuroPixels data. The (.imec) output file was preprocessed using the command-line tool CatGT (<https://billkarsh.github.io/SpikeGLX/#catgt>) to apply a highpass filter (cut-off 300 Hz) and global demux filters, a common average referencing that takes in account the probe channels subgrouping during data acquisition. The spike sorting step was conducted using the open-source software Kilosort 2 (<https://github.com/MouseLand/Kilosort>), which has shown better performance for cerebellar recordings than Kilosort 3 [148]; this software groups spikes into units, each representing the activity of a distinct putative neuron. Manual curation of sorted units was done with the open-source Python-library Phy (<https://github.com/cortex-lab/phy>) (Figure 3.2), and consisted in merging and splitting units, as well as categorising them in ‘good’, ‘bad’ and ‘mua’ (multiunit activity) units. In all analysis, only ‘good’ units located in the cerebellar cortex were used: in order to isolate the cortical population from cerebellar nuclei neurons, which were occasionally recorded on the lower channels of the probe, we retained units based on their approximate position in the cerebellum, informed by electrophysiological landmarks (e.g., deepest complex spike recorded) and visual inspection of histological data of the shank location in the brain.

### 3.2.4 Behavioural analysis

Whisking was recorded using a high speed camera (Dalsa Genie-HM640). The output (.avi) file was transcoded (.MP4, libx265 encoder), re-sampled (299 Hz) and cropped using the ffmpeg

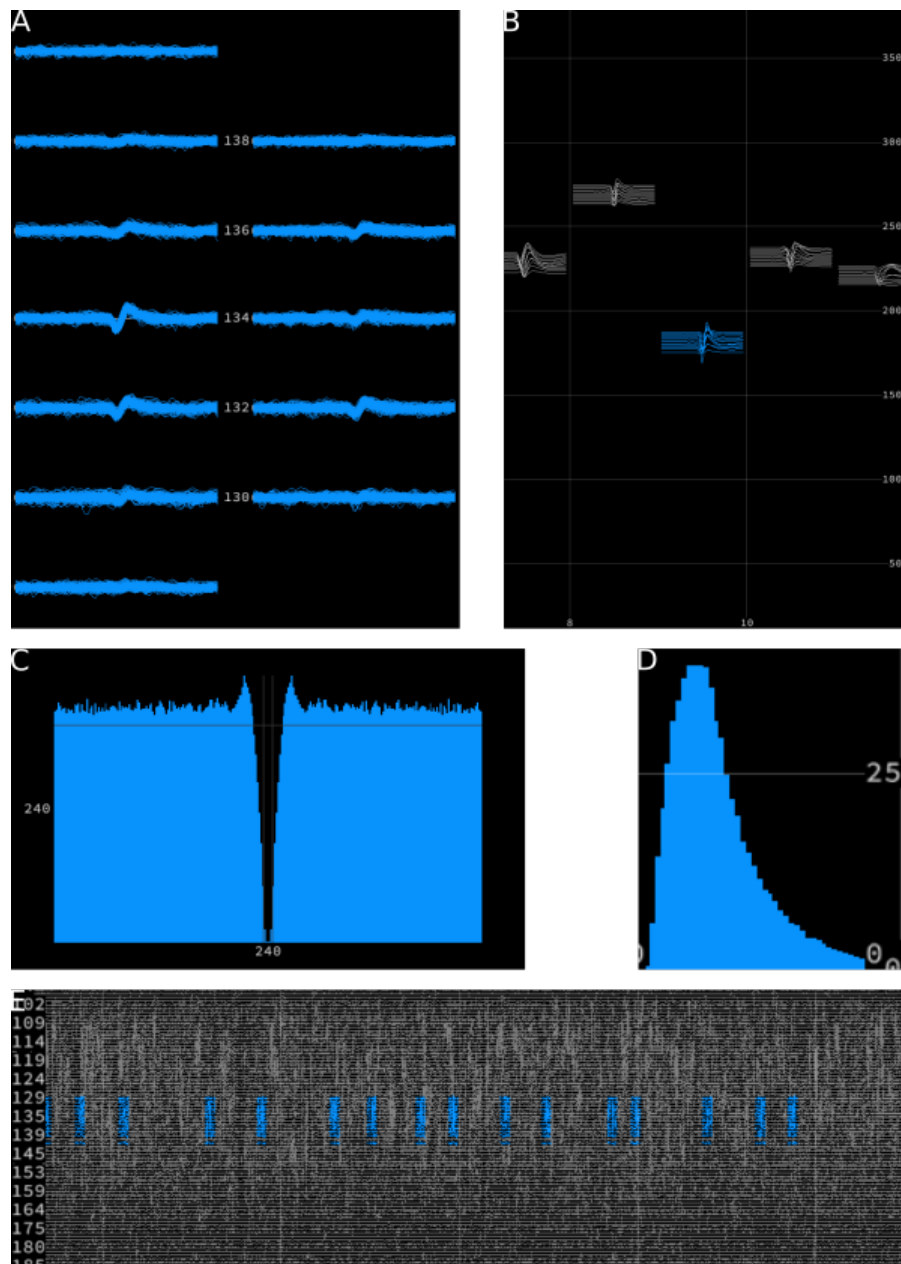


Figure 3.2: Exemplar unit. Detected spikes were sorted in units by Kilosort 2 based on the similarity of their waveform. The software phy2 was used to visualise and manually curate the output of Kilosort 2. (A) Waveforms of a unit in different channels, that is, recording sites on the probe. (B) Template associated with the unit. (C) Autocorrelogram. (D) Inter-spike-interval histogram. (E) Trace view showing the occurrence of the unit spikes across channels (y axis) and time (x axis).

software. We used the open-source toolbox Deeplabcut (<https://github.com/DeepLabCut/DeepLabCut>) to label four landmarks for each whiskers (C1, C2 and C3) (Figure 3.3) across the entire recording; these landmarks were then used to compute various whisking properties, following the work of [105]. Specifically, we first used the arctan function to measure the azimuth angle between the first whisker segment (traced from the first, basal marker to the second marker) and the horizontal line passing through the basal marker; given the fixed camera positioning, increases in angle correspond to whisker protraction, whereas decreases correspond to whisker retraction. Next, the phase of the whisking cycles was extracted using the Hilbert transform, and was used to compute the slowly changing whisking amplitude and setpoint across cycles. Finally, the whisking amplitude was low-pass filtered and used to identify periods of whisking: this was done using a heaviside function with a threshold of  $10^\circ$ , which allowed whisking to be discriminated from resting periods. If not alternatively specified, all whisking analysis focused on the C3 (most anterior) whisker.

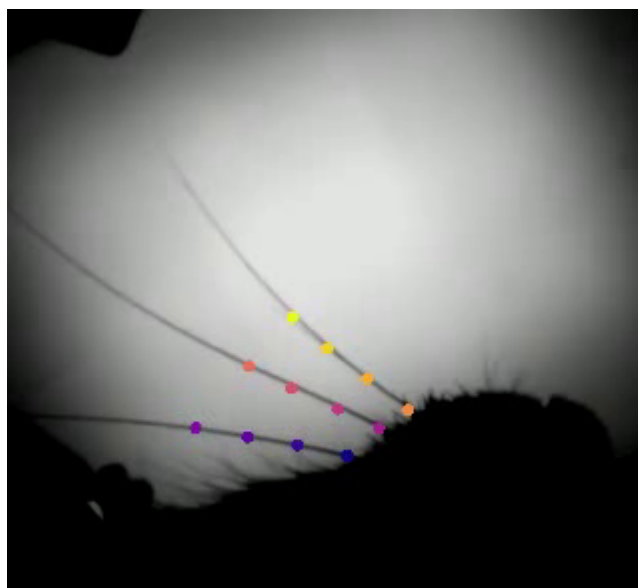


Figure 3.3: DLC whisker tracing. Example of DLC output frame. A high-speed camera was used to record whisking behaviour of head-fixed mice, and the ensuing videos were analysed with the DLC software. Previous to the analysis, the DLC deep neural network was trained to recognise 4 landmarks on each whisker, denoted by filled circles with different colors.

### 3.2.5 Histology

Brains were extracted and left in 4% PFA solution for 24-48 hours at 4°. After washing out the PFA with PBS, coronal sections (50-100  $\mu\text{m}$ ) were sliced using a vibrating microtome (Leica VT1000S). Fluorescent images were acquired using a confocal microscope (Leica DM4000 B) (Figure 3.4).

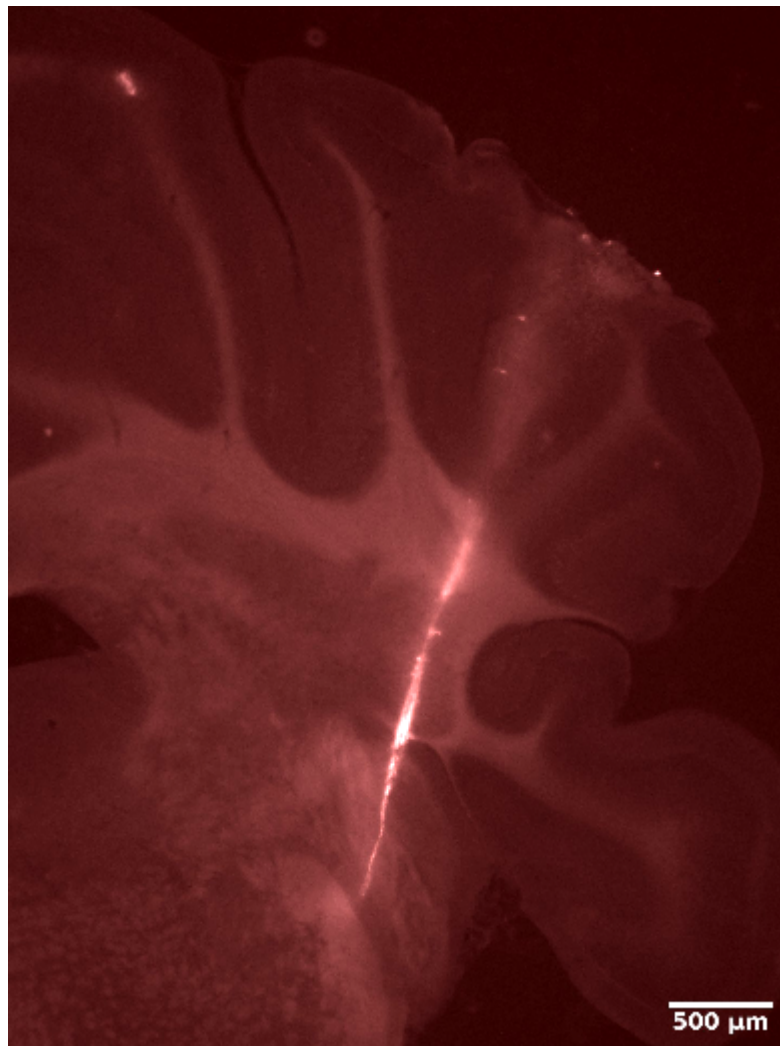


Figure 3.4: NeuroPixels trace. Fluorescent microscopy image of the DiI trace left by a NeuroPixels probe inserted in the lateral cerebellum. The probe was inserted for about 3 mm, crossing Crus I and the cerebellar nuclei.

### 3.2.6 Golgi cell manipulation

Manipulation of Golgi cells was achieved via activation of inhibitory DREADDs (designer receptors exclusively activated by designer drugs, hM4Di), which causes a reduction of neurotransmitters released by the cells expressing these receptors. Localised expression of DREADDs (Figure 3.5) was driven by the AAV-DIO-hM4D(Gi)-mCherry virus in a Cre-dependent manner, and was therefore restricted to Golgi cells, because in the GlyT2 mouse line used for this experiment Cre-recombinase is only expressed in Golgi cells in the cerebellar cortex [127]. Viral injection targeted the lateral cerebellum, and in particular Crus I. DREADDs were activated by dropping CNO on top of the site of the Neuropixels penetration into the brain, which in turn targeted the site of virus injection (Figure 3.6); this method was used to minimise possible side effects of the CNO, and afforded within-minute temporal precision to our manipulation.

### 3.2.7 Unit encoding of setpoint

We used a generalised linear model to predict spike counts (50 ms time bins) from the whisking setpoint. The model predicts spike counts with a Poisson distribution, whose rate is given by the linear combination of past, present and future setpoint data (time window ranging from -4 to +4 time bins) transformed with an log-link function. The posterior distributions over the nine  $\beta$  parameters (one for each time bin) were obtained with the probabilistic programming library Pymc (v4, <https://www.pymc.io/welcome.html>) from a training dataset (first 6000 time bins). From these posterior distributions, the expected (mean) rate was computed for the subsequent 6000 time bins; the expected rate was then used to draw samples from which the highest-density interval (HDI) was calculated. In addition, we accounted for temporal correlations among  $\beta$ 's by using a multivariate normal distribution as a prior, with correlations among  $\beta$ 's exponentially decaying with distance.

### 3.2.8 Tuning curve analysis

To compute the tuning curve for each unit, we first discretised the time in bins of  $\sim 33$  msec; second, we computed the total spike count and average whisker position (angle) for each time bin; third, we discretised the average whisking angles in 11 bins, ranging from the minimum to

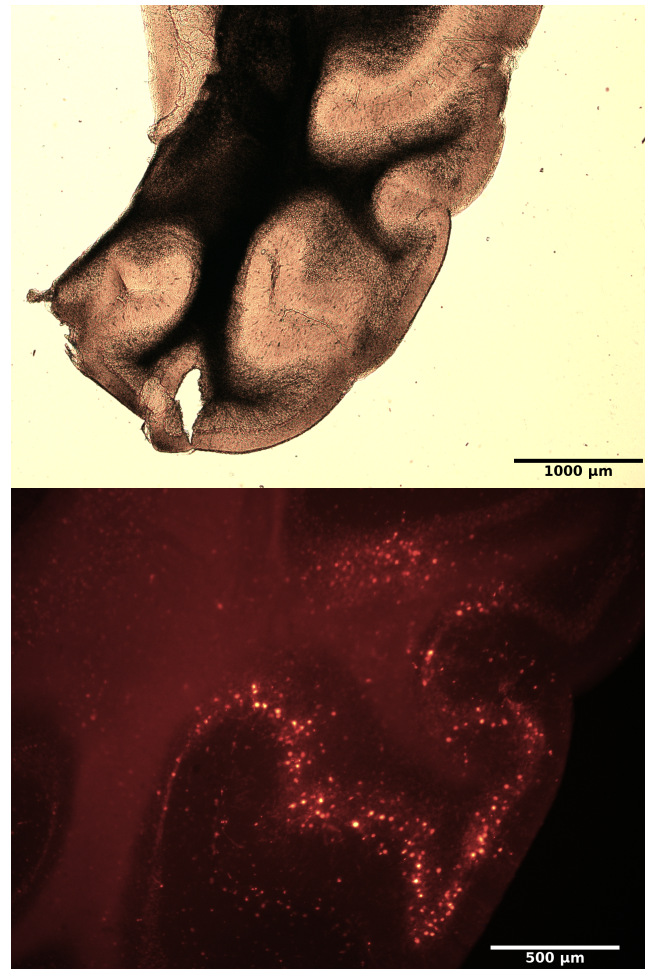


Figure 3.5: DREADD receptors expression. Fluorescent microscopy image of a cerebellar coronal slice from a GlyT2-Cre mouse injected with the AAV-DIO-hM4D(Gi)-mCherry. Top: brightfield microscopy image showing the lateral cerebellum. Bottom: fluorescent microscopy image showing selective expression of DREADDs in Golgi cells in Crus I.

the maximum angle observed in each recording; fourth, we paired the spike count at each time bin with the corresponding whisker angle. These data were finally used to plot the firing rate, together with their standard error, against the 11 angle bins.

We then tried to cluster tuning curves in groups that may represent different patterns of whisking encoding, by using the k-means clustering algorithm (`sklearn.cluster.KMeans` package). The estimation of the tuning curves can be noisy, due to, for example, errors during the spike sorting process, which may lead to the contamination of the spike history assigned to one unit by the activity of nearby neurons. This noise, in turn, could affect clustering of tuning curves



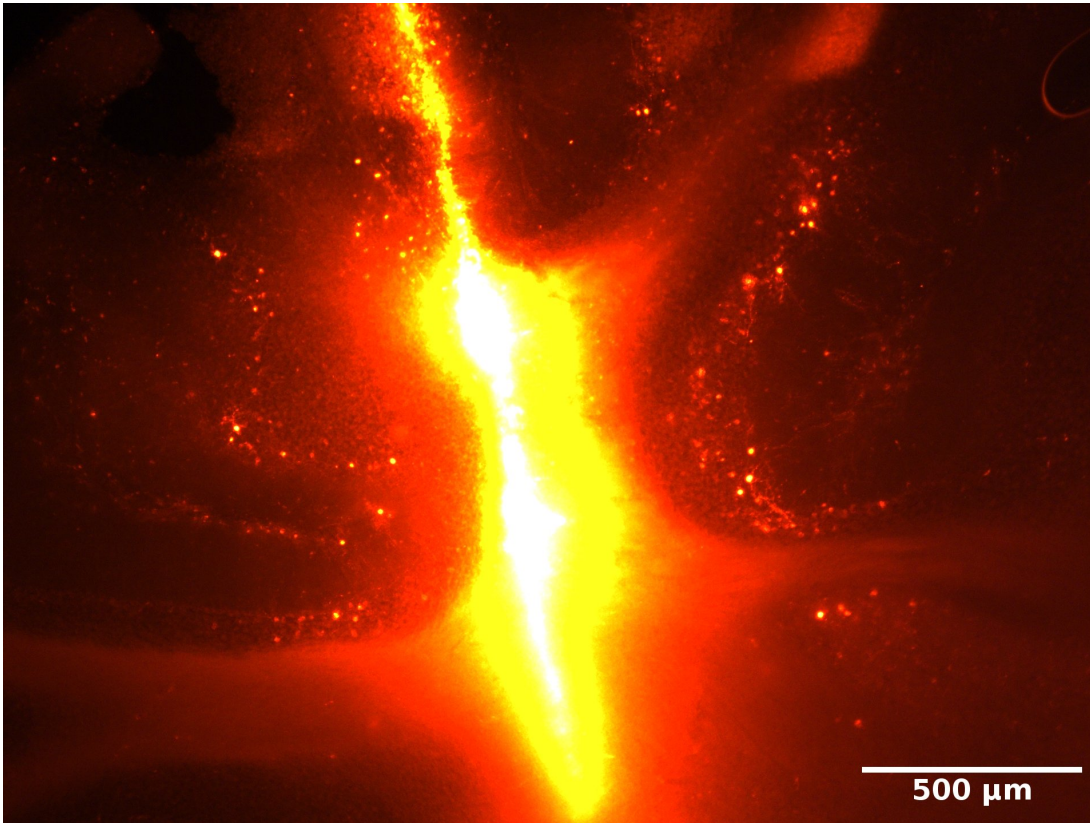


Figure 3.6: DREADD receptors and NeuroPixels trace. Fluorescent microscopy image of a cerebellar slice where the DiI NeuroPixels trace crosses a region where Golgi cells express DREADDs.

into meaningful groups. Thus, to reduce the impact of this source of noise on our clustering analysis, we fitted a spline model to each tuning curve: the model used 7 cubic b-spline functions, and allowed us to smooth the firing rate associated to each angle bin based on the firing rate of adjacent bins. The smoothed tuning curves were then clustered using a k-means cluster algorithm: this algorithm is an unsupervised machine learning technique that allows to group observations in  $k$  groups, where  $k$  is the user-provided number of groups. Here we used  $k=5$ , because visual inspection of the tuning curves suggested that at least 4 patterns of whisking encoding existed (Figure 3.11), and because the sum of squared distances of samples to their cluster's centre kept decreasing at least until  $k=7$ , after which it started to plateau (Figure 3.12). To visualise possible tuning curve subgroups, we reduced the dimensionality of the tuning curves (dim=7, equal to the number of b-splines) to 3 using the non-linear dimensionality reduction

method T-distributed Stochastic Neighbor Embedding (t-SNE, sklearn.manifold.TSNE package).

### 3.2.9 PCA analysis, whisking-pc cross correlation, and pc loadings

We used principal component analysis (PCA) to describe the population activity of each recording with its projections onto the its first three eigenvectors, which describe the first three orthogonal axes in neuronal space along which the activity varies the most. The projections are also called principal components (pc's). We used PCA as it provides a succinct description of high-dimensional data, while preserving its original properties as much as possible, such the geometry of population dynamics. The neuronal data used to derive the eigenvalues and eigenvectors were the units' firing rate obtained by averaging spike activity over trials from the whole recording (1 hour), where each trial encompasses the time from -2 to +3 seconds around the start of the whisking bouts. The eigenvector for each recording has length equal to the number of units present in that recording. The values of the eigenvector are known as loads, and correspond to the weight associated to each unit used when linearly combining the firing rate from all units; hence, the loadings correspond to how much each unit contributes to a pc. To derive the pc for single trial activity, we first smoothed single trial spike counts with a Gaussian window of  $sd=20$  (we also used  $sd=5$  but the results are equivalent; time bin width=3.3 ms).

The cross-correlation between whisking position and each pc was obtained using the 'scipy signal correlate' package. All cross-correlations were normalised by the absolute maximum value of the first pc. For analysis involving CNO manipulation, the cross-correlation peaks for pre- and post-drop periods were computed, and the respective distributions were compared using a two-sided Wilcoxon signed-rank test.

### 3.2.10 Setpoint decoding

To decode the whisking setpoint from the neuronal population activity we used a linear model. The neuronal data were the first three pc's, augmented in time with a lag of approximately 0, -30, -70, -100 and -130 ms compared to the time of the setpoint data; for example, the pc's with lag -130 ms anticipated whisking data by 130 ms. This was done to give the model the freedom to relate information in each pc to whisking setpoint with a different temporal separation, as it



is known that information in the same cerebellar cortical area can encode behavioural variables with different lags [183]. The model linearly combined the three pc’s with different lags. Thus, the posterior distribution of the 15  $\beta$  parameters (3 pc \* 5 lags) were obtained using the Pymc library and data from the first 20 minutes of the recording. The posteriors were then used to predict whisking setpoint (expected value together with the highest density interval) during the subsequent 20 minutes.

### 3.2.11 Statistical analysis for the CNO manipulation

A multilevel model was used to account for the variability in the total cerebellar cortical spike counts detected over time across recordings; the counts were the sum of the spikes assigned to ‘good’ (putative single units) cortical units. The counts were computed for each successive 5 minutes time bin, with the 0 time bin including the time of drug application, and with all counts scaled by the -5 minutes bin count; we also repeated the analysis by scaling all counts by the +20 minutes bin count, which gave the same results. In the model, spike counts were described using an inverse Gamma distribution, as it afforded a good fit of the model to the data, as well as a good sampling from the posterior probability distributions:

$$\begin{aligned}
 spkcount &\sim InverseGamma(\alpha, \beta) \\
 \alpha &= exp(\theta_\alpha + \theta_{\alpha cond} + \theta_{\alpha aid} + \theta_{\alpha time}) \\
 \beta &= exp(\theta_\beta + \theta_{\beta cond} + \theta_{\beta aid} + \theta_{\beta time})
 \end{aligned} \tag{3.1}$$

The  $\alpha$  and  $\beta$  are respectively the shape and scale parameter, linked each to a linear model by a loglink function. Both linear models involve a coefficient  $\theta$  for each explanatory variable, namely, the experimental condition, the time of the recording (dim=9) and the animal id (aid, dim=17). The experimental conditions included the one of interest, pairing CNO with Glyt2 mice (‘gCNO’, n=19 recordings), and two controls, one pairing CNO with wild-type mice (‘wCNO’, n=5 recordings), and the other pairing PBS with wild-type or Glyt2 mice (‘PBS’, n=9 recordings). The experimental conditions were split by recording period, one for bins before 0 (pre-drop or baseline period) and one for bins from 0 onward (post-drop period), for a total dimensionality of 3x2 (dim=6) for the  $\theta_{\alpha cond}$  and  $\theta_{\beta cond}$  coefficient. The contrasts between pre- and post-drop

coefficient  $\theta_{cond}$  were used to assess the effect of the experimental manipulation.

The additional explanatory variables, namely, the time of the recording and the animal id, were used to explain respectively spike count variability within each time bin due to natural changes in network activity over recording time, and variability due to the particular conditions of the network in each animal (e.g., affected by the surgical procedure). Thus, the addition of these explanatory variables allowed us to test within conditions for a difference in pre- and post-drop spike count distribution, after having accounted for variability explained by temporal correlations and between-animal differences.

Each  $\theta$  was drawn from a vector of independent normal distributions (of length equal to dimensionality of  $\theta$ ), except  $\theta_{time}$ , whose prior distribution was a multivariate normal distribution with covariance decaying with time distance, therefore accounting for temporal correlations within the data:

$$\begin{aligned}
 \Sigma_\alpha &= I * \exp(-dist_t) & \Sigma_\beta &= I * \exp(-dist_t) \\
 \theta_\alpha &\sim Normal(\mu_\alpha, \sigma_\alpha) & \theta_\beta &\sim Normal(\mu_\beta, \sigma_\beta) \\
 \theta_{\alpha cond} &\sim Normal(\mu_\alpha, \sigma_\alpha) & \theta_{\beta cond} &\sim Normal(\mu_\beta, \sigma_\beta) \\
 \theta_{\alpha aid} &\sim Normal(\mu_\alpha, \sigma_\alpha) & \theta_{\beta aid} &\sim Normal(\mu_\beta, \sigma_\beta) \\
 \theta_{\alpha time} &\sim MVNormal(\mu_\alpha, \Sigma_\alpha) & \theta_{\beta time} &\sim Normal(\mu_\beta, \Sigma_\beta)
 \end{aligned} \tag{3.2}$$

Finally, the hyperpriors:

$$\begin{aligned}
 \mu_\alpha &= 1 & \mu_\beta &= 1.2 \\
 \sigma_\alpha &= 0.2 & \sigma_\beta &= 0.2
 \end{aligned} \tag{3.3}$$

were chosen to sample prior predictive samples within a similar scale of the observed population spike counts, including extreme values; in other words, the hyperpriors were chosen to be as uninformative as possible, while still constraining the sampling from the posterior distributions to leave in a reasonable probability space, given the data.

For this analysis we used the  $\alpha$  and  $\beta$  parametrisation of the inverse Gamma distribution, because in our case it improved sampling from the posterior posterior distributions. However, an alternative, more intuitive parametrisation uses mean and variance parameters of the inverse Gamma distribution, which are related to the  $\alpha$  and  $\beta$  parameter by  $mean = \frac{\beta}{\alpha-1}$  and

$variance = \frac{\beta^2}{(\alpha-2)^2(\alpha-1)}$ . Our analysis of the posterior contrasts highlighted a change in the scale parameter  $\beta$  of the inverse Gamma distribution: we therefore derived for each experimental condition the posterior samples for the variance parameter, which also characterises the spread of the distribution, and calculated their post- and pre-drop period contrast. As for the previous contrasts, these contrasts for the variance parameter capture the difference in observed cortical spike counts only due to the experimental manipulation. In practice, the contrasts were calculated using the posterior samples for the variance parameter associated to the pre- and post-drop period, which in turn were derived using the same  $\alpha$  and  $\beta$  posterior samples and the identity above, except that for post-drop variance samples we used posterior samples for the  $\theta_{\alpha cond}$  and  $\theta_{\beta cond}$  coefficients associated with the post-drop period. This allowed us to compare samples which were identical other than for the effect of the experimental manipulation.

### 3.2.12 Analysis of pre- and post-drop neuronal and whisking data

For all analyses involving the manipulation of Golgi cell activity, except for the statistical analysis of the total cortical spike counts presented in the previous subsection, we used a subset of data excluding recordings with no or poor (almost absent) whisking activity (25 out of 33 recording left, please see Table 3.1). In these analyses, we compared data from pre- and post-drop period: the former entails the entire baseline period, which in five recordings is of length 10 minutes, in the other of length 20 minutes; the latter is of the same length of the baseline period, and starts 5 minutes after drug application.

### 3.2.13 Comparison of the pre- and post-drop standard deviations (std's) of the units' activity absolute peaks.

For each recording, we computed the absolute peak of the trial-averaged neuronal activity (PETH) aligned to whisking onset within a chosen subwindow. The trials, as for previous analyses, ranged from -2 to 3 sec centred around whisking onset; the subwindow used to compute the absolute peaks spanned -0.7 to 1.3 sec around whisking onset, and was chosen to focus the subsequent analysis around the initial whisking protraction period. We used the absolute peak of the PETH as a proxy of the timing of the neuronal response to whisking-related input. The

peaks for one recording are shown in Figure 3.26 (violet dots). For each recording we computed the standard deviation (std) of the peaks, for pre- and post-drop data. For each experimental condition, the pre- and post-drop std's were compared using a two-sided Wilcoxon signed-rank test.

### **3.2.14 Comparison of the pre- and post-drop linear fits of the initial whisking protraction phase.**

We used a linear model to fit a line to the average whisking position pre- and post-drop. Whisking data were delimited by a time window ranging from -0.06 to 0.21 sec centred around whisking onset; the time window was chosen to focus on the period of initial whisking protraction. We computed the difference between post-drop and pre-drop slopes to compare the effects of Golgi cell manipulation on the whisking protraction phase. To test whether the variance of the distribution slope contrasts in the two experimental conditions are different, we used a Levene's test.

Recording	Animal	Strain	Condition	Whisking	# cortical units	Time CNO/PBS drop (min)
1	1	GlyT2	gCNO	poor	18	10
2	1	GlyT2	gCNO	good	5	10
3	2	GlyT2	gCNO	good	8	10
4	2	GlyT2	gCNO	good	12	10
5	3	GlyT2	gCNO	good	10	10
6	3	GlyT2	gCNO	good	10	10
7	4	GlyT2	gCNO	good	8	20
8	5	GlyT2	gCNO	absent	27	20
9	6	GlyT2	gCNO	good	61	20
10	7	GlyT2	gCNO	good	76	20
11	7	GlyT2	gCNO	good	24	20
12	8	GlyT2	gCNO	absent	5	20
13	8	GlyT2	gCNO	poor	30	20
14	9	GlyT2	gCNO	good	58	20
15	9	GlyT2	gCNO	good	23	20
16	10	GlyT2	gCNO	good	46	20
17	10	GlyT2	gCNO	good	49	20
18	11	GlyT2	gCNO	poor	9	20
19	11	GlyT2	gCNO	poor	29	20
20	12	WT	wCNO (control)	good	96	10
21	13	WT	wCNO (control)	good	28	20
22	13	WT	wCNO (control)	good	31	20
23	14	WT	wCNO (control)	good	14	20
24	14	WT	wCNO (control)	good	55	20
25	4	GlyT2	PBS (control)	good	8	20
26	5	GlyT2	PBS (control)	absent	23	20
27	6	GlyT2	PBS (control)	good	31	20

28	15	WT	PBS (control)	good	88	20
29	15	WT	PBS (control)	poor	38	20
30	16	WT	PBS (control)	good	61	20
31	16	WT	PBS (control)	good	28	20
32	17	WT	PBS (control)	good	52	20
33	17	WT	PBS (control)	good	25	20

Table 3.1: Neuronal and behavioural data. Each animal underwent two recordings (except animal 12). Each recording was performed on either GlyT2 or WT (wild-type) mice; GlyT2 mice expressed Cre-recombinase selectively in Golgi cells in the cerebellar cortex, and therefore only in these mice CNO could selectively decrease Golgi cell inhibition. The three experimental conditions are called ‘gCNO’, in which CNO was used on GlyT2 mice, ‘wCNO’ in which CNO was used on WT mice, and ‘PBS’, in which PBS was used on either GlyT2 mice (3 recordings) or WT mice (6 recordings); the ‘wCNO’ and ‘PBS’ conditions were pooled into one ‘control’ condition, after assessing for the specific effect of our manipulation on total cerebellar cortical spike counts using the statistical model described in subsection 3.2.11. For this statistical analysis of spike counts (subsection 3.3.2), we used all recordings (n=33); however, we excluded recordings with absent/poor whisking activity in all other analyses (n=25 left after exclusion), as they required whisking data or were related to whisking analysis. In particular, the remaining 12 recordings in the ‘control’ condition were used in the analyses without Golgi cell manipulation (subsection 3.3.1), while 25 recordings from in the ‘gCNO’ and ‘control’ condition were used in the analyses assessing the effect of Golgi cell manipulation on neuronal and whisking dynamics and their relationship (subsection 3.3.3). Poor whisking behaviour was defined as almost absent and extremely small whisking activity.

## 3.3 Results

### 3.3.1 Whisking representations in the lateral cerebellar cortex

Previous work from our lab found that the cerebellar cortex accurately represents setpoint and angle parameters of whisking activity at a single cell level [37, 38]; here we will focus on the same parameters to extend previous results using recording from neuronal populations in the cerebellar cortex.

#### Whisking activity is represented at a single cell level

We first set out to investigate the whisking-related information content in the neuronal activity recorded from the lateral cerebellar cortex, during normal functioning of the circuit. Figure 3.7 shows for one recording the activity of identified units (putative neurons,  $n=88$ ) during whisking epochs, defined as the time window ranging from -2 to +3 seconds centred around whisking onset. On the left, the activity of a subset of units during a single epoch ( $n=24$ ) is shown, together with the concomitant changes in whisking position; on the right is shown the peri-event time histogram (PETH, average activity) for the entire population recorded, along with average whisking activity. In both cases, there is a clear alignment of neuronal and whisking activity dynamics. Accordingly, it was possible to partially reconstruct neuronal activity from whisking setpoint using a generalised linear model (Figure 3.8, please see method section 3.2.7). Together, these data show that whisking activity is well represented at a single cell level.

#### Heterogeneous encoding of whisking activity across neurons

A more detailed characterisation of these representations is offered by the tuning curve of single units to whisker angle (please see method section 3.2.8). Figure 3.9 shows the tuning curves of all units in one recording, with whisker angle discretised in 11 bins. Three examples of tuning curves are instead shown in Figure 3.10 (on the left), which were putatively assigned to different cell types (molecular layer interneurons and Purkinje cells) or modes of activity (simple spikes and complex spikes), based on the unit's firing rates, auto- and cross-correlogram (on the right). In more detail, the putative simple spike unit had an average firing rate of 70 Hz, which is within the

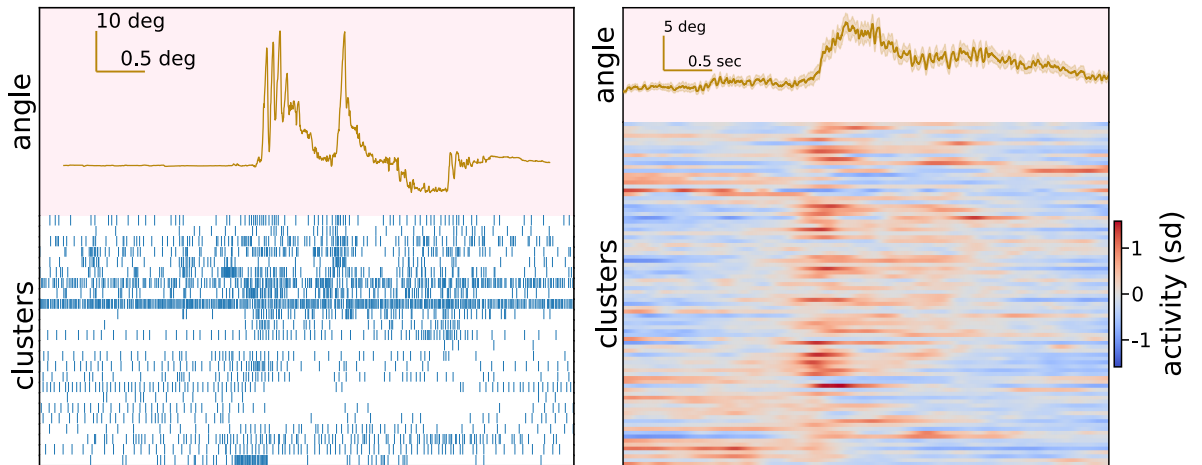


Figure 3.7: Neuronal and whisker activity. Left: neural and whisker activity during a single trial, defined as a -2 to +3 second window centred on whisking onset. Whisking dynamics are displayed at the top; the raster plot at the bottom shows the concomitant units' activity (subgroup of units shown on the right). Right: average neural and whisker activity across trials. The average changes in whisker angle, together with its standard error, are displayed at the top; beneath is shown the peri-event time histogram of the entire population for this recording. Units in the lateral cerebellar cortex appear to clearly encode information about whisking behaviour both on average and at a single trial level.

elevated and variable range of 20-200 Hz observed *in vivo* [8, 125, 37]. The average firing rate of the putative complex spike unit, on the other hand, matched the lower  $\sim 1$  Hz firing rate observed experimentally for complex spikes [207]. As for the putative molecular layer interneuron, this had an average firing rate of 15-30m Hz, which is consistent with the firing frequency of molecular layer interneuron observed *in vivo*, ranging from 1-35 Hz [132]. Moreover, the molecular layer interneuron exhibited an autocorrelogram characterised by two peaks separated by a trough of width  $\sim 100$  ms, which indicates the tendency of the neuron to fire regularly with an inter-spike interval around 50 ms [99]. On the other hand, the simple spikes and complex spikes exhibited a classical cross-correlogram, showing a short refractory period for simple spikes following the occurrence of complex spikes [88, 219], indicating that these units originated from the same Purkinje cells. Together, these examples indicate that our recordings could capture the activity of different cell types present in the lateral cerebellar cortex.

We next addressed the question of whether and how neurons across the cerebellar cortex encode differently whisking dynamics. Figure 3.11 displays four tuning curves that possibly



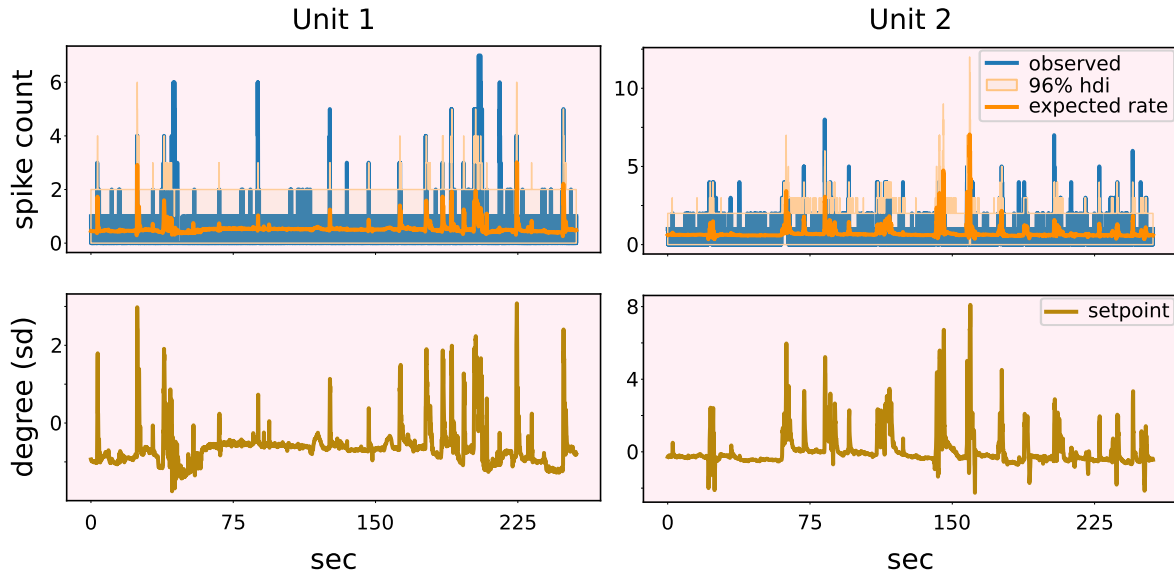


Figure 3.8: Single unit encoding of whisking setpoint. We used a generalised linear model with Poisson noise to predict the spike counts of two units (top, blue line) from the whisking setpoint (bottom). The predicted mean or expected rate of the Poisson distribution (top, orange line), together with the 96% highest density interval (hdi, light orange area) is superimposed on top of the observed spike counts. The expected rate tracks well changes in spike counts that are concomitant to changes in whisking setpoint. Time bin is 50 ms.

exemplify different ways of encoding the whisker position, namely, a monotonic increase or decrease of neuronal activity with whisker protraction (left to right bins), as well as a more localised change in activity around a certain whisker position. To describe this diversity at a population level, we attempted to cluster the tuning curves in groups that may be associated to different whisking encoding patterns. To do this, we first fitted a spline model with 7 cubic b-spline to each tuning curve in all recordings ( $n=508$ , 13 recordings): this allowed us to better capture the shape of the tuning curves by reducing variability due to noise (please see method section 3.2.8). Then, we used k-means clustering with  $k=5$  number of clusters on the smoothed tuning curves. The results are shown in Figure 3.12: on the top left is shown the sum of squared distances of each tuning curve from their cluster’s centre, which can be used to assess the possible number of existing clusters in the data; here, the sum starts to plateau after 7 clusters, meaning that  $k=5$  may be a conservative value. On the right is shown the projection of the tuning curves in the 3d space found using t-SNE, a non-linear dimensionality reduction technique; each dot (tuning

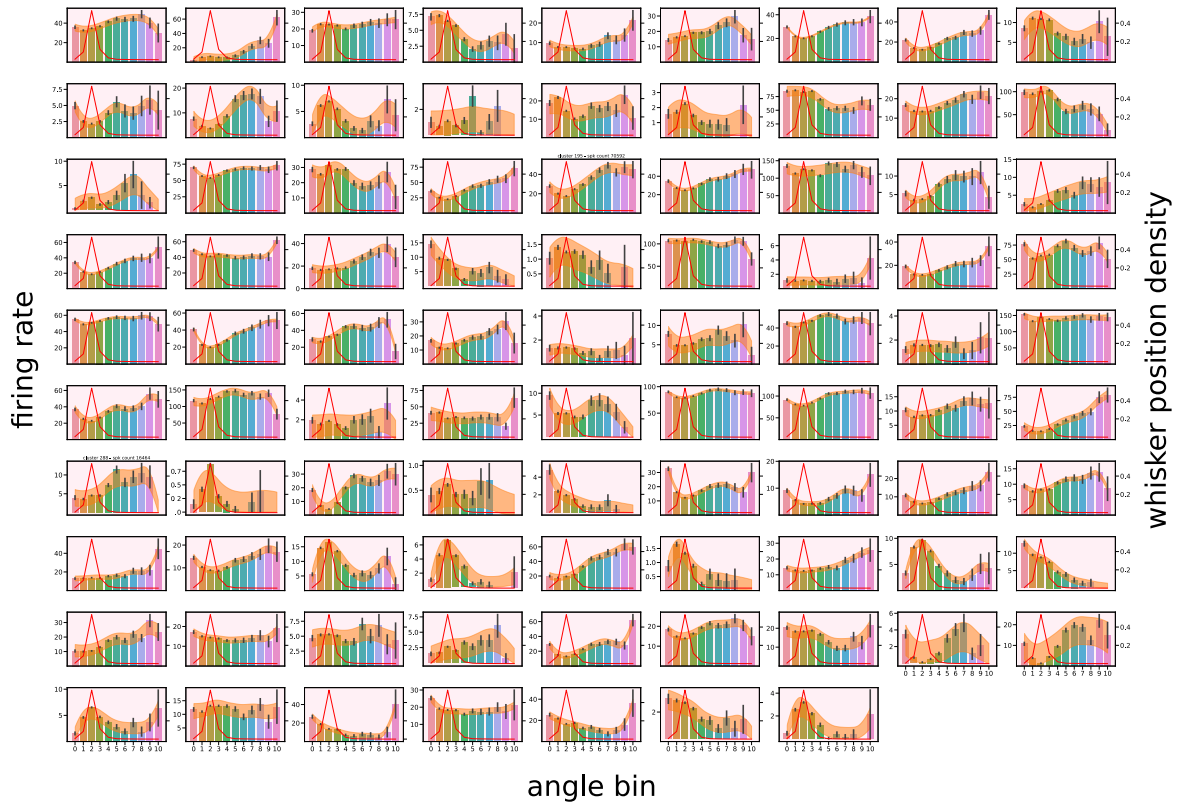


Figure 3.9: Tuning curves from one recording. The figure shows the firing rate tuning to whisker position of all units in one recording ( $n=88$ ): each colored bar is the firing rate of one unit (together with the standard error) associated to the corresponding whisker position, here discretised in 11 bins. The whisker position density (time spent on each position) is overlaid on top of the tuning curves (red line). To better characterise the shape of the tuning curves and reduce noise, we smoothed the tuning curves by fitting a spline model with 7 cubic b-splines to each tuning curve: the orange shaded area displays the highest density interval (hdi, 68%) of the posterior predictive sample for each tuning curve.

curve) is color-coded based on the cluster assigned to it by the k-means clustering: there seems to be a good correspondence between the output of the k-means clustering and the clusters that visually appeared using t-SNE, in the sense that clusters with the same color tend to be placed next to each other. Together, these results suggest the existence of heterogeneity in neuronal

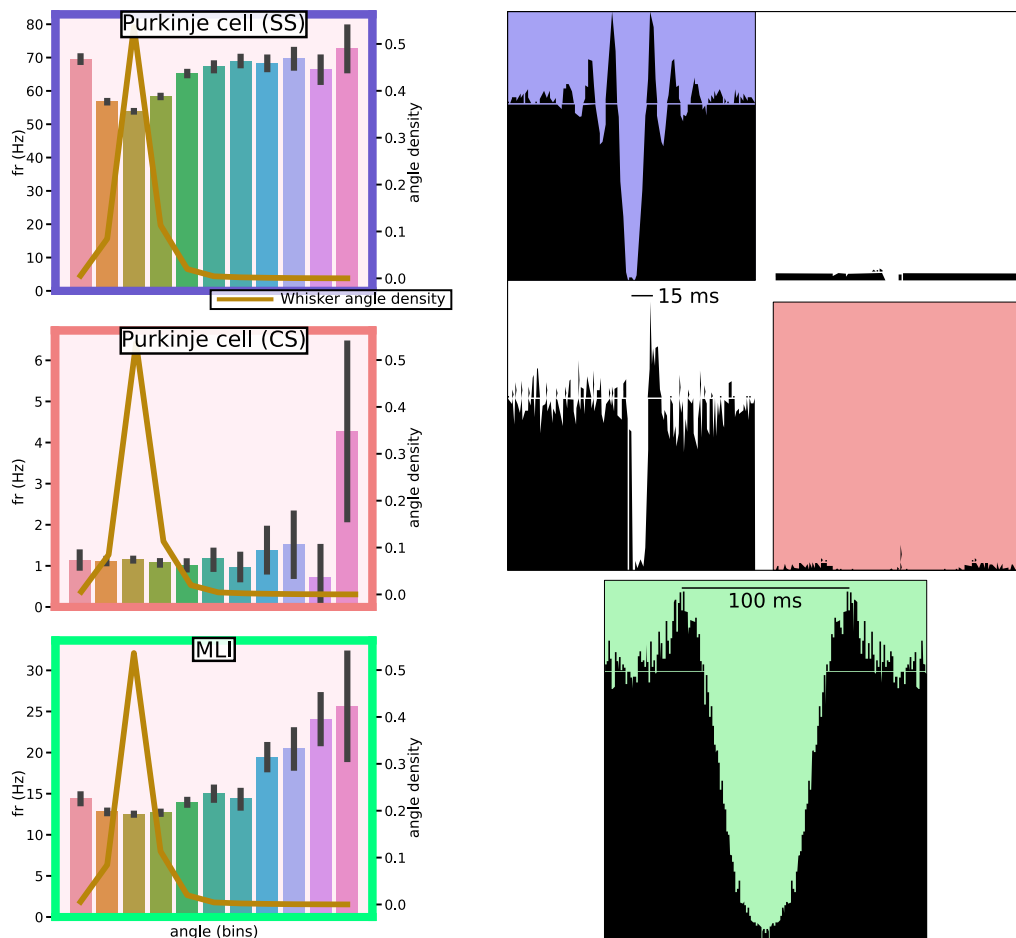


Figure 3.10: Example of unit tuning curves. Same layout as used for Figure 3.9, without hdi's. Three units with their respective tuning curves (left) and auto-/cross-correlogram (right) are shown. The three units are putatively assigned to different cell types or responses, namely, Purkinje cells simple spikes, complex spikes and molecular layer interneuron; a different box or background color is assigned to each. The assignment is based on their firing rates, the shape of their auto-correlogram, and temporal relationship of their activity displayed in the cross-correlogram.

tuning to whisking activity. Notably, there is no clear evidence of a change in sum-of-squared-distances decaying pattern, or elbow, which can be used as an indicator of the optimal number of clusters to be considered. Analogously, in the t-SNE space, different groups of clusters labeled with different colors do not appear to be completely isolated. Thus, this analysis does not appear to indicate a clear number of patterns used by cerebellar neurons to encode whisking activity; rather, it suggests that neurons form a continuum in the space of possible tuning curves.

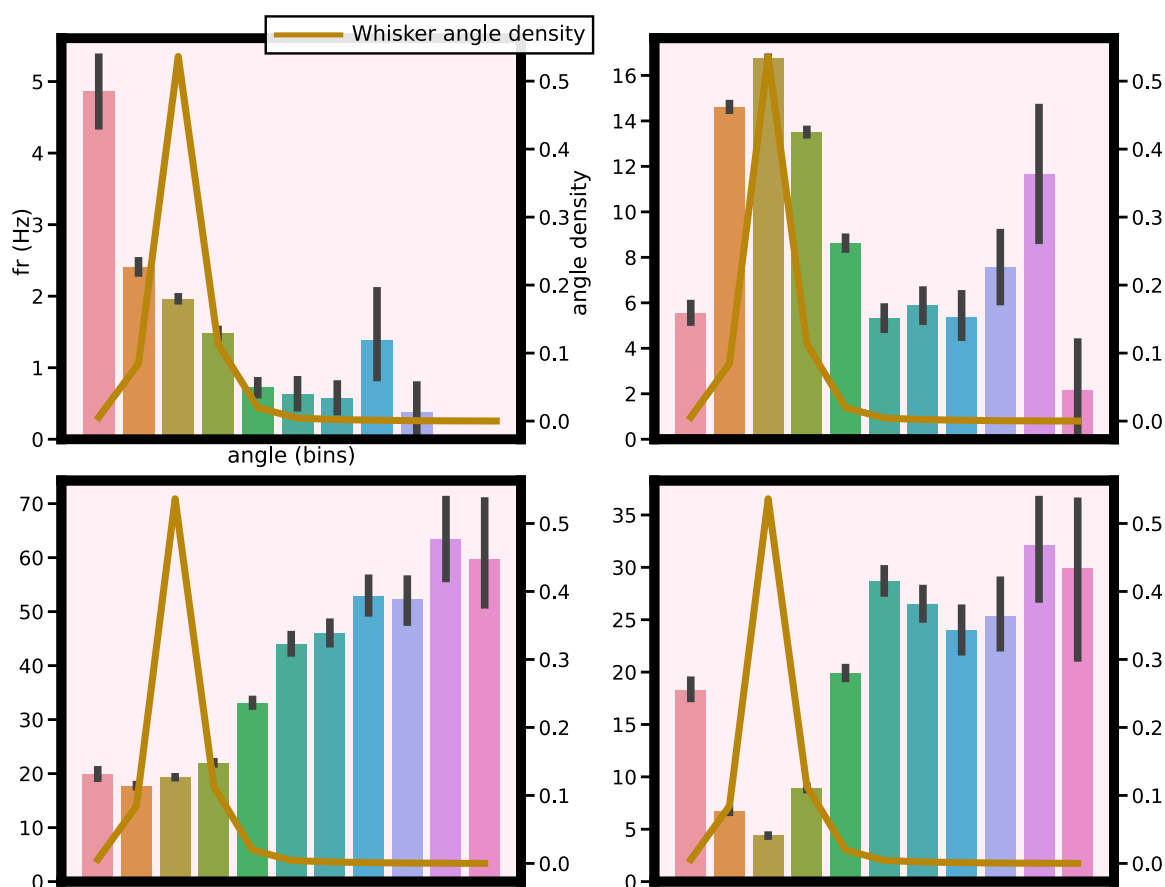


Figure 3.11: Tuning curve heterogeneity. Same layout as used for Figure 3.9, without hdi's. Four tuning curves, highlighting the heterogeneity in whisker encoding across units: they exemplify a monotonic decrease (top left), increase (bottom left), localised increase (top right) and decreased (bottom right) of activity with whisker protraction (left to right angle bis).

Finally, we investigated whether these groups reflect meaningful whisking encoding patterns across neurons, by visually inspecting the different tuning curve clusters. Figure 3.13 shows the same tuning curves displayed in Figure 3.9 (one recording) but now color-coded by group: the tuning curves show some consistency within groups, and can be distinguished from tuning curves belonging to other groups, although there is also some overlap. When visually inspecting the same examples shown in Figure 3.11 (indicated with a black background), it appears that the clustering procedure distinguished units that increase their firing rate with whisker protraction from units showing the reverse pattern, and possibly distinguished units based on more subtle differences in their tuning curves. Altogether, these results suggest that cerebellar cortical neurons can

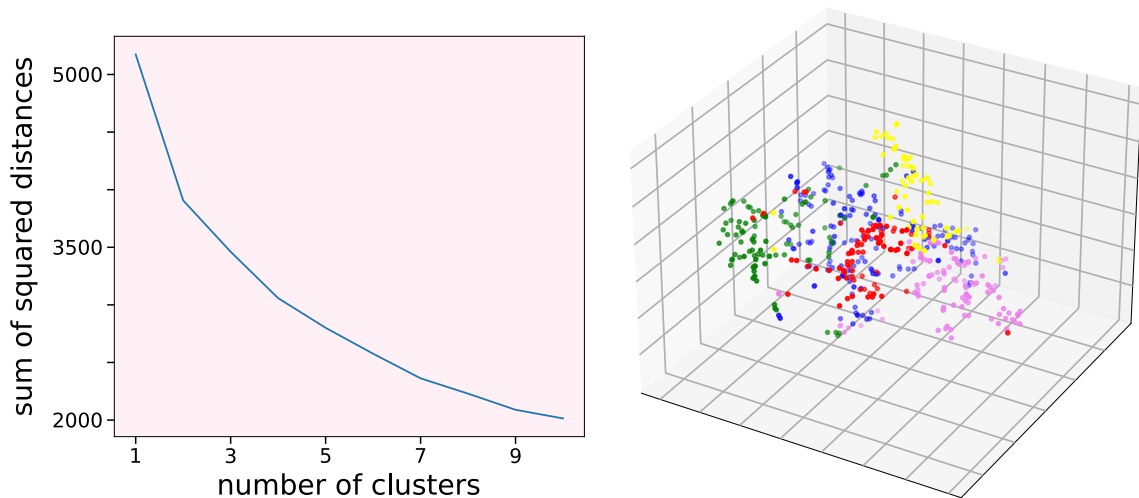


Figure 3.12: Tuning curve clustering. We used k-means clustering on the smoothed tuning curves (spline fit of the original tuning curves) to investigate whether there exist different groups in the tuning curve data. Left: the sum of squared distances of each tuning curve ( $n=508$ , all units from 13 recordings) from their cluster’s centre as a function of the number of clusters used to group the tuning curves. This metric can be used to judge the quality of clustering at the expense of model complexity (number of clusters): here the quality of clustering increases at least up to 7, after which it starts to plateau, which may justify the use of up to 7 clusters. Top right: all tuning curves were projected in a 3d space using t-SNE; the colors indicate the clusters found by the k-means algorithm, using 5 clusters: there seems to be a good correspondence between the output of the k-means clustering and the clusters that visually appear using t-SNE. This suggests the existence of different clusters in the tuning curve data.

display heterogeneous encoding of whisking position, which may support accurate behavioural representations at the population level.

### Neuronal populations preferentially represent upcoming whisking activity with a distributed code

To examine neuronal representations of whisking activity at the population level, we used principal component analysis (PCA), retaining the 3 principal components (pc’s) (Figure 3.14, please see method section 3.2.9). The analysis was restricted to whisking trials (-2 to +3 seconds from whisking onset), during which changes in neuronal activity are more likely to be associated to whisking behaviour. Figure 3.15 shows the results of this analysis for one recording ( $n=22$  units), focusing on a -0.5 to 1 subtime window around whisking onset for visualisation purposes: at the

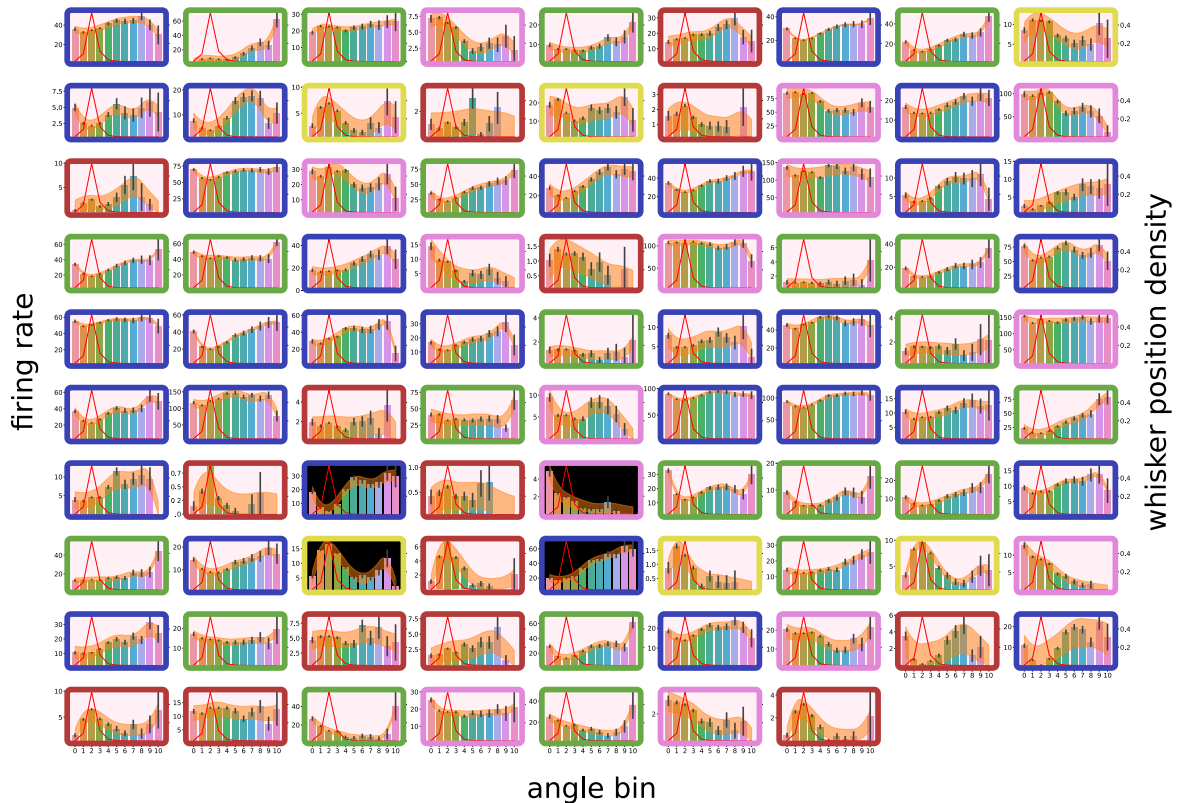


Figure 3.13: Tuning curve subgroups are associated to different whisking encoding patterns. We tried to relate the tuning curve subgroups found with k-means clustering ( $k=5$  number of clusters) to different whisking encoding patterns. Displayed are the same tuning curves as in Figure 3.9, but color-coded based on the output of the k-means clustering. The groups show some internal consistency, and can be used to distinguish different tuning curve patterns, but they also show some overlap. Comparing the tuning curves used in Figure 3.11 (highlighted by a black background), for example, shows that the clustering procedure can distinguish units that increase their firing rate with whisker protraction from units showing the reverse pattern; moreover, these examples show that k-means clustering can also distinguish between units based on more subtle features of their tuning curve. Overall, unsupervised clustering of tuning curves suggests that neurons in the lateral cerebellar cortex can display different profiles of whisking encoding.

top is shown the projection of the trial-averaged population activity onto the first three eigenvectors (left, average pc's), as well as the projected activity during a single trial (right, single trial pc's); at the bottom is shown the whisking activity during the same trial. Time is color-coded. These plots show that the pc's, both on average and at a single trial level, appear to have a clear structure in neuronal space during both behavioural quiescence and activity. This struc-

ture in turn suggests that population activity may contain accurate information about whisking dynamics.

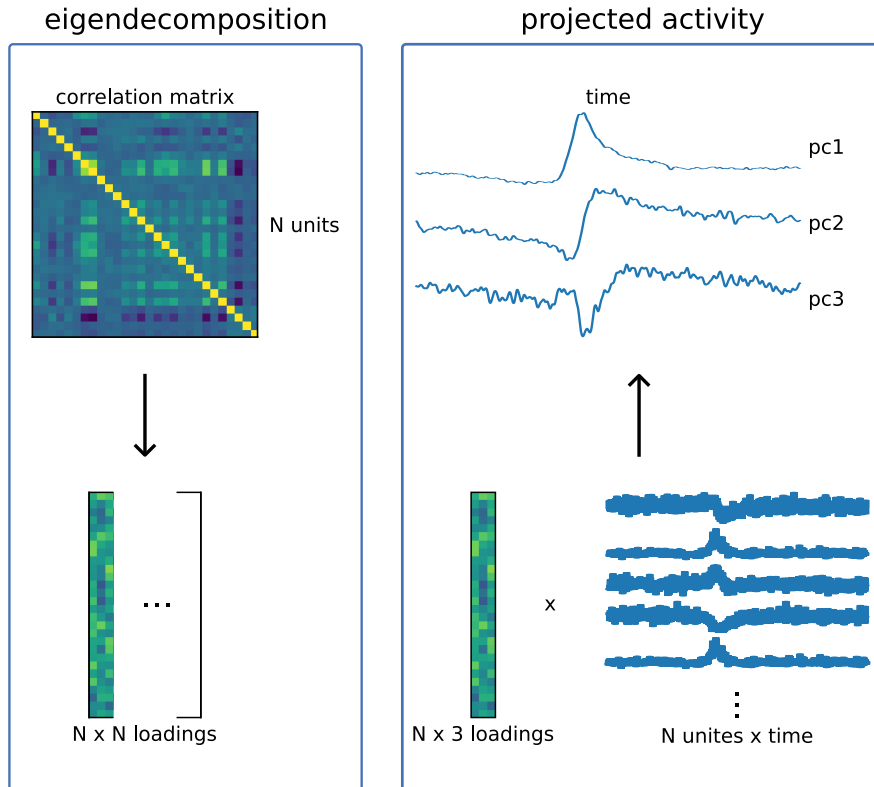


Figure 3.14: Extraction of the first 3 principal components. Left: we calculated the  $N \times N$  correlation matrix from the  $N$  unit's average responses, aligned to whisking onset. We then used the eigendecomposition of the correlation matrix to extract the  $N$  eigenvectors, sorted by their corresponding eigenvalues. The eigenvalues report how much variance is captured by each eigenvector; the  $N$  components of an eigenvectors are called loadings, and express the contribution of single units to total variance captured by the eigenvector. Right: we retained the first 3 eigenvectors to describe population activity with the first 3 principal components.

To better quantify this relationship, we computed the normalised cross-correlation between the average angle and the first 3 average pc's. Figure 3.16 shows the cross-correlation for each pc, together with its absolute peak (time indicated by a vertical line), for one recording: in this case, information related to whisking activity contained in pc1 tends to anticipate movement, whereas information in pc2 and 3 tends to lag behind behaviour. We then repeated the analysis for all recordings ( $n=12$ ). The distribution of cross-correlation peaks for each pc is shown in Figure 3.17:

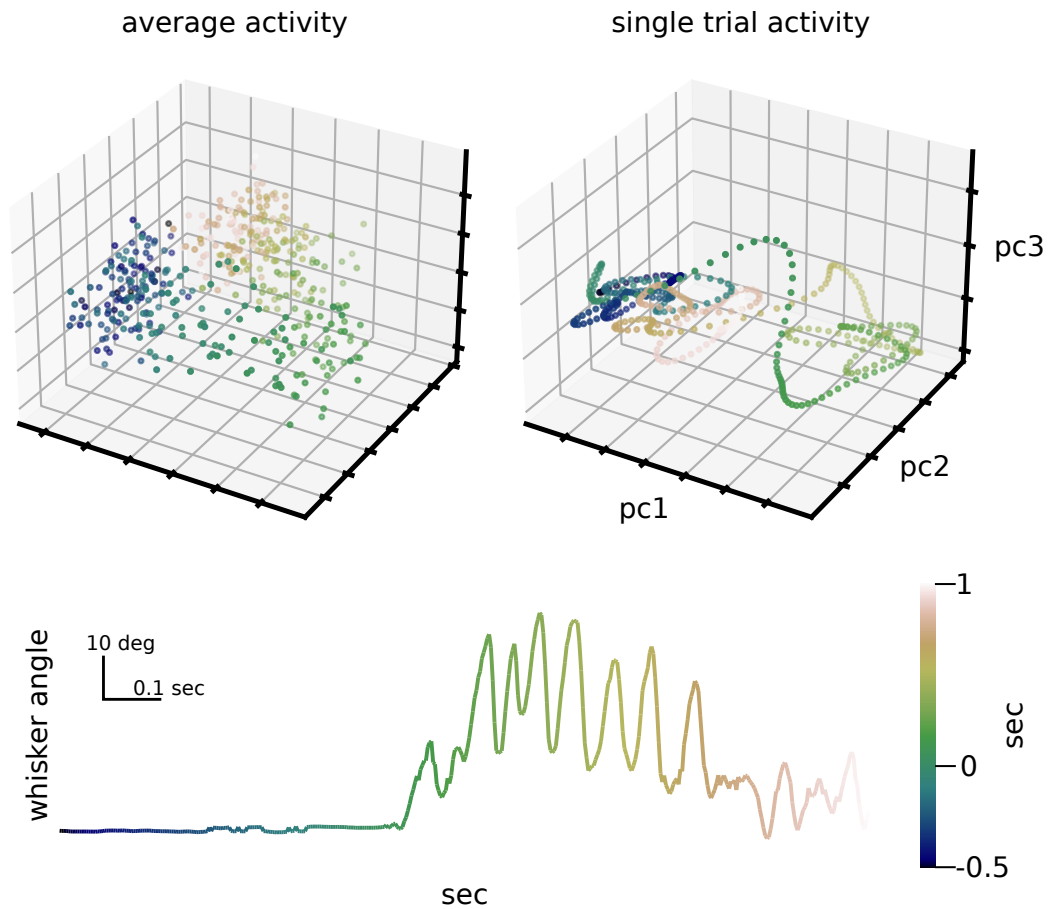


Figure 3.15: Projected population activity. PCA was used to extract the axis along which the population activity varies the most. Here are shown the results for one recording. The time, spanning 1.5 second length for each trial (-0.5 to +1 seconds from whisking onset), is color-coded. In the top left is shown the population activity averaged across trials in the PCA space, using the first three eigenvectors; in the top right is displayed the activity during a single trial (computed from smoothed spike counts); at the bottom is shown angle dynamics for one whisker during the same trial. The population activity, both in the trial shown and on average, tends to live in a confined space during quiescence (beginning and end of trials), while wondering in a seemingly structured manner during whisking activity.

all peaks for pc1 fall after whisking onset, indicating that, across recordings, variation in the whisking-aligned average neuronal activity expressed by the first pc tends to anticipate behaviour (one sample t test,  $t=4.71$ ,  $p=0.0006$ ,  $\text{mean}=36$  ms). On the other hand, the peaks for pc2 almost



always fall before whisking onset, indicating that whisker-related information contained in pc2 tends to lag behind whisking activity ( $t=-4.44$ ,  $p=0.009$ ,  $\text{mean}=-194$  ms). Finally peaks for pc3 have a distribution that includes 0 ( $t=-1.44$ ,  $p=0.17$ ,  $\text{mean}=-92$  ms). Notably, the peaks across recordings associated with the first pc are narrowly distributed in time; this may suggest that the first pc, specifically, contains precise information about whisking behaviour, and in particular behaviour occurring within  $\sim 40$  ms in the future.

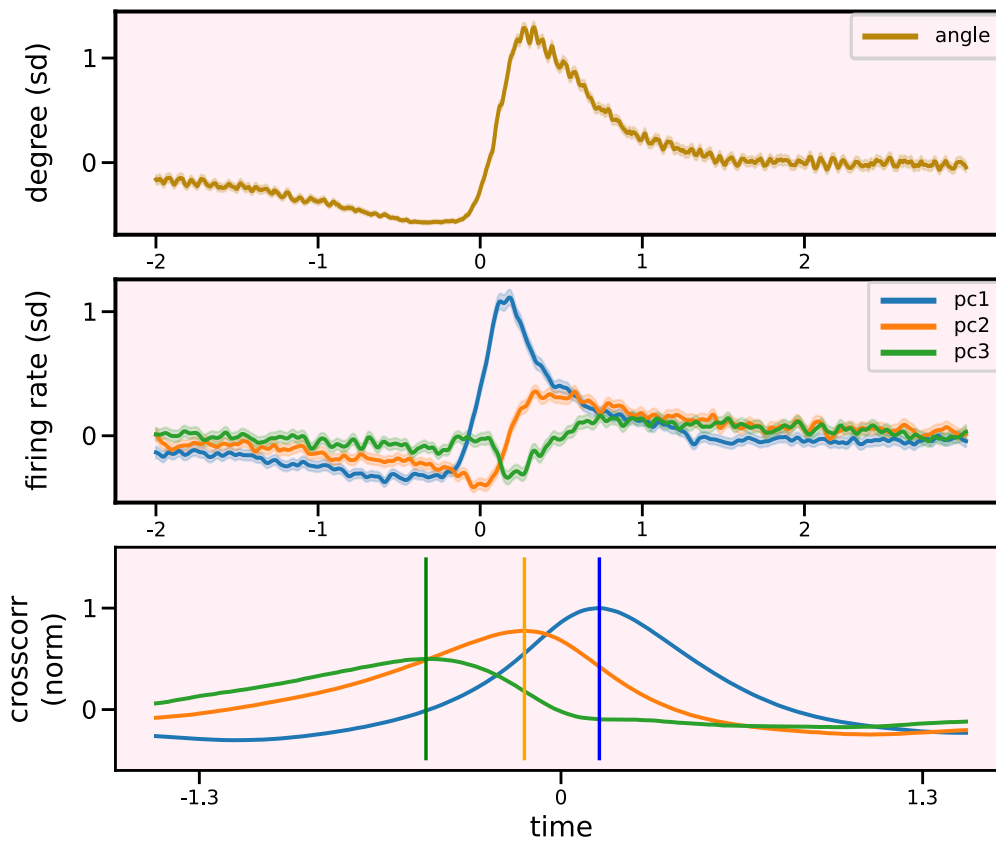


Figure 3.16: Neuronal activity-angle cross-correlation. Top: trial-averaged whisker angle with standard error. Middle: projection of the trial-averaged population activity onto the first three eigenvectors, with the standard error (computed from single trial pc's). Bottom: normalised cross-correlation between average angle and projections; positive times correspond to the shift of the time of whisking with respect to the time of neuronal population dynamics. Thus, the cross-correlation shows that neuronal activity captured by pc1 tends to correlate more with the upcoming whisking position; on the other hand, population activity described by pc2 tends to contain information lagging behind behaviour; as for pc3, the distribution of peaks include 0.

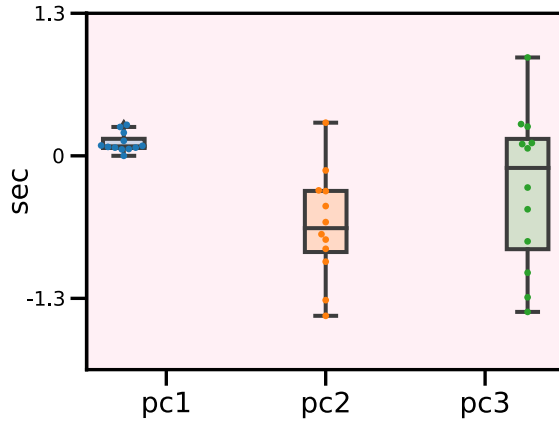


Figure 3.17: Cross-correlation peaks. Each dot is the peak for one recording (total  $n=12$ ) of the cross-correlation between the first three principal components (pc) and average whisker position. The box of the boxplots shows the quartiles (including 50% of data), whereas the whiskers show the entire distribution. The average for pc1 is positive (one sample t test,  $t=4.71$ ,  $p=0.0006$ ,  $\text{mean}=36$  ms), indicating its tendency to precede whisking behaviour; instead, pc2 peaks show the opposite trend, by lagging after behaviour ( $t=-4.44$ ,  $p=0.009$ ,  $\text{mean}=-194$  ms), whereas the distribution of pc3 peaks includes 0 ( $t=-1.44$ ,  $p=0.17$ ,  $\text{mean}=-92$  ms). The distribution of peaks for the first pc are concentrated around the mean; this indicates that the information contained in the first pc is particularly time locked to whisking behaviour, and therefore may represent this behaviour more accurately than information in other pc's.

For this recording, the first three eigenvalues accounted for only a moderate amount of the total variance in the population activity ( 30%), and we found similar results in all recordings (Figure 3.18). Therefore the first three pc's provided only a coarse description of population activity, which suggests that neuronal dynamics were quite heterogeneous. This analysis was performed on data restricted to the initial period of whisking activity, during which population dynamics, described by the first 3 pc's, well reflect whisking behaviour. Thus, the fact that a large portion of neuronal variability was not captured by the first 3 pc's strengthens the general idea that the cerebellar cortex integrates information about different behaviourally relevant variables at all times.

The whisker-related information contained in each pc can originate from few units in the population, whose activity may be particularly responsive to whisking; alternatively, the information could be more distributed, whereby each unit contributes to some extent to the population en-

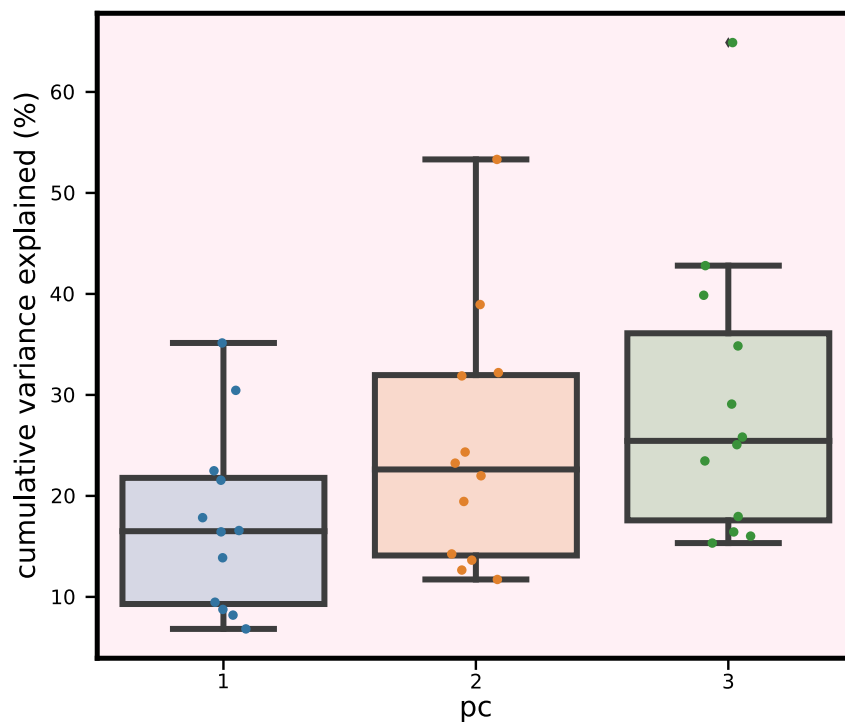


Figure 3.18: Variance explained by the first 3 principal components. We computed the cumulative variance explained by up to the third principal component. Notably, pca was computed on data restricted to the initial period of whisking, and therefore the first 3 pc's well reflected whisking behaviour. However, the total variance explained by the first 3 pc's was modest, and therefore population activity could not be exhaustively explained in terms of variability along these three orthogonal axes in neuronal space. This in turn suggests that neuronal dynamics in the lateral cerebellar cortex, at all times, encodes different types of information.

coding of behaviour. To measure how much behavioural information is distributed across units, we used the pc loading of each unit, indicating the contribution of a unit to the corresponding pc (please see method section 3.2.9). Figure 3.19 shows for each pc the loading of the units from all recordings ( $n=517$ ). The loading distribution for each pc is centred around 0 and is roughly symmetric, meaning that units can contribute both positively or negatively to each pc. The number of outliers in each distribution can then be used to quantify how much each pc is dominated by the activity of few units. We therefore calculated the excess kurtosis of each distribution, which is a measure of the frequency of outliers observed, using as a point of reference the frequency expected from normally distributed data. The distribution for the first pc has an excess kurtosis of -2.76, indicating infrequent outliers; this in turn suggests that the contribution of units across recordings to the first pc is fairly distributed. In contrast, the excess kurtosis for the third pc is 4.97, indicating a high frequency of outliers, and therefore of units which tend alone to contribute mostly to the third pc. The excess kurtosis for the second pc is instead -0.43, meaning that outliers are neither frequent nor infrequent. Thus, these results suggest that for the first pc, which reflects more accurately whisking behaviour, information is quite distributed across units.

Finally, we focused on how well population activity represents whisking information at a single trial level. Linearly combining the first three principal components, it was possible to decode whisking setpoint during a single trial (Figure 3.20, please see method section 3.2.10). In this analysis, neuronal data were augmented in time by shifting the projections by lags of approximately 0, -30, -70, -100, -130 ms, so that population activity up to 130 ms prior to whisking movement could be used to predict the latter. In summary, these results show that the population activity in the lateral cerebellar cortex, even when approximated within a low-dimensional space, accurately reflects upcoming slow whisking dynamics.

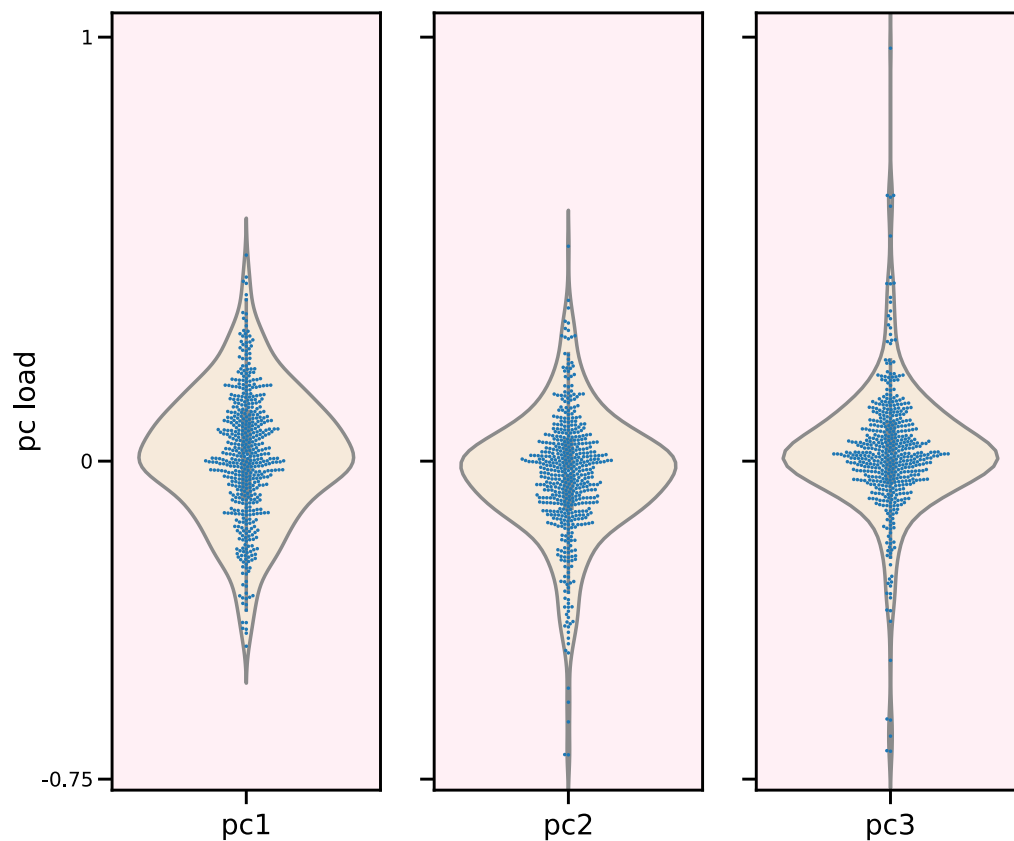


Figure 3.19: Principal component loads. Each dot is the load of one unit on the corresponding principal component (pc). Here we aggregated units from all recordings ( $n=12$ , total units 517). The violinplots show the distribution of the loads for each pc. The distribution for the first pc has an excess kurtosis of  $-2.76$  (platykurtic distribution), therefore the frequency of outliers (dots far from the mean) is low compared to what is expected from a gaussian distribution. This in turn means that the contribution to the first principal component is fairly distributed across units. For the third pc, instead, the excess kurtosis is  $4.97$ , which indicates a high frequency of units that alone contribute for the most part to the third pc. The excess kurtosis associated to the second pc, instead, sits close to  $0$  ( $-0.43$ ), meaning that the frequency of outliers is neither high nor low.

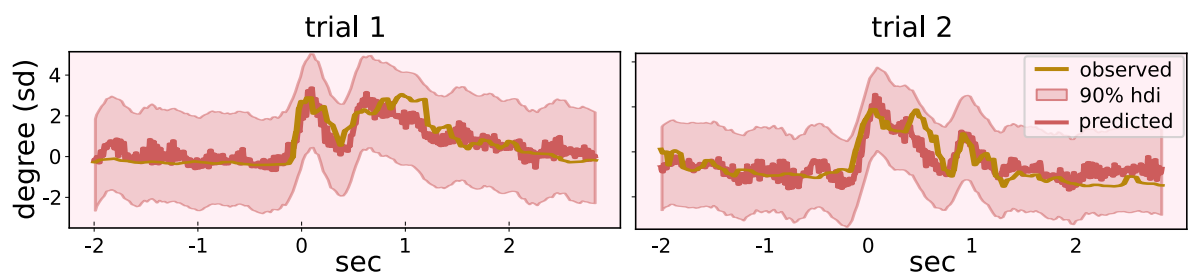


Figure 3.20: Setpoint decoding from neuronal population activity. Reconstruction of the whisking setpoint using a linear combination of the first three pc's; pc's were augmented by repeating them shifted with different time lags (0, -30, -70, -100, -130 ms). Here we show the setpoint (brown line) during two trials, together with the predicted setpoints (red) and the highest density interval (hdi, red shade). The results indicate that whisking activity can be accurately reconstructed using present and past information contained in the population activity.

### 3.3.2 Golgi cell manipulation

#### Testing topical drug application in the lateral cerebellar cortex

Next, we investigated how the manipulation of Golgi cell inhibition impacts whisking behaviour and its representations in the cerebellar cortex. In particular, we reduced Golgi cell inhibition via activation of inhibitory DREADDs; DREADDs were activated by dropping CNO on top of the recording site, a method that aimed to afford good spatial and temporal precision to our manipulation (please see method section 3.2.6). To our knowledge, this is the first time this method is used to manipulate activity in the cerebellar network.

To control for the dynamics of drug diffusion in the cerebellar cortex, we tested the effects of muscimol ( $1.665 \frac{\mu\text{g}}{\mu\text{l}}$  concentration in PBS) during recording in three mice. Muscimol was dropped on top of the recording site, similar to what is done in the experiment using CNO (please see method section 3.2.2). Muscimol is a potent  $GABA_A$  receptor agonist that causes a drastic reduction in cell activity. Figure 3.21 shows the results of this set of control experiments: the total spike count recorded across the cerebellar cortex, normalised by the count occurring at the time of muscimol application (0 time bin), started to decrease within minutes after drug administration, and reached its minimum within 10-30 minutes. These results thus show the viability of applying CNO topically onto cerebellar cortex.

#### Effects of reduced Golgi cell inhibition on coarse network activity

As the following step, we examined whether the CNO-dependent reduction in Golgi cell activity had an impact on the overall cerebellar cortical population activity. We therefore compared the dynamics of the total cortical spike count across experimental conditions, which included a condition with the manipulation of Golgi cell activity using CNO on Glyt2 mice ('gCNO', n=19 recordings), and two controls, one using CNO on wild-type mice ('wCNO', n=5 recordings), and the other using PBS on both wild-type and Glyt2 mice ('PBS', n=9 recordings). Notably, for all mice but one (n=16) we performed two recordings, which could belong to two different experimental conditions (e.g., using CNO or PBS on GLYT2 mice). (Please see Table 3.1 for a description of all data used in this analysis.) At the top of figure 3.22 is displayed the temporal evolution of the cortical spike count for each recording (n=33), with experimental conditions

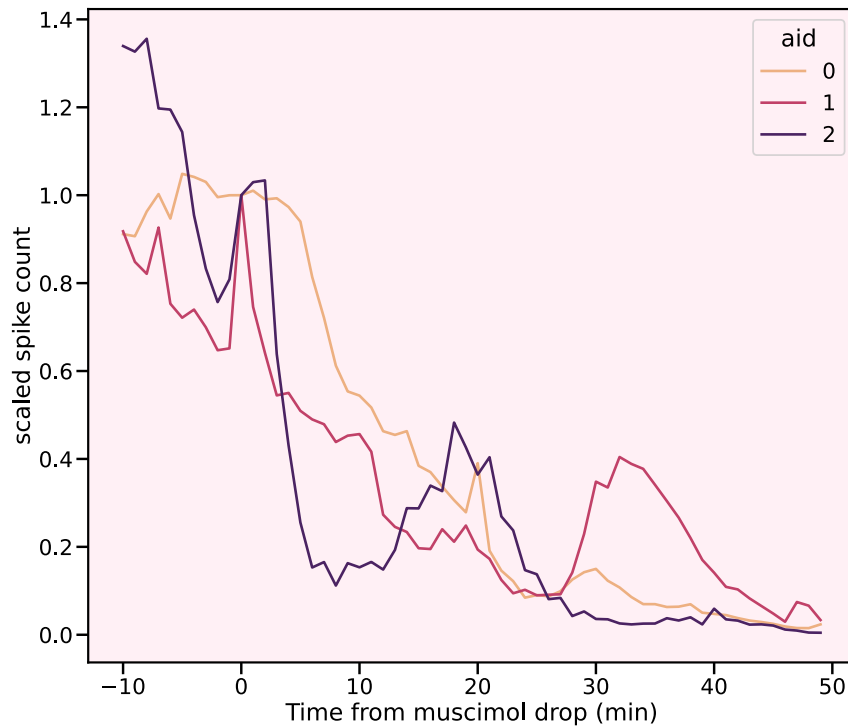


Figure 3.21: Muscimol reduces cortical population spike count. We tested the dynamics of drug diffusion in the lateral cerebellar cortex by topically applying muscimol in three wild-type mice while recording; line color denotes animal id. The plot shows the total cortical population spike count during 1 hour recording. The spike count is stable during baseline (first 10 minutes), then rapidly starts to drop within minutes, to reach a minimum around 10-30 minutes after muscimol administration, reflecting efficient diffusion of the drug. Occasional rebounds of activity were observed. Time bin width is 1 minute.

color-coded, and count computed within time windows of width 1 minute. At the bottom, instead, are displayed the same data scaled by the spike count occurring at -5 minutes from PBS/CNO drop, which helps to highlight different spike count dynamics between ‘gCNO’ and control conditions after drug application: in particular, the spike count in ‘gCNO’ recordings tends to increase compared to baseline. In order to test for evidence of an effect of the experimental manipulation, we therefore compared data pre and post CNO/PBS drop within each experimental condition, as explained below. For this analysis we used scaled spike count data computed with bins of width 5 minutes (Figure 3.23); this was done to average out variability in spike counts naturally occurring in a neuronal network, and to reduce the number number of parameters used in the analysis.



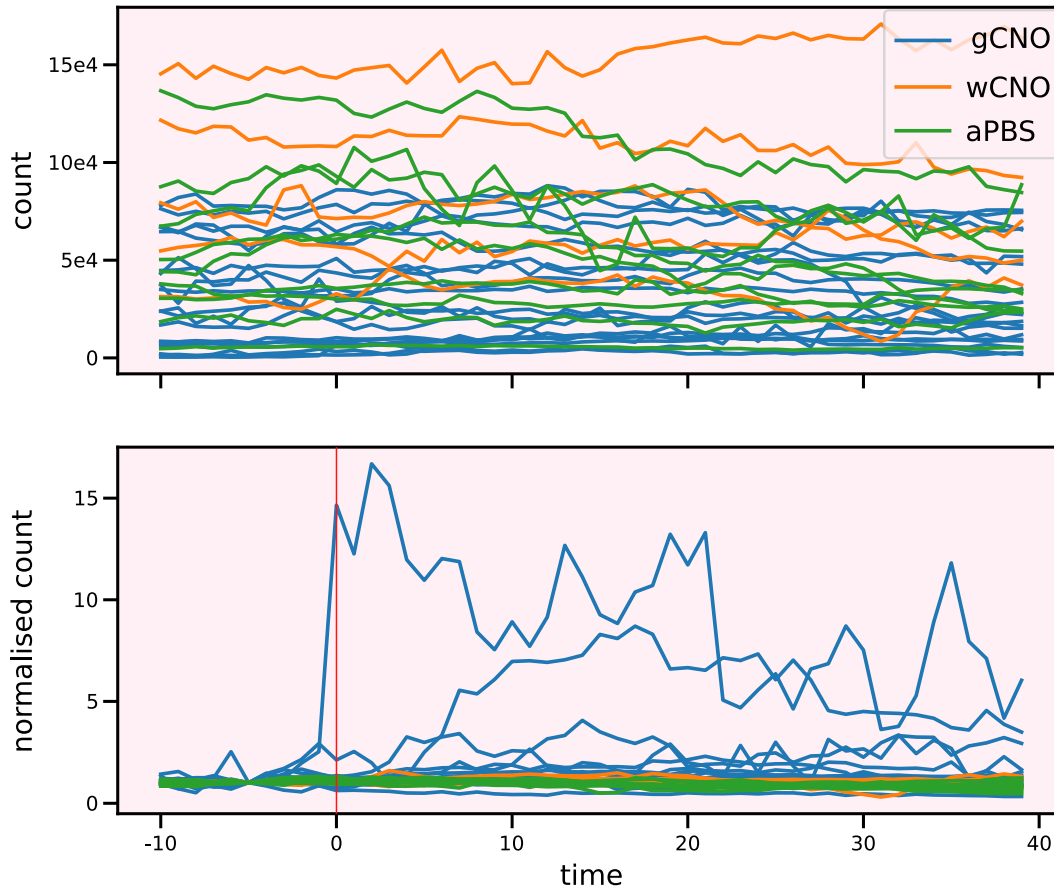


Figure 3.22: Spike count dynamics (bin width 1 minute). At the top is shown the dynamics of the spike counts for each recording ( $n=33$ ), color-coded by experimental condition. Counts were computed using bins of 1 minute width. At the bottom are shown the same data, but scaled by the count at -5 minutes from CNO/PBS drop (0 time bin). Vertical red line signals the 0 time bin.

In more detail, to explain the variance in the spike count observed across recordings that was possibly due to the experimental manipulation, we used a multilevel model (please see method section 3.2.11). The model described the distribution of spike counts for each time bin with an inverse Gamma distribution, parameterised by a shape parameter  $\alpha$  and a scale parameter  $\beta$ . The model used as explanatory variables the experimental conditions, associated to pre- and post-drop periods, to find the  $\alpha$  and  $\beta$  parameters that best explained the pre- and post-drop data. Therefore, for each parameter of the gamma distribution ( $\alpha$  and  $\beta$ ) and each condition ('gCNO', 'wCNO', 'PBS'), the model had a coefficient  $\theta$  associated to the pre-drop period and

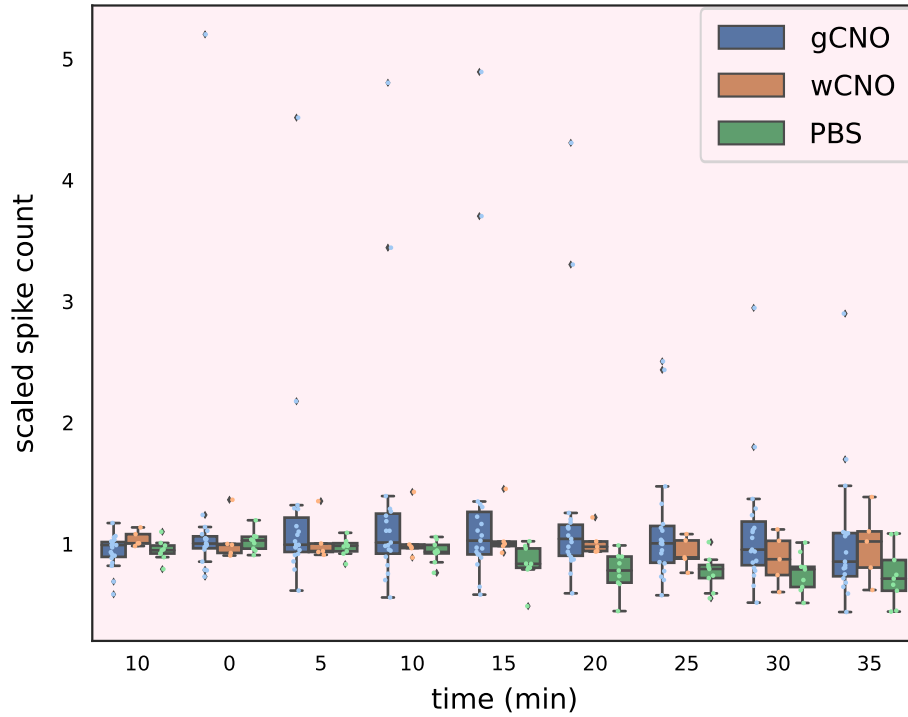


Figure 3.23: Spike count dynamics (bin width 5 minute). The spike counts for each recording (single dots,  $n=33$ ) are computed within bins of 5 minutes, and scaled by the count in the -5 minutes bin (not shown). The 0 bin includes the time of CNO/PBS drop. The underlying boxplots show the mean and quartiles of the distribution of spike counts for each time bin, while the whiskers extend to include the rest of the distribution, without covering outliers (beyond 1.5 times the IQR). These data were included in the statistical analysis used to check whether the experimental manipulation had an effect on population spike counts.

one for the post-drop period. The contrast between the two coefficients was then used to measure the change in spike counts due to the experimental manipulation.

The results are shown in Figure 3.24. On the left is shown the distribution of all spike counts observed, together with the model fit: the overlap between the two distributions indicates that the model was able to capture the overall structure of the data reasonably well. On the right, instead, are shown the contrasts between the model coefficients associated with the pre-drop and post-drop period (pre minus post samples). These contrasts reflect the effect of the experimental manipulation on spike count distribution for each experimental condition. For each experimental

condition there are two contrasts, one associated to the shape parameter  $\alpha$  and one for the scale parameter  $\beta$  of the distribution describing spike counts. Comparing the contrasts and highest density intervals (hdi, 94%) for the parameter across conditions reveals a specific effect of the CNO manipulation, and in particular an effect on the scale parameter,  $\beta$ , which describes the spread of observed spike counts.

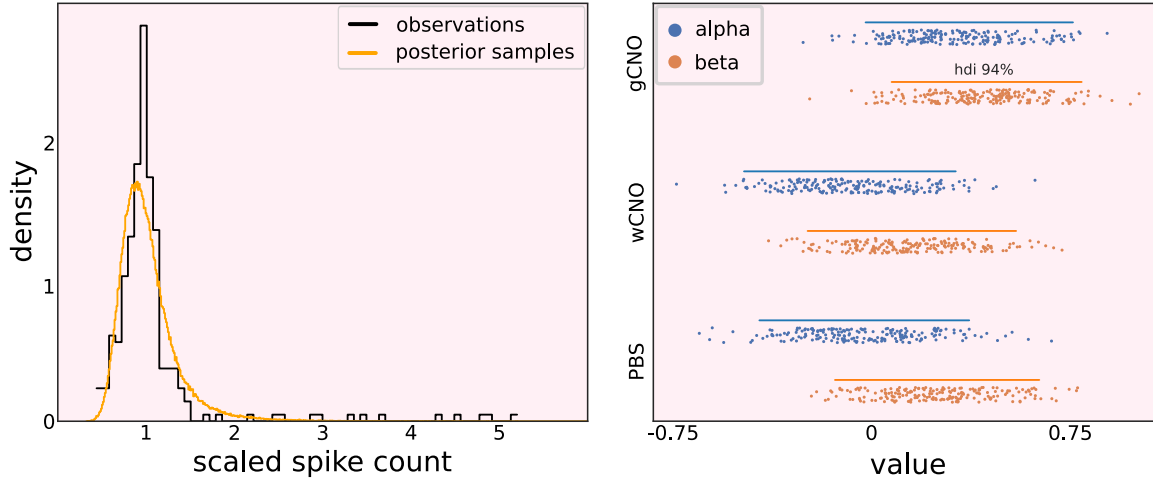


Figure 3.24: Statistical analysis of CNO application. We used a multilevel model to explain spike count variability: the model includes as explanatory variables the three experimental conditions, divided in pre and post drop (six in total), time and animal id. The left panel shows the distributions of posterior predictive samples and observations. These results show that the model is able to capture the distribution of observed spike counts. The right panel shows the contrast between experimental condition parameters associated with pre- and post-drop periods; for each condition there are two contrasts, associated to either the shape parameter  $\alpha$  or scale parameter  $\beta$  of the inverse Gamma distribution used to describe the spike counts. Comparing the contrasts and highest density intervals (hdi, 94%) for the shape and scale parameter across conditions reveals a specific effect of the CNO manipulation on observed spikes, and especially on the spread of their distribution.

To gain a better intuition of the implications of these results, we used the posterior samples of the  $\alpha$  and  $\beta$  to derived samples for the variance parameter of the inverse Gamma distribution; the variance, indeed, offers an alternative parametrisation that characterises more intuitively the spread of spike counts pre- and post- drug application (please see supplementary section 3.2.11 for more details). Figure 3.25 shows the contrasts between post- and pre-drop variance samples (post minus pre samples) for each experimental condition. These contrasts show that

the variance tends to increase after drug application in the ‘gCNO’ condition, whereas it remains stable in the two control conditions. Thus, these results suggest our manipulation of Golgi cell inhibition made high population spike counts more likely.

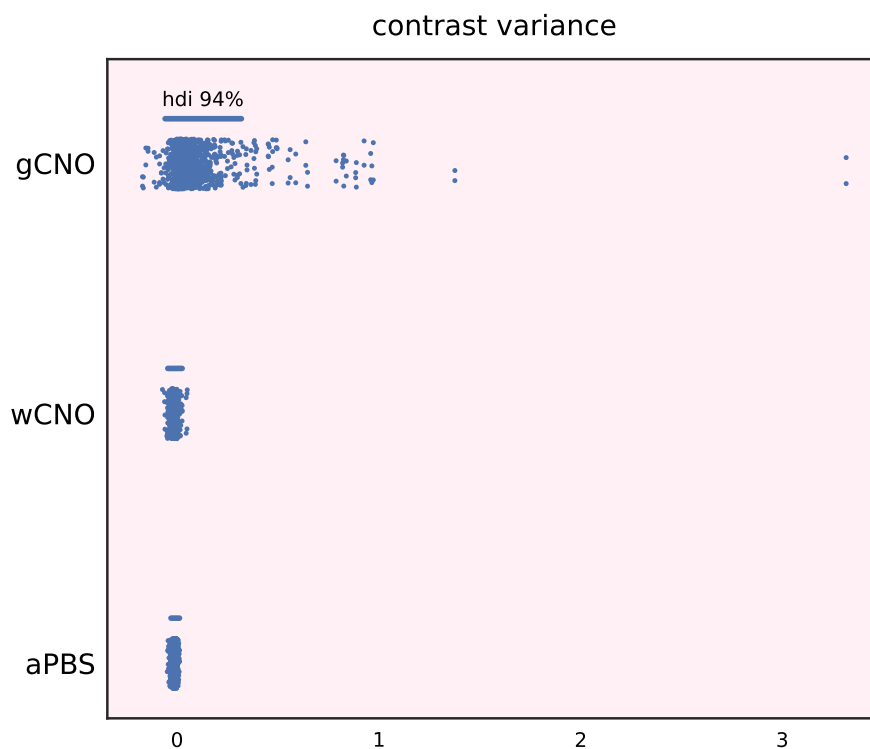


Figure 3.25: Inverse Gamma variance contrasts. We compared the pre- and post-drop posterior samples of the variance parameter of the inverse Gamma distribution, used to describe the distribution of observed cerebellar cortical spike counts. These samples were derived from the samples of the  $\alpha$  and  $\beta$  using the identity  $var = \frac{\beta^2}{(\alpha-1)^2(\alpha-2)}$ . The contrasts show that the application of CNO in GlyT2 tends to increase the variance of population spike counts (although the highest density interval, hdi 94%, crosses 0). In other words, elevated spike counts were more likely after CNO administration.

Based on these results, in subsequent analyses we pooled the ‘wCNO’ and ‘PBS’ condition in one ‘control’ condition to increase power of the analyses. In addition, because in these analysis we also used whisking behaviour, we discarded 8 recordings with no or poor whisking behaviour, for a total of 25 recordings left (please see Table 3.1).

### 3.3.3 Contribution of Golgi cells to whisking representations

#### Effects of reduced Golgi cell inhibition on network dynamics

To describe in more detail how decreasing Golgi cell inhibition may affect whisking representations in the cerebellar cortex, we compared the trial-averaged PETH and average whisking activity from pre- and post-drop data, defined respectively as baseline data and data acquired after CNO/PBS application (please see method section 3.2.12). Figure 3.26 shows the comparison for one recording (‘gCNO’ condition), with pre- and post-drop data shown respectively at the top and bottom of the figure. In this recording, the post-drop whisking activity (brown line) appeared to be faster on average during the initial protraction period, while neuronal responses tended to be more aligned with each others; this alignment becomes more evident when taking in consideration the absolute peak in activity for each unit (violet dots) and comparing the pre- and post-drop temporal dispersion of these peaks; peaks were computed within a subwindow focusing on the initial whisking period (-0.7 to 1.3 sec), and used as a proxy of the timing of the neuronal response to whisking-related input to the network.

To follow up these observations, we first checked whether reduction in Golgi cell activity may have an effect on the dispersion of neuronal activity aligned to whisking onset, using data from all recordings ( $n=25$ ) and comparing the two experimental conditions (‘gCNO’ and ‘control’). To this end, we computed for each recording the standard deviation (std) of the distribution of peaks, for both pre- and post-drop periods (please see method section 3.2.13). The std’s are shown in Figure 3.27: notably, only in the ‘gCNO’ condition the pre- and post-drop distribution of the recordings std’s are different (two-sided Wilcoxon signed-rank test,  $T=12$ ,  $p=0.017$ ). Moreover, comparing the two experimental conditions, in terms of the mean and variance of the normal distributions fit to the post-pre drop contrasts, also highlights a change in the std of the spread of peaks of neuronal activity due to Golgi cell manipulation (Figure 3.28). In more detail, these results suggest that decreased Golgi cell inhibition has an impact on the temporal heterogeneity or dispersion of neuronal responses around the onset of whisking activity, and in particular reduces it.

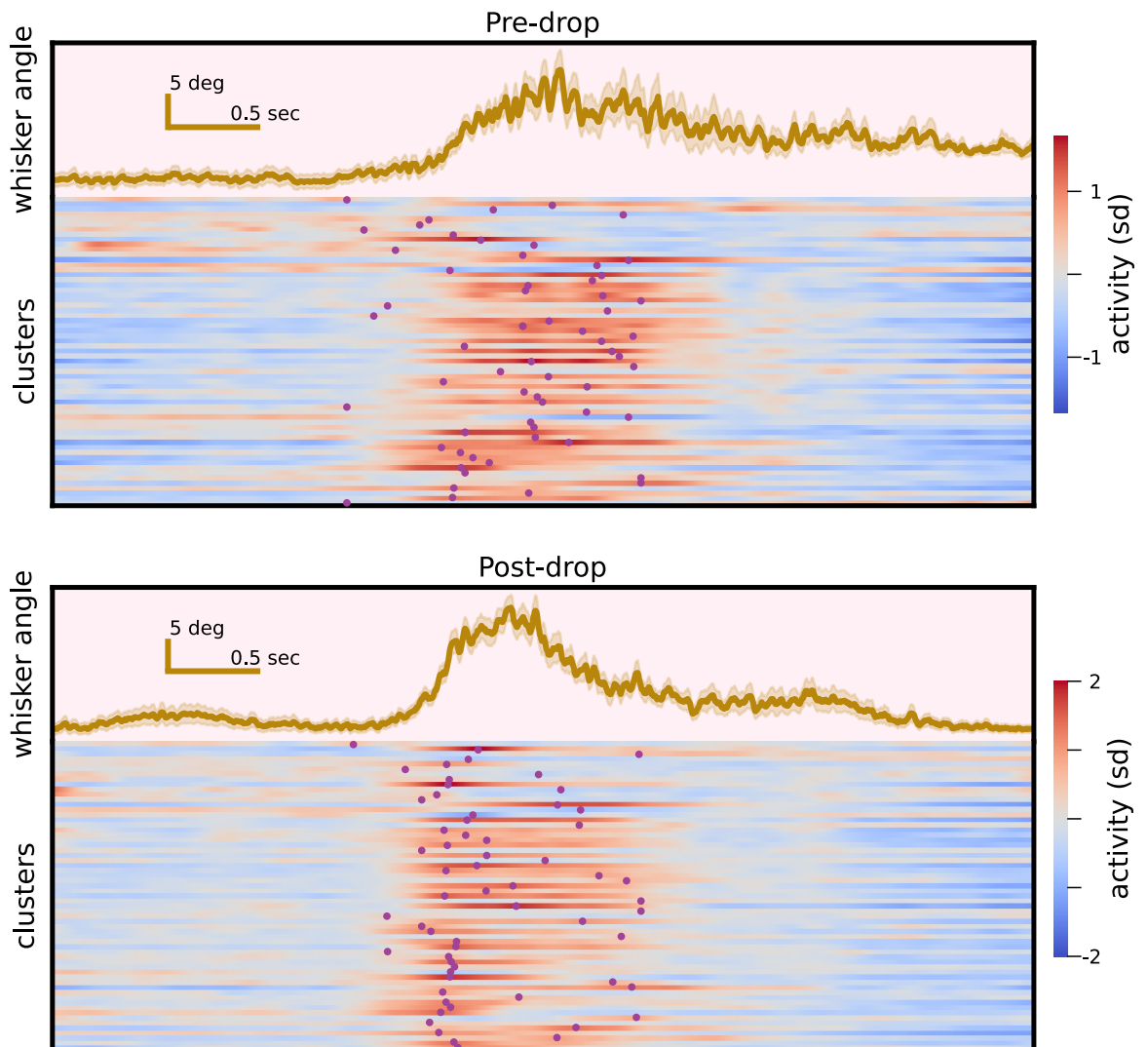


Figure 3.26: Comparison of average whisking and neuronal activity pre- and post-drop. Same analysis as for the PETH in Figure 3.7, with neuronal activity aligned to the onset of whisking bouts. Top: PETH from one recording before CNO application in a GlyT2 mouse, and associated mean whisking activity. Bottom: average activity after CNO application. In this recording, Golgi cell manipulation seems to fasten the average initial whisking protraction, while increasing the alignment of average neuronal activity. Violet dots indicate the absolute peak in activity for each unit within a subwindow ranging from -0.7 to 1.3 seconds centred around whisking onset.

### Effects of reduced Golgi cell inhibition on whisking dynamics

Then, we addressed the possible effects of Golgi cell manipulation specifically on velocity of whisking protraction (please see method section 3.2.14). To this end, for each recording we used

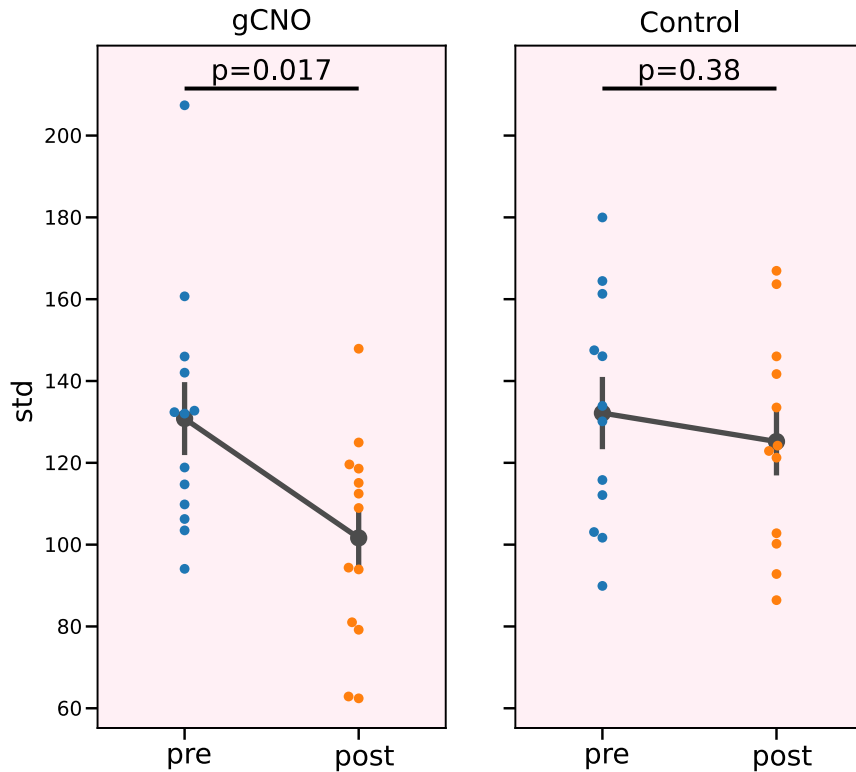


Figure 3.27: Comparison of the std's of absolute peaks in neuronal activity pre- and post-drop. For each recording ( $n=25$ ), we computed the standard deviation (std) of the distribution of the absolute peaks of the units' activity aligned to whisking onset (violet dots in Figure 3.26 for one recording). The peaks were used as proxy for the timing of a neuron's response to its input. The left and right plot shows the results for the 'gCNO' and control condition, respectively. Blue and orange colors are used to label pre- and post-drop data, respectively. Only the pre-drop std's in the 'gCNO' condition are systematically different than those in the post-drop condition (two-sided Wilcoxon signed-rank test,  $T=12$ ,  $p=0.017$ ). These results suggest that decreased Golgi cell inhibition reduces heterogeneity in the timing of units' whisking-related responses on average.

a linear model to approximate the slope of the average whisking activity during its protraction phase (Figure 3.29, orange area); the coefficient for each linear fit was thus used as a proxy for the velocity of average pre- and post-drop whisking protraction. The comparison between post- and pre-drop slopes, in terms of their difference (post-drop minus pre-drop slope), is shown on the left of Figure 3.30 for the two experimental conditions: the differences are centred around 0 in both cases, but the variance in the 'gCNO' condition is different from that in the 'control'

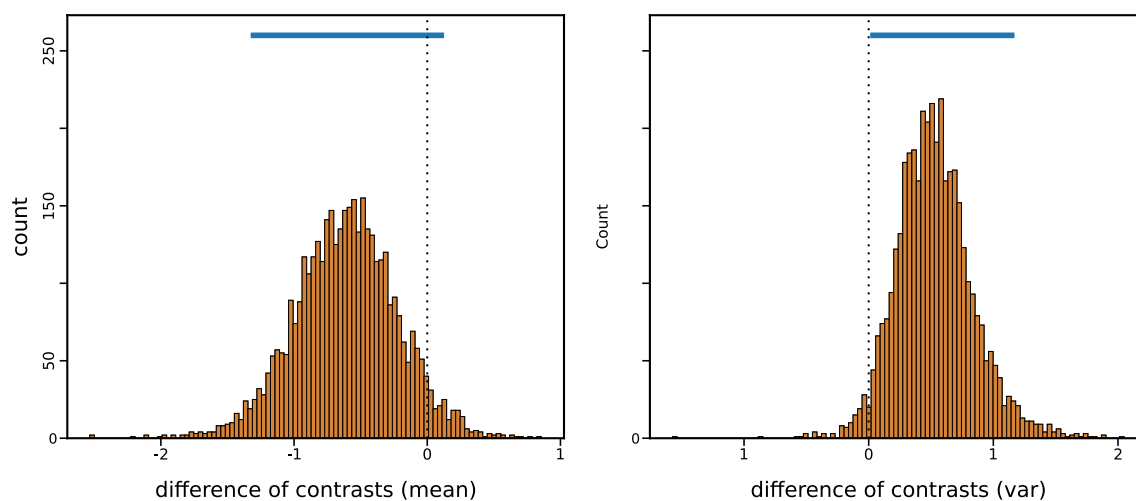


Figure 3.28: Difference between conditions in post-pre contrasts of std of absolute peaks in neuronal activity. For each recording in the ‘gCNO’ and ‘control’ conditions, the post-pre contrasts of the std was computed. The distribution of contrasts for the two conditions was then fit with a gaussian distribution, and the difference in posterior samples for the mean (left) and variance (right) are shown. The 94% hdi for the mean include 0, but there is a tendency for the post-pre drop contrasts in the ‘gCNO’ condition to be more negative than those in the ‘control’ condition. As for the variance, the hdi does not include 0, indicating stronger evidence for a difference between the two conditions: in particular, in the ‘gCNO’ condition the contrasts can take bigger values. Overall, these differences in contrasts suggest a change in the std of absolute peaks in neuronal activity, with std being smaller in the ‘gCNO’ condition.

condition (Levene’s test  $W=8.39$ ,  $p=0.008$ ). The (0-mean) slopes obtained from each linear fit are instead displayed on the right: in the ‘gCNO’ condition (top), there is less overlap between pre- and post-drop slopes, compared to that in the control condition (bottom). These results thus suggest that reduced Golgi cell activity leads to average changes in whisking protraction dynamics that are more pronounced than what can be observed in absence on a manipulation, in which case the dynamics remain instead relatively constant.



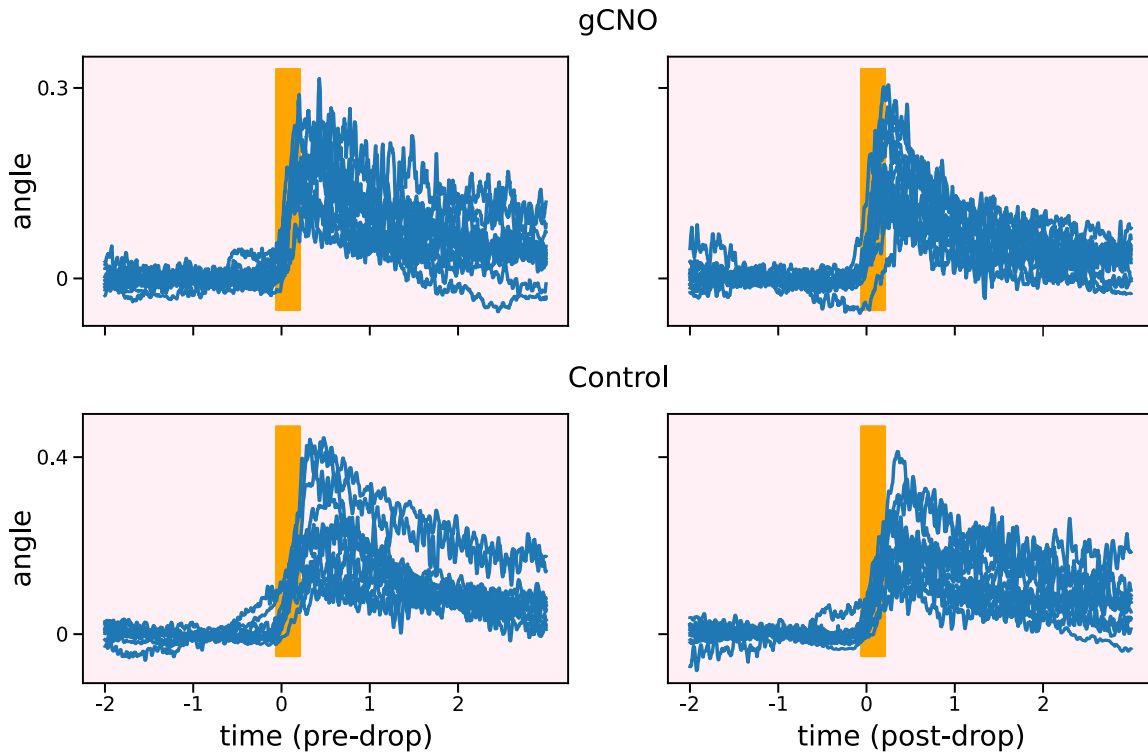


Figure 3.29: Time window for linear fit of whisking protraction. The time window highlighted by the orange area was used to delimit the period of average whisking protraction used for the linear fit in each recording ( $n=25$ ).

### Effects of reduced Golgi cell inhibition on the network representations of whisking behaviour

Finally, we addressed the question of whether and how the relationship between whisking activity and neuronal dynamics changes after experimental manipulation. In particular, we are interested in how population activity may differently reflect whisking-related information when reducing Golgi cell inhibition. To this end, we compared the distribution of absolute peaks of cross-correlation between neuronal and whisking activity before and after drug application in the ‘gCNO’ and ‘control’ condition (please see method section 3.2.9). Figure 3.31 shows the pre- and post-drop distributions of cross-correlation absolute peaks for pc1, pc2 and pc3 (left to right) and experimental condition (‘gCNO’ top, ‘control’ bottom). There is no strong evidence of a difference

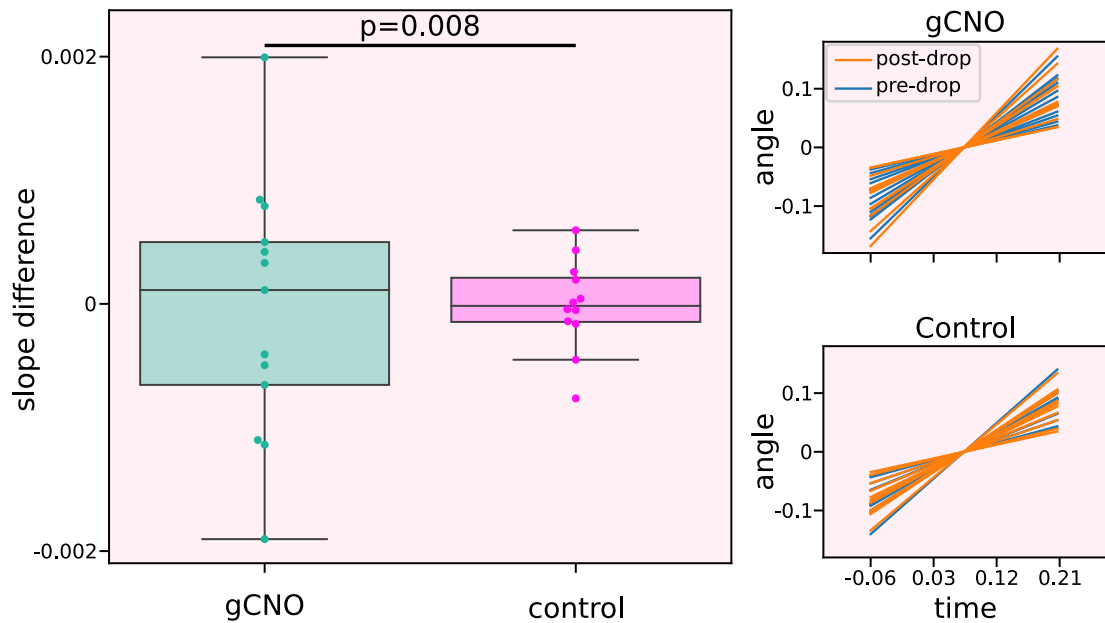


Figure 3.30: Comparison of whisking protraction linear fits pre- and post-drop. Left: each point is the difference in post- minus pre-drop slope obtained from fitting a line to the average whisking protraction (see Figure 3.29). In both the ‘gCNO’ and ‘control’ condition the slope differences are centred around 0, but the spread around 0 is different in the two conditions (Levene’s test,  $W=8.39$ ,  $p=0.008$ ). Right: comparison between the linear fits for pre- and post-drop data. In the control condition (bottom), pre- and post-drop fits show a high level of overlap; this overlap decreases in the ‘gCNO’ condition (top). These results suggest that decrease Golgi cell activity leads to increased variability in average whisking protraction dynamics..

in peak cross-correlation before and after drug application (Wilcoxon test, T:31, 35, 27, 17, 14, 22; p-value:0.33, 0.49, 0.21, 0.09, 0.05, 0.20 for ‘gCNO’-pc1, -pc2, pc3 and ‘control’-pc1, -pc2, -pc3 respectively). The same results are found when comparing the cumulative sum of absolute cross-correlations instead of just their peak, which are shown in Figure 3.32. Altogether, these results may suggest that, despite affecting neuronal and whisking activity, moderate decrease of inhibition in the lateral cerebellum does not impact neuronal representations of whisking behaviour.

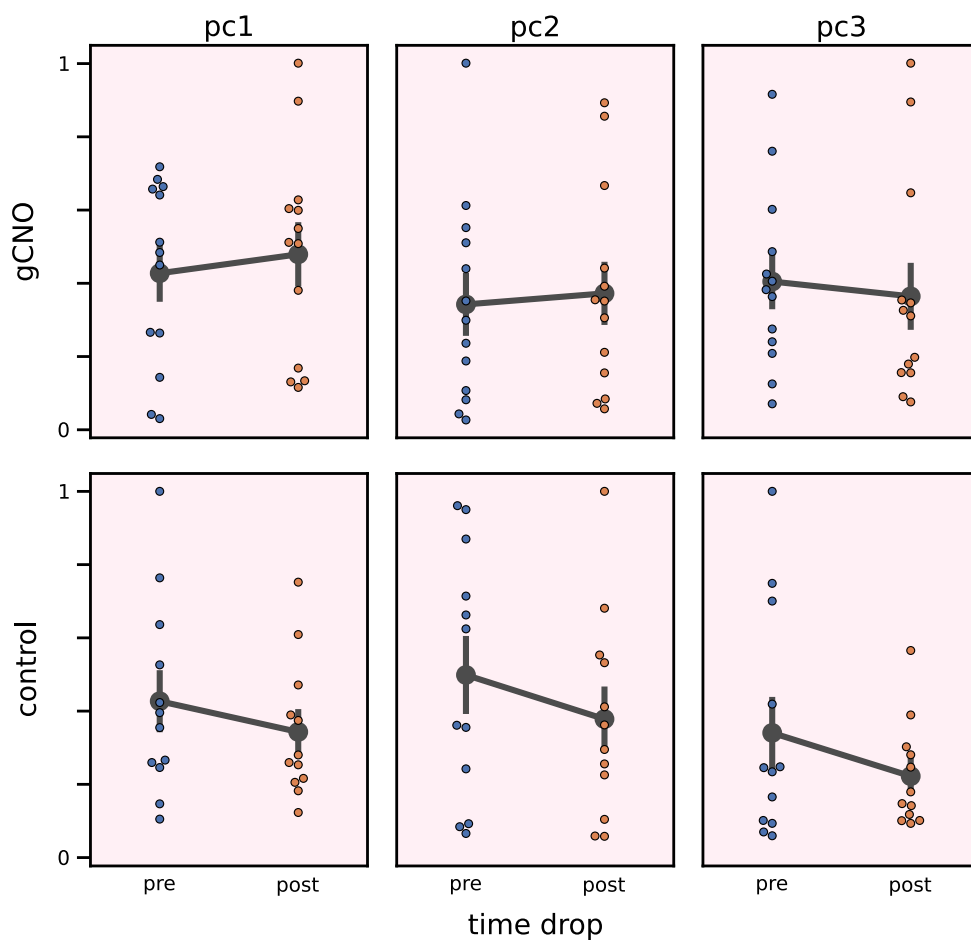


Figure 3.31: Pre- and post-drop cross-correlation peaks. Each subplot shows the distribution of absolute peaks of the cross-correlation for pre- and post-drop data. The cross-correlation is between pc1, pc2 and pc3 (left to right subplots) and average whisking activity. Top: data from the ‘gCNO’ condition (n=13). Bottom: data from the ‘control’ condition (n=12). In neither conditions there is a strong evidence of a difference in peaks before and after CNO/PBS drop (Wilcoxon test, T:31, 35, 27, 17, 14, 22; p-value:0.33, 0.49, 0.21, 0.09, 0.05, 0.20 for ‘gCNO’-pc1, -pc2, pc3 and ‘control’-pc1, -pc2, -cp3 respectively). This may suggest that the reduction of Golgi cell inhibition did not affect whisking representations in the lateral cerebellar cortex.

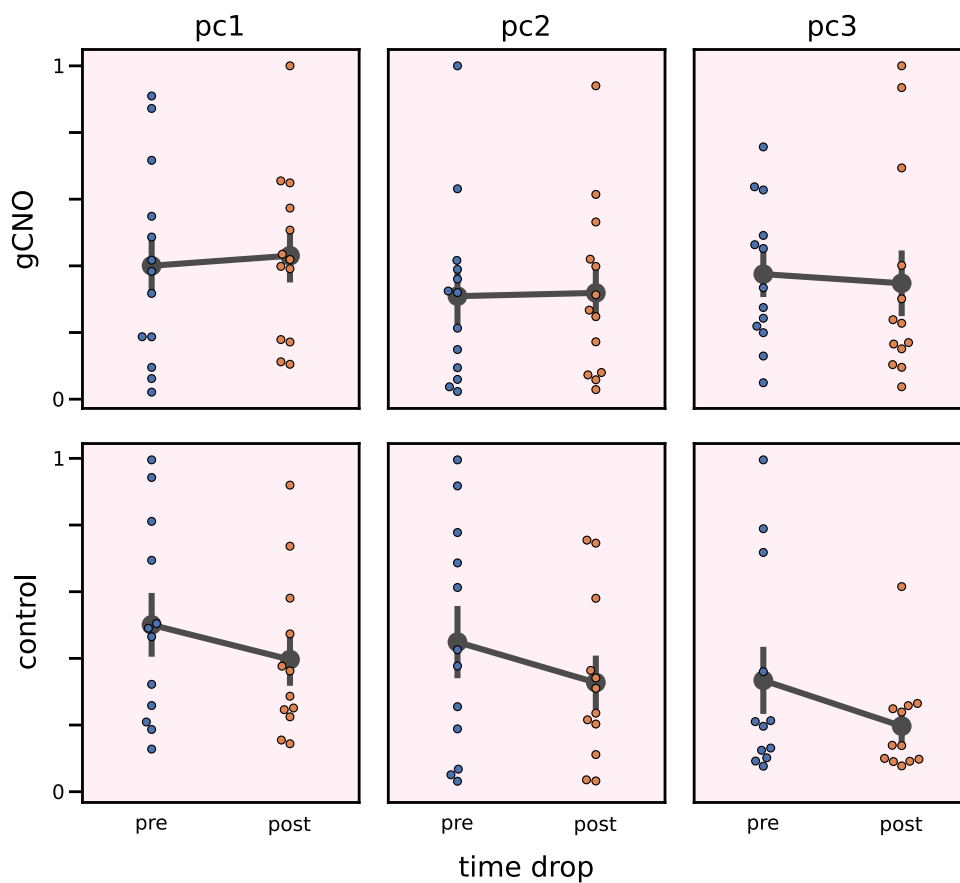


Figure 3.32: Pre- and post-drop cross-correlation cumulative sums. Same layout as in Figure 3.31, but here we compare the cumulative sum of the absolute cross-correlation between pc1, pc2 and pc3 and average whisking activity. Again, there is no strong evidence of a difference in cross-correlation cumulative sums before and after drug application (Wilcoxon test, T:24, 42, 29, 19, 18, 20; p-value:0.14, 0.83, 0.27, 0.12, 0.10, 0.15 for 'gCNO'-pc1, -pc2, pc3 and 'control'-pc1, -pc2, -cp3 respectively).

### 3.3.4 Discussion

The aim of this work was to investigate how sensorimotor activity is represented in the lateral cerebellar cortex, and how changes in the network state, in the form of decreased Golgi cell inhibition, affect these representations as well as behaviour. To this end, we simultaneously performed Neuropixels I recording of neuronal activity in the lateral cerebellar cortex and recording of whisking activity in mice. We analysed whisking behaviour and its neuronal representations both in an intact network and in a network where the level of Golgi cell inhibition was reduced. This experimental setting allowed us to study how inhibition may affect the overall state of the network, how this network encodes behaviourally relevant variables, and how changes of these representations may affect downstream behaviour.

#### **Cerebellar cortical neurons heterogeneously encode whisking behaviour**

The data obtained from recording in the intact network showed that the cortical population in the lateral cerebellum accurately represent whisking behaviour. At a single cell level, we observed that neuronal spike counts could be well explained by dynamics of the whisking setpoint, even when using a simple linear model with Poisson noise. Moreover, we observed that units could exhibit different tuning profiles to whisking position, including monotonic increase, decrease, localised increase or decrease of the firing rate. Using an unsupervised clustering method to group tuning curves from all recordings also suggested that the profile of single unit tuning to whisking position is heterogeneous, and form a continuum in the t-SNE space. Previous studies have found that Purkinje cells use a linear code to represent whisking activity, and that this code may arise from the combination of more specific tuning curves of upstream neurons [37, 38]; thus, future analysis of the present data should investigate whether different cell types are particularly associated with specific tuning curve profiles. Overall, these results are in line with previous findings, highlighting how single cell activity at all levels of the cerebellar cortex precisely encodes whisking dynamics [184, 37, 38, 21, 140]. Given the critical role of the cerebellum in coordination of behaviour, one possibility is that the observed neuronal code, used to accurately represent whisking activity, may be optimised to efficiently integrate information about whisker behaviour with information related to other sensory and motor domains.

### **Population activity preferentially encodes upcoming whisking behaviour**

The whisking tuning found at a single cell level was reflected at a population level. We used PCA analysis to describe population activity with three independent variables, the principal components (pc's), subject to the constraint of retaining as much variance as possible. The first three pc's captured only a moderate amount of the total variance in the population activity, despite the fact that this analysis was restricted to periods centred around whisking onset. This may be explained in light of the fact that neuronal activity in the cerebellar cortex integrates and reflects at all times many other behaviourally relevant variables [209, 34, 113, 227]. Nevertheless, neuronal dynamics projected in this 3d pc space still had a structure that well matched whisking dynamics. In fact, it was possible to decode single trial whisking setpoint from concomitant population activity, while cross-correlation analysis showed a good match between average whisking position and single pc's. Notably, the cross-correlation peaks for red pc1 were on average positive with mean 36ms, meaning that population dynamics captured by pc1 tended to anticipate whisking behaviour; on the other hand, peaks associated to pc2 lagged behind behavioural dynamics on average. Moreover, the distribution of peaks for the pc1 – but to the other pc's – was particularly narrow, which indicated that information contained in pc1 was precisely tuned to upcoming whisking activity. Thus, these results hint at a role of the cerebellum in controlling future behaviour, by possibly integrating information from multiple behaviourally relevant variables.

### **The cerebellar cortex uses a distributed code to represent whisking dynamics**

We then investigated how much information contained in each pc is distributed across units in the neuronal population; the contribution of each unit to the pc is reflected in the pc loadings. Plotting the loadings of all units recorded for each pc showed that information, especially in the first pc, was well distributed across units. These results indicate that information about whisking activity is broadly distributed in the recorded neuronal populations, with most units contributing to some extent to its encoding.

### Decreasing Golgi cell inhibition does not saturate population activity

Finally, we examined how changing the state of the cerebellar cortical network may affect neuronal representations, behaviour, and their relationship. In particular, we changed the state of the network by decreasing the level of Golgi cell inhibition: this was achieved by activating inhibitory DREADDs (hM4Di), selectively expressed by Golgi cells, via application of CNO directly on top of the recording site, which afforded a within-minute temporal precision to our manipulation. These receptors inhibit neuronal activity via moderate hyperpolarisation of the cell membrane, and by reducing presynaptic release of neurotransmitters [197].

Topical application of CNO onto the cerebellar cortex was followed by an increased spread of the population spike count distribution, with the average count remaining stable, but with higher counts becoming more likely across recordings. Hence, our manipulation of Golgi cell inhibition did not lead to an overall saturation of network dynamics, namely, a drastic and indiscriminate increase in excitation, but variably affected the course population activity. One reason explaining the absence of strong saturation of network activity may be the fact that the coarse level of granule cell excitability is mostly under the control of tonic inhibition, which arises in part from non-vesicular sources of GABA [194, 230, 142]. On the other hand, variable changes in population activity may be due to several reasons, including heterogeneity in the subpopulations of neurons recorded in each session: for example, neurons could have differed in terms of cell type, with some types more or less sensitive to increased granule cell activity; or in terms of the particular connectivity structure of the network in which they were embedded, including the Golgi cell network; or again in terms of their positioning relative to Golgi cells affected by our local manipulation. Altogether, these results suggest that dynamic Golgi cell inhibition may not be necessary for maintaining network excitation at the level required for the network to perform its computations, as postulated by sparse coding theories; instead our manipulation of Golgi cell inhibition may have had more subtle effects on cerebellar cortical neuronal dynamics.

### **Decreasing Golgi cell inhibition increases the temporal heterogeneity of neuronal dynamics during whisking activity**

Accordingly, when focusing on the temporal aspect of neuronal activity, we noticed that decreased Golgi cell inhibition was associated with an increased alignment or synchronisation of the average neuronal activity peaks during whisking onset. Golgi cell inhibition has indeed been shown to control spike timing of granule cells through various mechanisms, including changes in gain, determining the slope of the granule cell input-output curve, and spike threshold, controlling spike initiation [96, 161]. Golgi cells are the source of feedforward inhibition, whose general downstream consequence in other brain regions has been linked to an increase in temporal precision on neuronal dynamics, as normally inhibition trails behind excitation and sharpens the window of input integration [234, 82, 162]; however, Golgi cell inhibition, in the specific, can precede or be concomitant with mossy fibre excitation, in which case it can actually reduce the temporal precision of early granule cell responses [56]. Our results are in line with these findings, as decreasing Golgi cell inhibition leads to an increased temporal alignment of the overall network activity during whisking initiation. This control by Golgi cells of the timing of network activity, in turn, could support the specific cerebellar role in integrating information across different behavioural domains. In fact, the temporal heterogeneity of granule cell responses to mossy fibre input is deemed important for how the cerebellar network integrates and distinguishes parallel sensory and motor pathways [34], which is consistent with the idea that the cerebellum works as a hub for sensorimotor integration, and more in general behavioural coordination [175].

### **Decreasing Golgi cell inhibition decreases the stability of whisking behaviour**

As for the behavioural effects of our manipulation, we found that it lead to increased variability in the dynamics of whisking onset. In detail, we found that the velocity or slope of average whisking protraction during whisking initiation could change more over recording time, both increasing or decreasing, when Golgi cell inhibition was reduced. In contrast, with intact inhibition, whisking protraction remained mostly unchanged. This result highlights the importance of an intact cerebellum for precise whisking control, which, notably, is subject to the coordination with other motor and sensory systems [48, 138, 157, 191]. Thus, increased variability in motor initiation



may be linked with the possible contribution of Golgi cell inhibition to the representations of multiple streams of information – bound together at the level of the cerebellar cortex – that might improve the accuracy with which each single behaviour involved is performed.

### **Decreasing Golgi cell inhibition does not change the population representations of whisking behaviour**

Finally, we assessed whether reduction of inhibition in the lateral cerebellar cortex changed how population activity reflected whisking behaviour. We did not find strong evidence of a change in cross-correlation between neuronal and whisking activity, which indicates that neuronal representations of whisking behaviour were not deteriorated after Golgi cell manipulation. In other words, it is possible that our manipulation could have caused changes in neuronal dynamics in the cerebellar cortex, which in turn may have affected whisking behaviour, without however changing the quality of the encoding of whisking information by the network *per se*.

### **Limitations and future research**

These results, however, are subject to some limitations that may affect their validity or interpretation. In particular, it is important to notice that Golgi cells have different properties that may circumvent or decrease the efficacy of our chemogenetic manipulation [43]. For example, Golgi cells display pacemaker activity and activity rebound following hyperpolarisation, which may interact with the moderate hyperpolarisation caused by DREADDs activation. Golgi cells are also electrically coupled with each other, and this type of neuronal communication was not affected by presynaptic silencing. Finally, Golgi cells have extensive axonal arborisations, which means that the neuronal population recorded may still have received inhibition from Golgi cells located outside the site of DREADDs expression. A second limitation concerns instead the direct recording of granule cells. Our manipulation should have in the first instance altered the activity of this neuronal class; however, recording from these neurons is particularly difficult with Neuropixels I probes, due to their small size [104, 172]. Thus, our analyses addressed changes in the overall cerebellar network dynamics, but could not focus on the immediate target of Golgi cell inhibition. Overall, these caveats intimate prudence when assessing the effects of our manipulation on Golgi cell inhibition. Thus, future work should aim at replicating the present findings, while

also assessing more directly how activation of inhibitory DREADDs interact with the peculiar Golgi cell properties.

Our work suggests that altering Golgi cell inhibition changes the response of the network to its input, hence changing how the downstream behaviour is controlled. Golgi cell inhibition itself is under the control of many mechanisms, including feedback loops within the cerebellum [3] and its cortex [52, 237, 167], as well as neuromodulatory systems [63, 141, 66]. Thus, the Golgi cell population is in a key position to flexibly control cerebellar computations, based on the dynamic behavioural context, which may require to focus on different aspects of behaviour each time. Hence, in order to fully understand the pervasive involvement of the cerebellum in behavioural control, it will be critical to elucidate how different mechanisms contribute to fine tune the Golgi cell network in a context-dependent manner.

### Conclusions

In conclusion, the data presented in this chapter show that the cerebellar cortex can accurately encode whisking behaviour, and that these representations play a role in whisking dynamics. In particular, when decreasing the level of Golgi cell inhibition, which in a natural situation may correspond to a careful adjustment of the state of the network [174], we did not observe a saturation of neuronal activity, nor degradation of whisking representations *per se*. Instead, our manipulation increased the temporal alignment of neuronal dynamics during whisking, while, at the same time, increasing the variability in the dynamics of whisking initiation. Although at a first glance contradictory, these results could be reconciled by the idea that Golgi cell inhibition contributes to the temporal heterogeneity in granule cell activity, and therefore to how the granular layer encodes and integrates information about different sensory, motor and cognitive domains carried by mossy fibres; in turn, this integration may support behavioural coordination, which increases the precision of execution of each single behavioural domain, by constraining or regulating one domain based on the dynamics of the others. Thus, it would be particularly interesting in future experiments to track, in addition to whisking, other interrelated motor systems and sensory pathways, in order to investigate how Golgi cell inhibition supports their joint dynamics.

### 3.4 Covid statement

The experimental work presented in this thesis was seriously affected by the covid pandemic, which delayed the acquisition of data presented in this chapter. In particular, the Bristol Animal Unit experienced a significant staff shortage, which brought to extreme low numbers the mouse colony I am working with; this, together with difficulties in recovering the colony, imposed a prolonged period during which we could not perform experiments.



# Chapter 4: General discussion

The overarching aim of this thesis was to investigate how the cerebellum contributes to behaviour. We addressed how the cerebellum encodes behaviourally relevant variables, and how it uses these representations to produce functional behaviour, namely, behaviour where its components (i.e., sensory, motor, and cognitive ones) are seamlessly integrated and coordinated.

This work included both computational modelling of the cerebellum and experiments. The computational work described a general model of the cerebellum, illustrating how its computations may serve whole-brain neuronal dynamics underlying behavioural production. The experimental work, instead, involved simultaneous recording of whisking and cerebellar cortical activity in mice, coupled with chemogenetic manipulation of the cerebellar network state. This experimental setup allowed us to gain insights on how the cerebellum encodes whisking activity, and how this encoding, together with downstream behaviour, may be susceptible to changes in the network's state.

## 4.1 Computational modelling of the cerebellum

The cerebellum is involved in most aspects of behaviour, spanning sensory, motor, and cognitive domains [213, 6, 210, 199, 129, 61, 156]. Cerebellar computations have often been described in terms of a state estimation process, based on an internal model whose structure is learned through experience [180, 158, 239]. This view is supported by empirical research, showing that cerebellar activity encodes estimates of behaviourally relevant variables used to fine tune behaviour [147, 168, 10, 201, 220, 217]. However, it is still debated how cerebellar computations are integrated within whole-brain dynamics, especially when considering its involvement in so many different

behavioural contexts.

Theoretical treatments of the cerebellum have used various approaches to describe its functions, for example by modelling it as a Smith predictor, a forward model, a model predictive control, as an implementation of predictive coding [54, 179, 222, 201, 67, 137, 185, 74]. Notably, all these models include a state prediction and estimation process, which are commonly associated with the cerebellar functions. In this work, we used a formalism that generalises these approaches, the free energy principle (FEP).

The FEP is a theoretical framework primarily concerned with the description of how internal (e.g., neuronal) states of biological systems change over time, and has been successfully used to explain neuronal dynamics, cognition and behaviour [130, 76, 62, 77, 160, 177, 114]. Under the FEP, neuronal dynamics reflect an inference process, where the objects of inference are hidden environmental states, namely, external and somatic states such as conditioned stimuli and limb or whisking position. Notably, neuronal inference is based on a generative model of how environmental states produce available sensory input, the form of which is defined by the biophysical structure of the network itself.

Thus, the key question we addressed was: what is the form of the cerebellar generative model, and of the ensuing estimation process, that best explains the cerebellar role in behavioural control? In this work we argued that, at its simplest, the key cerebellar function is to coordinate different behavioural domains, and that this translates into a generative model that is able to learn and infer interactions between those domains. Thus, in this picture, cerebellar state estimation is focused on how behavioural variables interact with each other; these estimates, in turn, are used by the cerebellum to constrain extra-cerebellar dynamics, so that they conform with expectations about behavioural coordination. In other words, the cerebellar model is placed on top of the extra-cerebellar model, and serves the function of contextualising inference therein. Technically, the cerebellum infers the context of behaviour, and uses this context as an empirical prior, known in machine learning as inductive bias, to guide and adjust neuronal inference in other brain regions underlying behavioural production.

The proposed cerebellar model aims to be as simple and general as possible. For this reason we used a state space model with linear mapping and equations of motion, in accordance with empirical studies showing linear encoding of behavioural variables in the cerebellum [109, 190] –

although it would also be possible to include non-linearities in a biologically plausible manner [17]. Nevertheless, the model is able to capture many important aspects of the cerebellar circuitry that are often neglected. In particular, the cerebellum is usually described as a feedforward network; however, feedback loops within it play an increasingly recognised role in the generation of its dynamics, which is accounted for in the present model.

Finally, we presented numerical simulations that use as an exemplary case whisking-respiration coordination in rodents, for which the cerebellum is known to play a crucial role [191]. The results show that the cerebellum is capable of establishing and maintaining behavioural coordination in face of different perturbations, such as internal noise and external stimuli. Importantly, these findings can be generalised to any behavioural context, because in all cases functional behaviour relies on learned associations and coordination between task-relevant variables.

In conclusion, the cerebellar model described in this thesis offers a perspective on its computations that may guide interpretations of empirical results on how the cerebellum encodes or estimates behaviourally relevant variables, what role cerebellar components play in this estimation process, and how cerebellar outputs control or guide extra-cerebellar dynamics.

## 4.2 Cerebellar representations of whisking behaviour

The experimental part of this thesis investigated how the lateral cerebellar cortex, including Crus I, II and the simplex, represents whisking behaviour in mice, and how both neuronal and behavioural activity are affected by changing the state of the network. In particular, we used Neuropixels I and high-speed camera recordings of neuronal and behavioural activity in mice in two conditions: with and without altered levels of Golgi cell inhibition. Temporally precise manipulation of Golgi cell inhibition was achieved using inhibitory DREADDs, activated via topical application of CNO.

Data obtained from the intact network are in line with past results, showing accurate representations of whisking dynamics in the lateral cerebellar cortex. In particular, it has been found that Purkinje cells linearly encode whisking position [37], and that this tuning arises from the combination of more localised tuning curves in upstream neurons [38]. Accordingly, our results show the presence of both monotonically increasing and decreasing tuning curves, as well as

tuning curves with more localised changes in firing rates across whisker positions. Moreover, neuronal activity could be well predicted based on information about whisking setpoint, showing accurate representations of whisking activity in the lateral cerebellar cortex.

Not surprisingly, the analysis of population activity also showed accurate representations of whisking activity. These representations preferentially preceded behaviour by a few tens of milliseconds, which highlights the role of the cerebellum in fine tuning upcoming behaviour. Moreover, we found that information about whisking activity tended to be widely spread across the neuronal populations recorded; this distributed code may naturally arise from the characteristic neuronal connectivity patterns found in the granular layer and molecular layer layer, favouring an expansion and distribution of information across neurons.

When we perturbed the state of the network, by decreasing Golgi cell inhibition, we found no clear change in how the cerebellar cortex represents whisking activity. This may be due to the fact that our manipulation was moderate, and did not disrupt information processing in this network. Nevertheless, we found that our manipulation had an effect on the level of neuronal activity alignment, with peaks of average activity less scattered with reduced Golgi cell inhibition. Accordingly, Golgi cell inhibition has been linked to increased temporal dispersion of neuronal activity, especially during the first stage of the response to mossy fibre input [56]; notably, this was linked to the role of Golgi cells in integrating different streams of information at the level of the granular layer. Thus, one possibility is that our manipulation might have hampered integration of information related to different behavioural variables in the cerebellar cortex, which in turn may have decreased temporal variability of the network response to whisking-related input alone.

At a behavioural level, we found a concomitant increase in variability of average whisking responses across recording time, and in particular of the velocity of whisking initiation. This result resonates with other findings, showing how cerebellar activity plays an important role in motor initiation [21, 224, 45], and may support the idea that the cerebellum fine tunes behaviour by coordinating its different components. In other words, if our manipulation of Golgi cell inhibition had an effect on how the network integrates information in the granular layer, downstream behavioural changes may be due to the reduced capacity of the cerebellum to refine whisking activity based on other behavioural variables, which are normally coordinated with whisking.

This interpretation of our experimental results may also be linked to our computational model



of the cerebellum. In particular, in this model Golgi cell inhibition controls the precision of mossy fibre input, namely, the weight carried by these input in updating cerebellar state estimates. Notably, the precision is encoded in the correlation matrix, describing how noise co-varies across different streams of information. Practically, this means that these streams of information are not considered independent by the cerebellar model, but carry information about one another. Thus, our manipulation of Golgi cell inhibition, when read within the framework of cerebellar state estimation, may lead to the decreased ability of the network to integrate information across behaviorally relevant variables (in our case whisking and unobserved ones such as respiration and limb movements), which in turn may affect how well the cerebellum can fine tune behaviour.



# Chapter 5: References



# Bibliography

- [1] Rick A. Adams, Stewart Shipp, and Karl J. Friston. “Predictions not commands: active inference in the motor system”. In: *Brain Structure and Function* 218.3 (2013), pp. 611–643. ISSN: 1863-2661.
- [2] James S. Albus. “A theory of cerebellar function”. In: *Mathematical Biosciences* 10.1 (1971), pp. 25–61. ISSN: 0025-5564.
- [3] Lea Ankri et al. “A novel inhibitory nucleo-cortical circuit controls cerebellar Golgi cell activity”. In: *eLife* 4 (2015). Ed. by Michael Häusser, e06262. ISSN: 2050-084X.
- [4] Richard Apps and Richard Hawkes. “Cerebellar cortical organization: a one-map hypothesis”. In: *Nature Reviews Neuroscience* 10.9 (2009), pp. 670–681.
- [5] Richard Apps et al. “Cerebellar Modules and Their Role as Operational Cerebellar Processing Units”. In: *The Cerebellum* 17.5 (2018), pp. 654–682. ISSN: 1473-4230.
- [6] Georgios P.D. Argyropoulos. “The cerebellum, internal models and prediction in ‘non-motor’ aspects of language: A critical review”. In: *Brain and Language* 161 (2016), pp. 4–17.
- [7] Kendra Arkley et al. “Strategy Change in Vibrissal Active Sensing during Rat Locomotion”. In: *Current Biology* 24.13 (2014), pp. 1507–1512. ISSN: 0960-9822.
- [8] D M Armstrong and J A Rawson. “Activity patterns of cerebellar cortical neurones and climbing fibre afferents in the awake cat.” In: *The Journal of Physiology* 289.1 (1979), pp. 425–448.

- [9] Yuri I Arshavsky, Tatiana G Deliagina, and Grigori N Orlovsky. “Pattern generation”. In: *Current Opinion in Neurobiology* 7.6 (1997), pp. 781–789. ISSN: 0959-4388.
- [10] Amy J Bastian. “Learning to predict the future: the cerebellum adapts feedforward movement control”. In: *Current Opinion in Neurobiology* 16.6 (2006). Motor systems / Neurobiology of behaviour, pp. 645–649. ISSN: 0959-4388.
- [11] Oliver Baumann and Jason B. Mattingley. “The Emotional Cerebellum”. In: ed. by Michael Adamaszek, Mario Manto, and Dennis J. L. G. Schutter. Cham: Springer International Publishing, 2022. Chap. Cerebellum and emotion processing, pp. 25–39. ISBN: 978-3-030-99550-8.
- [12] Oliver Baumann et al. “Consensus paper: The role of the cerebellum in perceptual processes”. In: *Cerebellum* 14.2 (2015), pp. 197–220. ISSN: 1473-4230.
- [13] Curtis C. Bell, Victor Han, and Nathaniel B. Sawtell. “Cerebellum-Like Structures and Their Implications for Cerebellar Function”. In: *Annual Review of Neuroscience* 31.1 (2008). PMID: 18275284, pp. 1–24.
- [14] Mark C. Bellingham. “Driving respiration: The respiratory central pattern generator”. In: *Clinical and Experimental Pharmacology and Physiology* 25.10 (1998), pp. 847–856.
- [15] Ronny Bergmann et al. “Coordination between eye movement and whisking in head-fixed mice navigating a plus maze”. In: *eNeuro* 9.4 (2022).
- [16] Guy Billings et al. “Network structure within the cerebellar input layer enables lossless sparse encoding”. In: *Neuron* 83.4 (1998), pp. 960–974.
- [17] Rafal Bogacz. “A tutorial on the free-energy framework for modelling perception and learning”. In: *Journal of Mathematical Psychology* 76 (2017), pp. 198–211. ISSN: 0022-2496.
- [18] Gino Brochu, Leonard Maler, and Richard Hawkes. “Zebrin II: A polypeptide antigen expressed selectively by purkinje cells reveals compartments in rat and fish cerebellum”. In: *Journal of Comparative Neurology* 291.4 (1990), pp. 538–552.

- [19] Jessica X. Brooks, Jerome Carriot, and Kathleen E. Cullen. “Learning to expect the unexpected: rapid updating in primate cerebellum during voluntary self-motion”. In: *Nature Neuroscience* 18.9 (2015), pp. 1310–1317. ISSN: 1546-1726.
- [20] Amanda M. Brown et al. “Molecular layer interneurons shape the spike activity of cerebellar Purkinje cells”. In: *Scientific Reports* 9.1 (2019), p. 1742. ISSN: 2045-2322.
- [21] Spencer T. Brown and Indira M. Raman. “Sensorimotor Integration and Amplification of Reflexive Whisking by Well-Timed Spiking in the Cerebellar Corticonuclear Circuit”. In: *Neuron* 99.3 (2018), 564–575.e2. ISSN: 0896-6273.
- [22] Christopher L. Buckley et al. “The free energy principle for action and perception: A mathematical review”. In: *Journal of Mathematical Psychology* 81 (2017), pp. 55–79. ISSN: 0022-2496.
- [23] Randy L. Buckner et al. “The organization of the human cerebellum estimated by intrinsic functional connectivity”. In: *Journal of Neurophysiology* 106.5 (2011). PMID: 21795627, pp. 2322–2345.
- [24] Santiago Ramón y Cajal. “Textura del Sistema Nervioso del Hombre y de los Vertebrados, 1899–1904”. In: *The Art of Animal Anatomy*. Princeton: Princeton University Press, 2019, pp. 216–219. ISBN: 9780691183978.
- [25] Dylan J. Calame, Matthew I. Becker, and Abigail L. Person. “Cerebellar associative learning underlies skilled reach adaptation”. In: *Nature Neuroscience* 26.6 (2023), pp. 1068–1079. ISSN: 1546-1726.
- [26] JC Callaway, N Lasser-Ross, and WN Ross. “IPSPs strongly inhibit climbing fiber-activated  $[Ca^{2+}]_i$  increases in the dendrites of cerebellar Purkinje neurons”. In: *Journal of Neuroscience* 15.4 (1995), pp. 2777–2787. ISSN: 0270-6474.
- [27] Matteo Carandini and David J. Heeger. “Normalization as a canonical neural computation”. In: *Nature Reviews Neuroscience* 13.1 (2011), pp. 51–62.
- [28] Megan R Carey and Wade G Regehr. “Noradrenergic control of associative synaptic plasticity by selective modulation of instructive signals”. In: *Neuron* 62.1 (2009), pp. 112–122.

- [29] N. Alex Cayco-Gajic, Claudia Clopath, and R. Angus Silver. “Sparse synaptic connectivity is required for decorrelation and pattern separation in feedforward networks”. In: *bioRxiv* (2017).
- [30] N. Alex Cayco-Gajic and R. Angus Silver. “Re-evaluating Circuit Mechanisms Underlying Pattern Separation”. In: *Neuron* 101.4 (2019), pp. 584–602. ISSN: 0896-6273.
- [31] Nadia L. Cerminara, Richard Apps, and Dilwyn E. Marple-Horvat. “An internal model of a moving visual target in the lateral cerebellum”. In: *Journal of Physiology* 587.2 (2009), pp. 429–442.
- [32] Nadia L. Cerminara et al. “Redefining the cerebellar cortex as an assembly of non-uniform Purkinje cell microcircuits”. In: *Nature Reviews Neuroscience* 16.2 (2015), pp. 79–93. ISSN: 1471-0048.
- [33] Nadia L. Cerminara et al. “Redefining the cerebellar cortex as an assembly of non-uniform Purkinje cell microcircuits”. In: *Nature Reviews Neuroscience* 16.2 (2015), pp. 79–93. ISSN: 1471-0048.
- [34] François P Chabrol et al. “Synaptic diversity enables temporal coding of coincident multisensory inputs in single neurons”. In: *Nature Neuroscience* 18.5 (2015), pp. 718–727.
- [35] Francois P. Chabrol, Antonin Blot, and Thomas D. Mrsic-Flogel. “Cerebellar contribution to preparatory activity in motor neocortex”. In: *Neuron* 103.3 (2019), 506–519.e4. ISSN: 0896-6273.
- [36] Paul Chadderton, Troy W. Margrie, and Michael Häusser. “Integration of quanta in cerebellar granule cells during sensory processing”. In: *Nature* 428.6985 (2004), pp. 856–860. ISSN: 1476-4687.
- [37] Susu Chen, George J Augustine, and Paul Chadderton. “The cerebellum linearly encodes whisker position during voluntary movement”. In: *eLife* 5 (2016).
- [38] Susu Chen, George J. Augustine, and Paul Chadderton. “Serial processing of kinematic signals by cerebellar circuitry during voluntary whisking”. In: *Nature Communications* 8.1 (2017).



- [39] Claudia Clopath et al. “A cerebellar learning model of vestibulo-ocular reflex adaptation in wild-type and mutant mice”. en. In: *J Neurosci* 34.21 (2014), pp. 7203–7215.
- [40] Michiel Coesmans et al. “Bidirectional parallel fiber plasticity in the cerebellum under climbing fiber control”. In: *Neuron* 44.4 (2004), pp. 691–700. ISSN: 0896-6273.
- [41] John J. Crowley, Diasynou Fioravante, and Wade G. Regehr. “Dynamics of fast and slow inhibition from cerebellar Golgi cells allow flexible control of synaptic integration”. In: *Neuron* 63.6 (2009), pp. 843–853. ISSN: 0896-6273.
- [42] Egidio D’Angelo. “The organization of plasticity in the cerebellar cortex: From synapses to control”. In: *Cerebellar Learning*. Ed. by Narender Ramnani. Vol. 210. Progress in Brain Research. Elsevier, 2014, pp. 31–58.
- [43] Egidio D’Angelo et al. “The cerebellar Golgi cell and spatiotemporal organization of granular layer activity”. In: *Frontiers in Neural Circuits* 7 (2013).
- [44] Lancelot Da Costa et al. “Neural dynamics under active inference: Plausibility and efficiency of information processing”. In: *Entropy* 23.4 (2021). ISSN: 1099-4300.
- [45] Joshua Dacre et al. “A cerebellar-thalamocortical pathway drives behavioral context-dependent movement initiation”. In: *Neuron* 109.14 (2021), 2326–2338.e8. ISSN: 0896-6273.
- [46] Erik De Schutter. “Cerebellar Cortex: Computation by Extrasynaptic Inhibition?” In: *Current Biology* 12.10 (2002), R363–R365. ISSN: 0960-9822.
- [47] Paul Dean et al. “The cerebellar microcircuit as an adaptive filter: experimental and computational evidence”. In: *Nature Reviews Neuroscience* 11.1 (2010), pp. 30–43. ISSN: 1471-0048.
- [48] Martin Deschênes, Jeffrey Moore, and David Kleinfeld. “Sniffing and whisking in rodents”. In: *Current Opinion in Neurobiology* 22.2 (2012). Neuroethology, pp. 243–250. ISSN: 0959-4388.
- [49] Jean C. Desclin. “Histological evidence supporting the inferior olive as the major source of cerebellar climbing fibers in the rat”. In: *Brain Research* 77.3 (1974), pp. 365–384. ISSN: 0006-8993.

- [50] Ben Deverett et al. “Cerebellar involvement in an evidence-accumulation decision-making task”. In: *eLife* 7 (2018). Ed. by Megan R Carey and Richard B Ivry, e36781. ISSN: 2050-084X.
- [51] Mathew E. Diamond et al. “‘Where’ and ‘what’ in the whisker sensorimotor system”. In: *Nature Reviews Neuroscience* 9.8 (2008), pp. 601–612. ISSN: 1471-0048.
- [52] Stéphane Dieudonné and Andréa Dumoulin. “Serotonin-driven long-range inhibitory connections in the cerebellar cortex”. In: *Journal of Neuroscience* 20.5 (2000), pp. 1837–1848.
- [53] David A. Digregorio, Zoltan Nusser, and R. Angus Silver. “Spillover of glutamate onto synaptic AMPA receptors enhances fast transmission at a cerebellar synapse”. In: *Neuron* 35.3 (2002), pp. 521–533.
- [54] K. Doya. “What are the computations of the cerebellum, the basal ganglia and the cerebral cortex?” In: *Neural Networks* 12.7 (1999), pp. 961–974. ISSN: 0893-6080.
- [55] Guillaume P. Dugué et al. “Electrical coupling mediates tunable low-frequency oscillations and resonance in the cerebellar Golgi cell network”. In: *Neuron* 61.1 (2009), pp. 126–139. ISSN: 0896-6273.
- [56] Ian Duguid et al. “Control of cerebellar granule cell output by sensory-evoked Golgi cell inhibition”. In: *Proceedings of the National Academy of Sciences* 112.42 (2015), pp. 13099–13104. ISSN: 0027-8424.
- [57] Ian Duguid et al. “Tonic inhibition enhances fidelity of sensory information transmission in the cerebellar cortex”. In: *Journal of Neuroscience* 32.32 (2012), pp. 11132–11143. ISSN: 0270-6474.
- [58] John C. Eccles, Masao Ito, and Szentágothai János. *The cerebellum as a neuronal machine*. Springer, 1967.
- [59] Harriet Feldman and Karl Friston. “Attention, uncertainty, and free-energy”. In: *Frontiers in Human Neuroscience* 4 (2010), p. 215. ISSN: 1662-5161.
- [60] Katie A. Ferguson and Jessica A. Cardin. “Mechanisms underlying gain modulation in the cortex”. In: *Nature Reviews Neuroscience* 21.2 (2020), pp. 80–92. ISSN: 1471-0048.

- [61] F. R. FIOCCHI et al. “Stimulus generalization in mice during Pavlovian eyeblink conditioning”. In: *eNeuro* 9.2 (2022).
- [62] Thomas H. B. FITZGERALD et al. “Active Inference, Evidence Accumulation, and the Urn Task”. In: *Neural Computation* 27.2 (2015), pp. 306–328. ISSN: 0899-7667.
- [63] Elizabeth FLEMING and COURT HULL. “Serotonin regulates dynamics of cerebellar granule cell activity by modulating tonic inhibition”. In: *Journal of Neurophysiology* 121.1 (2019), pp. 105–114.
- [64] Elizabeth A. FLEMING et al. “Local synaptic inhibition mediates cerebellar granule cell pattern separation necessary for learned sensorimotor associations”. In: *bioRxiv* (2022).
- [65] Ehud FONIO et al. “Coordination of sniffing and whisking depends on the mode of interaction with the environment”. In: *Israel Journal of Ecology and Evolution* 61.2 (2015), pp. 95–105.
- [66] Taylor R. FORE et al. “Acetylcholine Modulates Cerebellar Granule Cell Spiking by Regulating the Balance of Synaptic Excitation and Inhibition”. In: *Journal of Neuroscience* 40.14 (2020), pp. 2882–2894.
- [67] Maarten FRENS and Opher DONCHIN. “Forward models and state estimation in compensatory eye movements”. In: *Frontiers in Cellular Neuroscience* (2009). ISSN: 1662-5102.
- [68] Daniel Ari FRIEDMAN et al. “Active Inference: An Active Inference Framework for Ant Colony Behavior”. In: *Frontiers in Behavioral Neuroscience* 15 (2021). ISSN: 1662-5153.
- [69] K.J. FRISTON, N. TRUJILLO-BARRETO, and J. DAUNIZEAU. “DEM: A variational treatment of dynamic systems”. In: *NeuroImage* 41.3 (2008), pp. 849–885.
- [70] Karl FRISTON. “Life as we know it”. In: *Journal of The Royal Society Interface* 10.86 (2013), p. 20130475.
- [71] Karl FRISTON. “The free-energy principle: a unified brain theory?” In: *Nature Reviews Neuroscience* 11.2 (2010), pp. 127–138. ISSN: 1471-0048.
- [72] Karl FRISTON. “What is optimal about motor control?” In: *Neuron* 72.3 (2011), pp. 488–498. ISSN: 0896-6273.

- [73] Karl Friston and Christopher Frith. “A duet for one”. In: *Consciousness and Cognition* 36 (2015), pp. 390–405. ISSN: 1053-8100.
- [74] Karl Friston and Ivan Herreros. “Active inference and learning in the cerebellum”. en. In: *Neural Computation* 28.9 (2016), pp. 1812–1839.
- [75] Karl Friston and Stefan Kiebel. “Predictive coding under the free-energy principle”. en. In: *Philosophical Transactions of the Royal Society B: Biological Sciences* 364.1521 (2009), pp. 1211–1221.
- [76] Karl Friston, Spyridon Samothrakis, and Read Montague. “Active inference and agency: optimal control without cost functions”. In: *Biological Cybernetics* 106.8 (2012), pp. 523–541. ISSN: 1432-0770.
- [77] Karl Friston et al. “Active inference and epistemic value”. In: *Cognitive Neuroscience* 6.4 (2015). PMID: 25689102, pp. 187–214.
- [78] Karl Friston et al. “Active inference: A process theory”. en. In: *Neural Computation* 29.1 (2016), pp. 1–49.
- [79] Karl Friston et al. *The free energy principle made simpler but not too simple*. 2022.
- [80] Q G Fu et al. “Movement kinematics encoded in complex spike discharge of primate cerebellar Purkinje cells”. en. In: *Neuroreport* 8.2 (1997), pp. 523–529.
- [81] M. Fujita. “Adaptive filter model of the cerebellum”. In: *Biological Cybernetics* 45.3 (1982), pp. 195–206. ISSN: 1432-0770.
- [82] Laetitia Gabernet et al. “Somatosensory Integration Controlled by Dynamic Thalamocortical Feed-Forward Inhibition”. In: *Neuron* 48.2 (2005), pp. 315–327.
- [83] Michael A. Gaffield, Audrey Bonnan, and Jason M. Christie. “Conversion of graded presynaptic climbing fiber activity into graded postsynaptic Ca<sup>2+</sup> signals by Purkinje cell Dendrites”. In: *Neuron* 102.4 (2019), 762–769.e4. ISSN: 0896-6273.
- [84] Jia-Hong Gao et al. “Cerebellum Implicated in Sensory Acquisition and Discrimination Rather Than Motor Control”. In: *Science* 272.5261 (1996), pp. 545–547.

- [85] Zhenyu Gao, Boeke J. Van Beugen, and Chris I. De Zeeuw. “Distributed synergistic plasticity and cerebellar learning”. In: *Nature Reviews Neuroscience* 13.9 (2012), pp. 619–635.
- [86] Zhenyu Gao et al. “A cortico-cerebellar loop for motor planning”. In: *Nature* 563.7729 (2018), pp. 113–116. ISSN: 1476-4687.
- [87] Samuel J. Gershman. “Dopamine, Inference, and Uncertainty”. In: *Neural Computation* 29.12 (2017), pp. 3311–3326. ISSN: 0899-7667.
- [88] Peter F.C. Gilbert. “Simple spike frequency and the number of secondary spikes in the complex spike of the cerebellar Purkinje cell”. In: *Brain Research* 114.2 (1976), pp. 334–338. ISSN: 0006-8993.
- [89] Andrea Giovannucci et al. “Cerebellar granule cells acquire a widespread predictive feedback signal during motor learning”. In: *Nature Neuroscience* 20 (2017), pp. 727–734.
- [90] David Golomb et al. “Theory of hierarchically organized neuronal oscillator dynamics that mediate rodent rhythmic whisking”. In: *Neuron* 110.22 (2022), 3833–3851.e22. ISSN: 0896-6273.
- [91] Robyn A. Grant, Vicki Breakell, and Tony J. Prescott. “Whisker touch sensing guides locomotion in small, quadrupedal mammals”. In: *Proceedings of the Royal Society B: Biological Sciences* 285.1880 (2018), p. 20180592.
- [92] Victoria A. Griffiths et al. “Real-time 3D movement correction for two-photon imaging in behaving animals”. In: *Nature Methods* 17.7 (2020), pp. 741–748. ISSN: 1548-7105.
- [93] Chong Guo et al. “Purkinje cells directly inhibit granule cells in specialized regions of the cerebellar cortex”. In: *Neuron* 91.6 (2016), pp. 1330–1341. ISSN: 0896-6273.
- [94] Harsha Gurnani and R. Angus Silver. “Multidimensional population activity in an electrically coupled inhibitory circuit in the cerebellar cortex”. In: *Neuron* 109.10 (2021), 1739–1753.e8. ISSN: 0896-6273.
- [95] Zachary J. Hall, Sally E. Street, and Susan D. Healy. “The evolution of cerebellum structure correlates with nest complexity”. In: *Biology Letters* 9.6 (2013), p. 20130687.

- [96] Martine Hamann, David J Rossi, and David Attwell. “Tonic and spillover inhibition of granule cells control information flow through cerebellar cortex”. In: *Neuron* 33.4 (2002), pp. 625–633.
- [97] Christian Hansel, David J. Linden, and Egidio D’Angelo. “Beyond parallel fiber LTD: the diversity of synaptic and non-synaptic plasticity in the cerebellum”. In: *Nature Neuroscience* 4.5 (2001), pp. 467–475. ISSN: 1546-1726.
- [98] R. J. Harvey and R. M. A. Napper. “Quantitative study of granule and Purkinje cells in the cerebellar cortex of the rat”. In: *Journal of Comparative Neurology* 274.2 (1988), pp. 151–157.
- [99] Michael Häusser and Beverley A. Clark. “Tonic Synaptic Inhibition Modulates Neuronal Output Pattern and Spatiotemporal Synaptic Integration”. In: *Neuron* 19.3 (1997), pp. 665–678. ISSN: 0896-6273.
- [100] William Heffley and Court Hull. “Classical conditioning drives learned reward prediction signals in climbing fibers across the lateral cerebellum”. en. In: *Elife* 8 (2019).
- [101] William Heffley et al. “Coordinated cerebellar climbing fiber activity signals learned sensorimotor predictions”. In: *Nature Neuroscience* 21.10 (2018), pp. 1431–1441. ISSN: 1546-1726.
- [102] Hermann von Helmholtz. *Handbuch der physiologischen Optik*. ger. Allgemeine Encyclopädie der Physik. Leipzig: Voss, 1867.
- [103] Julia U Henschke and Janelle MP Pakan. “Disynaptic cerebrotocerebellar pathways originating from multiple functionally distinct cortical areas”. In: *eLife* 9 (2020). Ed. by Megan R Carey, Richard B Ivry, and Roy V Sillitoe, e59148. ISSN: 2050-084X.
- [104] D.J. Herzfeld et al. “Behavioral responses of expert-identified cerebellar cell types during smooth pursuit eye movements in primates”. In: *SFN poster* (2022).
- [105] Daniel N. Hill et al. “Primary Motor Cortex Reports Efferent Control of Vibrissa Motion on Multiple Timescales”. In: *Neuron* 72.2 (2011), pp. 344–356. ISSN: 0896-6273.
- [106] Jakob Hohwy. “The self-evidencing brain”. In: *Noûs* 50.2 (2016), pp. 259–285.

- [107] Tahl Holtzman et al. “Cerebellar Golgi cells in the rat receive multimodal convergent peripheral inputs via the lateral funiculus of the spinal cord”. In: *Journal of Physiology* 577.1 (2006), pp. 69–80.
- [108] Tahl Holtzman et al. “Different responses of rat cerebellar Purkinje cells and Golgi cells evoked by widespread convergent sensory inputs”. In: *Journal of Physiology* 574.2 (2006), pp. 491–507.
- [109] Sungho Hong et al. “Multiplexed coding by cerebellar Purkinje neurons”. In: *eLife* 5 (2016). Ed. by Fred Rieke, e13810. ISSN: 2050-084X.
- [110] Brenda D. Houck and Abigail L. Person. “Cerebellar premotor output neurons collateralize to innervate the cerebellar cortex”. In: *Journal of Comparative Neurology* 523.15 (2015), pp. 2254–2271.
- [111] Cheng-Chiu Huang et al. “Convergence of pontine and proprioceptive streams onto multimodal cerebellar granule cells”. In: *eLife* 2 (2013).
- [112] Koji Ikezoe et al. “Cerebellar climbing fibers convey behavioral information of multiplex modalities and form functional modules”. In: *bioRxiv* (2022).
- [113] Taro Ishikawa, Misa Shimuta, and Michael Häusser. “Multimodal sensory integration in single cerebellar granule cells in vivo”. In: *eLife* 4 (2015).
- [114] Takuya Isomura et al. “Experimental validation of the free-energy principle with in vitro neural networks”. In: *Nature Communications* 14.1 (2023), p. 4547. ISSN: 2041-1723.
- [115] Philippe Isope and Boris Barbour. “Properties of Unitary Granule Cell→Purkinje Cell Synapses in Adult Rat Cerebellar Slices”. In: *Journal of Neuroscience* 22.22 (2002), pp. 9668–9678. ISSN: 0270-6474.
- [116] M Ito. “Cerebellar long-term depression: characterization, signal transduction, and functional roles”. en. In: *Physiol Rev* 81.3 (2001), pp. 1143–1195.
- [117] M Ito. “Experimental verification of Marr-Albus’ plasticity assumption for the cerebellum”. en. In: *Acta Biol Acad Sci Hung* 33.2-3 (1982), pp. 189–199.
- [118] M Ito. “Long-Term Depression”. In: *Annual Review of Neuroscience* 12.1 (1989). PMID: 2648961, pp. 85–102.

- [119] M. Ito, M. Itō, and J. Eccles. *The Cerebellum and Neural Control*. Raven Press, 1984. ISBN: 9780890041062.
- [120] Masao Ito. “Cerebellar circuitry as a neuronal machine”. In: *Progress in Neurobiology* 78.3 (2006). The Contributions of John Carew Eccles to Contemporary Neuroscience, pp. 272–303. ISSN: 0301-0082.
- [121] Masao Ito. “Control of mental activities by internal models in the cerebellum”. In: *Nature Reviews Neuroscience* 9.4 (2008), pp. 304–313.
- [122] Masao Ito. “Neural design of the cerebellar motor control system”. In: *Brain Research* 40.1 (1972), pp. 81–84. ISSN: 0006-8993.
- [123] R. L. Jakab and J. Hámori. “Quantitative morphology and synaptology of cerebellar glomeruli in the rat”. In: *Anatomy and Embryology* 179.1 (1988), pp. 81–88.
- [124] Jan Jansen and Alf Brodal. “Experimental studies on the intrinsic fibers of the cerebellum. II. The cortico-nuclear projection”. In: *Journal of Comparative Neurology* 73.2 (1940), pp. 267–321.
- [125] Dan-Anders Jirenhed, Fredrik Bengtsson, and Henrik Jörntell. “Parallel fiber and climbing fiber responses in rat cerebellar cortical neurons in vivo”. In: *Frontiers in Systems Neuroscience* 7 (2013). ISSN: 1662-5137.
- [126] Chiheng Ju et al. “Neurons of the inferior olive respond to broad classes of sensory input while subject to homeostatic control”. en. In: *Journal of Physiology* 597.9 (2019), pp. 2483–2514.
- [127] Toshikazu Kakizaki et al. “A glycine transporter 2-Cre knock-in mouse line for glycinergic neuron-specific gene manipulation”. In: *IBRO Reports* 3 (2017), pp. 9–16.
- [128] Justus M. Kubschull et al. “Cerebellar nuclei evolved by repeatedly duplicating a conserved cell-type set”. In: *Science* 370.6523 (2020), eabd5059.
- [129] Elyza Kelly et al. “Regulation of autism-relevant behaviors by cerebellar–prefrontal cortical circuits”. In: *Nature Neuroscience* 23.9 (2020), pp. 1102–1110. ISSN: 1546-1726.
- [130] Stefan J Kiebel and Karl J Friston. “Free energy and dendritic self-organization”. en. In: *Frontiers in Systems Neuroscience* 5 (2011), p. 80.



- [131] Stefan J. Kiebel et al. “Recognizing sequences of sequences”. In: *PLOS Computational Biology* 5.8 (2009), pp. 1–13.
- [132] Jinsook Kim and George J. Augustine. “Molecular Layer Interneurons: Key Elements of Cerebellar Network Computation and Behavior”. In: *Neuroscience* 462 (2021). In Memoriam: Masao Ito—A Visionary Neuroscientist with a Passion for the Cerebellum, pp. 22–35. ISSN: 0306-4522.
- [133] Rhea R Kimpo et al. “Gating of neural error signals during motor learning”. In: *eLife* 3 (2014). Ed. by Dora E Angelaki, e02076. ISSN: 2050-084X.
- [134] David Kleinfeld, Ehud Ahissar, and Mathew E Diamond. “Active sensation: insights from the rodent vibrissa sensorimotor system”. In: *Current Opinion in Neurobiology* 16.4 (2006). Sensory systems, pp. 435–444. ISSN: 0959-4388.
- [135] David C. Knill and Alexandre Pouget. “The Bayesian brain: the role of uncertainty in neural coding and computation”. In: *Trends in Neurosciences* 27.12 (2004), pp. 712–719.
- [136] Dimitar Kostadinov et al. “Predictive and reactive reward signals conveyed by climbing fiber inputs to cerebellar Purkinje cells”. In: *Nature Neuroscience* 22.6 (2019), pp. 950–962. ISSN: 1546-1726.
- [137] Leonard F Koziol et al. “Consensus paper: The cerebellum’s role in movement and cognition”. en. In: *Cerebellum* 13.1 (2014), pp. 151–177.
- [138] Anastasia Kurnikova et al. “Coordination of orofacial motor actions into exploratory behavior by rat”. In: *Current Biology* 27.5 (2017), pp. 688–696. ISSN: 0960-9822.
- [139] Jeanne Lainé and Herbert Axelrad. “Lugaro cells target basket and stellate cells in the cerebellar cortex”. In: *NeuroReport* 9.10 (1998). ISSN: 0959-4965.
- [140] Frederic Lanore et al. “Cerebellar granule cell axons support high-dimensional representations”. en. In: *Nat Neurosci* 24.8 (2021), pp. 1142–1150.
- [141] Frederic Lanore et al. “Norepinephrine controls the gain of the inhibitory circuit in the cerebellar input layer”. In: *bioRxiv* (2019).
- [142] Soojung Lee et al. “Channel-mediated tonic GABA release from glia”. In: *Science* 330.6005 (2010), pp. 790–796. ISSN: 0036-8075.

- [143] Elise Lesage et al. “Cerebellar rTMS disrupts predictive language processing”. In: *Current Biology* 22.18 (2012), R794–R795. ISSN: 0960-9822.
- [144] Varda Lev-Ram et al. “A new form of cerebellar long-term potentiation is postsynaptic and depends on nitric oxide but not cAMP”. In: *Proceedings of the National Academy of Sciences* 99.12 (2002), pp. 8389–8393.
- [145] Stephen G. Lisberger. “Visual Guidance of Smooth-Pursuit Eye Movements: Sensation, Action, and What Happens in Between”. In: *Neuron* 66.4 (2010), pp. 477–491. ISSN: 0896-6273.
- [146] Ashok Litwin-Kumar et al. “Optimal degrees of synaptic connectivity”. In: *Neuron* 93.5 (2017), 1153–1164.e7. ISSN: 0896-6273.
- [147] Xuguang Liu, Edwin Robertson, and R Christopher Miall. “Neuronal activity related to the visual representation of arm movements in the lateral cerebellar cortex”. en. In: *Journal of Neurophysiology* 89.3 (2002), pp. 1223–1237.
- [148] Victor Llobet, Aurélien Wyngaard, and Boris Barbour. “Automatic post-processing and merging of multiple spike-sorting analyses with Lussac”. In: *bioRxiv* (2022).
- [149] Lianyi Lu et al. “Medial cerebellar nuclear projections and activity patterns link cerebellar output to orofacial and respiratory behavior”. In: *Frontiers in Neural Circuits* 7 (2013). ISSN: 1662-5110.
- [150] Wei Ji Ma et al. “Bayesian inference with probabilistic population codes”. In: *Nature Neuroscience* 9.11 (2006), pp. 1432–1438. ISSN: 1546-1726.
- [151] Ana S Machado et al. “A quantitative framework for whole-body coordination reveals specific deficits in freely walking ataxic mice”. In: *eLife* 4 (2015). Ed. by Indira M Raman, e07892. ISSN: 2050-084X.
- [152] Ana S Machado et al. “Shared and specific signatures of locomotor ataxia in mutant mice”. In: *eLife* 9 (2020). Ed. by Ronald L Calabrese, e55356. ISSN: 2050-084X.
- [153] David Marr. “A theory of cerebellar cortex”. In: *Journal of Physiology* 202.2 (1969), pp. 437–470.

- [154] Jun Maruta, Robert A. Hensbroek, and John I. Simpson. “Intraburst and Interburst Signaling by Climbing Fibers”. In: *Journal of Neuroscience* 27.42 (2007), pp. 11263–11270. ISSN: 0270-6474.
- [155] D A McCormick and R F Thompson. “Neuronal responses of the rabbit cerebellum during acquisition and performance of a classically conditioned nictitating membrane-eyelid response”. en. In: *J Neurosci* 4.11 (1984), pp. 2811–2822.
- [156] Samuel D McDougle et al. “Continuous manipulation of mental representations is compromised in cerebellar degeneration”. In: *Brain* 145.12 (2022), pp. 4246–4263. ISSN: 0006-8950.
- [157] Lauren E. McElvain et al. “Circuits in the rodent brainstem that control whisking in concert with other orofacial motor actions”. In: *Neuroscience* 368 (2018). Barrel Cortex Function, pp. 152–170. ISSN: 0306-4522.
- [158] R. Chris Miall et al. “Is the cerebellum a Smith predictor?” In: *Journal of Motor Behavior* 25 3 (1993), pp. 203–16.
- [159] F. A. Miles and J. H. Fuller. “Visual Tracking and the Primate Flocculus”. In: *Science* 189.4207 (1975), pp. 1000–1002.
- [160] M. Berk Mirza et al. “Scene Construction, Visual Foraging, and Active Inference”. In: *Frontiers in Computational Neuroscience* 10 (2016). ISSN: 1662-5188.
- [161] Simon J. Mitchell and R. Angus Silver. “Shunting inhibition modulates neuronal gain during synaptic excitation”. In: *Neuron* 38.3 (2003), pp. 433–445. ISSN: 0896-6273.
- [162] Wolfgang Mittmann, Ursula Koch, and Michael Häusser. “Feed-forward inhibition shapes the spike output of cerebellar Purkinje cells”. In: *The Journal of Physiology* 563.2 (2005), pp. 369–378.
- [163] Michael Moutoussis et al. “A formal model of interpersonal inference”. In: *Frontiers in Human Neuroscience* 8 (2014). ISSN: 1662-5161.
- [164] Enrico Mugnaini and Alessandra Floris. “The unipolar brush cell: A neglected neuron of the mammalian cerebellar cortex”. In: *Journal of Comparative Neurology* 339.2 (1994), pp. 174–180.

- [165] R M Napper and R J Harvey. “Number of parallel fiber synapses on an individual Purkinje cell in the cerebellum of the rat”. en. In: *J Comp Neurol* 274.2 (1988), pp. 168–177.
- [166] Thomas A. Nielsen, David A. Digregorio, and R. Angus Silver. “Modulation of glutamate mobility reveals the mechanism underlying slow-rising AMPAR EPSCs and the diffusion coefficient in the synaptic cleft”. In: *Neuron* 42.5 (2004), pp. 757–771.
- [167] Angela K Nietz et al. “Non-synaptic signaling from cerebellar climbing fibers modulates Golgi cell activity”. In: *eLife* 6 (2017).
- [168] Dennis A. Nowak et al. “Predictive and reactive finger force control during catching in cerebellar degeneration”. In: *The Cerebellum* 3.4 (2004), pp. 227–235. ISSN: 1473-4230.
- [169] Sean M. O’Connor, Rune W. Berg, and David Kleinfeld. “Coherent Electrical Activity Between Vibrissa Sensory Areas of Cerebellum and Neocortex Is Enhanced During Free Whisking”. In: *Journal of Neurophysiology* 87.4 (2002). PMID: 11929931, pp. 2137–2148.
- [170] Tatsuya Ohyama et al. “What the cerebellum computes”. In: *Trends in Neurosciences* 26.4 (2003), pp. 222–227. ISSN: 0166-2236.
- [171] Filiz Onat and Safiye Çavdar. “Cerebellar connections: hypothalamus”. In: *Cerebellum* 2.4 (2003), pp. 263–269.
- [172] M. Oostland et al. “Identifying cell types in Neuropixels recordings from cerebellar cortex in awake mice using optotagging”. In: *SFN poster* (2022).
- [173] Thomas S. Otis. “Simple Spikes and Complex Spikes”. In: *Essentials of Cerebellum and Cerebellar Disorders: A Primer For Graduate Students*. Ed. by Donna L. Gruol et al. Cham: Springer International Publishing, 2016, pp. 299–303. ISBN: 978-3-319-24551-5.
- [174] Ensor Rafael Palacios, Conor Houghton, and Paul Chadderton. “Accounting for uncertainty: inhibition for neural inference in the cerebellum”. In: *Proceedings of the Royal Society B: Biological Sciences* 288.1947 (2021), p. 20210276.
- [175] Ensor Rafael Palacios et al. “Cerebellar state estimation enables resilient coupling across behavioural domains”. In: *bioRxiv* (2023).
- [176] Ensor Rafael Palacios et al. “On Markov blankets and hierarchical self-organisation”. In: *Journal of Theoretical Biology* 486 (2020), p. 110089. ISSN: 0022-5193.

- [177] Ensor Rafael Palacios et al. “The emergence of synchrony in networks of mutually inferring neurons”. In: *Scientific Reports* 9.1 (2019), p. 6412. ISSN: 2045-2322.
- [178] Chan-Palay V Palay SL. *Cerebellar Cortex: Cytology and Organizatio*. Springer-Verlag Berlin Heidelberg, 1974. ISBN: 9780890041062.
- [179] M G Paulin. “Evolution of the cerebellum as a neuronal machine for Bayesian state estimation”. In: *Journal of Neural Engineering* 2.3 (2005), S219–S234.
- [180] Michael G. Paulin. “A model of the role of the cerebellum in tracking and controlling movements”. In: *Human Movement Science* 12.1 (1993), pp. 5–16. ISSN: 0167-9457.
- [181] Hannah L Payne et al. “Cerebellar Purkinje cells control eye movements with a rapid rate code that is invariant to spike irregularity”. In: *eLife* 8 (2019). Ed. by Richard B Ivry and David J Herzfeld, e37102. ISSN: 2050-084X.
- [182] Laurentiu Popa, Angela Hewitt, and Timothy Ebner. “Predictive and feedback performance errors are signaled in the simple spike discharge of individual Purkinje cells”. In: *Journal of Neuroscience* 32 (2012), pp. 15345–58.
- [183] Laurentiu S. Popa and Timothy J. Ebner. “Cerebellum, Predictions and Errors”. In: *Frontiers in Cellular Neuroscience* 12 (2019).
- [184] Rémi D. Proville et al. “Cerebellum involvement in cortical sensorimotor circuits for the control of voluntary movements”. In: *Nature Neuroscience* 17.9 (2014), pp. 1233–1239. ISSN: 1546-1726.
- [185] Narender Ramnani. “Automatic and controlled processing in the corticocerebellar system”. In: *Cerebellar Learning*. Ed. by Narender Ramnani. Vol. 210. Progress in Brain Research. Elsevier, 2014, pp. 255–285.
- [186] Narender Ramnani. “The primate cortico-cerebellar system: anatomy and function”. In: *Nature Reviews Neuroscience* 7.7 (2006), pp. 511–522.
- [187] Maxwell James Désormeau Ramstead, Paul Benjamin Badcock, and Karl John Friston. “Answering Schrödinger’s question: A free-energy formulation”. In: *Physics of Life Reviews* 24 (2018), pp. 1–16. ISSN: 1571-0645.

- [188] Ede A. Rancz et al. “High-fidelity transmission of sensory information by single cerebellar mossy fibre boutons”. In: *Nature* 450 (2007), pp. 1245–1248.
- [189] Jennifer L. Raymond, Stephen G. Lisberger, and Michael D. Mauk. “The Cerebellum: A Neuronal Learning Machine?” In: *Science* 272.5265 (1996), pp. 1126–1131.
- [190] Jennifer L. Raymond and Javier F. Medina. “Computational principles of supervised learning in the cerebellum”. In: *Annual Review of Neuroscience* 41.1 (2018), pp. 233–253.
- [191] Vincenzo Romano et al. “Functional convergence of autonomic and sensorimotor processing in the lateral cerebellum”. In: *Cell Reports* 32.1 (2020), p. 107867. ISSN: 2211-1247.
- [192] Hana Roš et al. “Neocortical Networks Entrain Neuronal Circuits in Cerebellar Cortex”. In: *Journal of Neuroscience* 29.33 (2009), pp. 10309–10320. ISSN: 0270-6474.
- [193] Christian Rössert, Paul Dean, and John Porrill. “At the edge of chaos: How cerebellar granular layer network dynamics can provide the basis for temporal filters”. In: *PLOS Computational Biology* 11.10 (2015), pp. 1–28.
- [194] D. J Rossi, M. Hamann, and D. Attwell. “Multiple modes of GABAergic inhibition of rat cerebellar granule cells”. In: *Journal of Physiology* 548.1 (2003), pp. 97–110.
- [195] D. J. Rossi et al. “Properties of transmission at a giant glutamatergic synapse in cerebellum: the mossy fiber-unipolar brush cell synapse”. In: *Journal of Neurophysiology* 74.1 (1995). PMID: 7472327, pp. 24–42.
- [196] David J Rossi and Martine Hamann. “Spillover-Mediated Transmission at Inhibitory Synapses Promoted by High Affinity  $\alpha 6$  Subunit GABA<sub>A</sub> Receptors and Glomerular Geometry”. In: *Neuron* 20.4 (1998), pp. 783–795.
- [197] Bryan L. Roth. “DREADDs for Neuroscientists”. In: *Neuron* 89.4 (2016), pp. 683–694.
- [198] Paul A Salin, Robert C Malenka, and Roger A Nicoll. “Cyclic AMP Mediates a Presynaptic Form of LTP at Cerebellar Parallel Fiber Synapses”. In: *Neuron* 16.4 (1996), pp. 797–803. ISSN: 0896-6273.
- [199] Jeremy D. Schmahmann. “The cerebellum and cognition”. In: *Neuroscience Letters* 688 (2019). *The Cerebellum in Health and Disease*, pp. 62–75. ISSN: 0304-3940.

- [200] Naveen Sendhilnathan et al. “Neural correlates of reinforcement learning in mid-lateral cerebellum”. en. In: *Neuron* 106.1 (2020), 188–198.e5.
- [201] Reza Shadmehr and John W. Krakauer. “A computational neuroanatomy for motor control”. In: *Experimental Brain Research* 185.3 (2008), pp. 359–381.
- [202] G M Shambes, J M Gibson, and W Welker. “Fractured somatotopy in granule cell tactile areas of rat cerebellar hemispheres revealed by micromapping”. en. In: *Brain Behav Evol* 15.2 (1978), pp. 94–140.
- [203] Ari A. Shemesh and David S. Zee. “Eye Movement Disorders and the Cerebellum”. In: *Journal of Clinical Neurophysiology* 36.6 (2019). ISSN: 0736-0258.
- [204] Y. Shinoda et al. “Axon collaterals of mossy fibers from the pontine nucleus in the cerebellar dentate nucleus”. In: *Journal of Neurophysiology* 67.3 (1992). PMID: 1578244, pp. 547–560.
- [205] Roy V. Sillitoe, YuHong Fu, and Charles Watson. “Chapter 11 - Cerebellum”. In: *The Mouse Nervous System*. Ed. by Charles Watson, George Paxinos, and Luis Puelles. San Diego: Academic Press, 2012, pp. 360–397. ISBN: 978-0-12-369497-3.
- [206] Maria Caterina Silveri. “Contribution of the Cerebellum and the Basal Ganglia to Language Production: Speech, Word Fluency, and Sentence Construction—Evidence from Pathology”. In: *The Cerebellum* 20.2 (2021), pp. 282–294. ISSN: 1473-4230.
- [207] J. I. Simpson, D. R. Wylie, and C. I. De Zeeuw. “On climbing fiber signals and their consequence(s)”. In: *Behavioral and Brain Sciences* 19.3 (1996), pp. 384–398.
- [208] Ray S. Snider and Averill Stowell. “Receiving areas of the tactile, auditory, and visual systems in the cerebellum”. In: *Journal of Neurophysiology* 7.6 (1944), pp. 331–357.
- [209] Noam Sobel et al. “Odorant-induced and sniff-induced activation in the cerebellum of the human”. In: *Journal of Neuroscience* 18.21 (1998), pp. 8990–9001.
- [210] Hitomi Soumiya et al. “Neonatal Whisker Trimming Impairs Fear/Anxiety-Related Emotional Systems of the Amygdala and Social Behaviors in Adult Mice”. In: *PLOS ONE* 11.6 (2016), pp. 1–16.

- [211] Tevye J. Stachniak, Anirvan Ghosh, and Scott M. Sternson. “Chemogenetic Synaptic Silencing of Neural Circuits Localizes a Hypothalamus→Midbrain Pathway for Feeding Behavior”. In: *Neuron* 82.4 (2014), pp. 797–808. ISSN: 0896-6273.
- [212] L S Stone and S G Lisberger. “Visual responses of Purkinje cells in the cerebellar flocculus during smooth-pursuit eye movements in monkeys. I. Simple spikes”. en. In: *J Neurophysiol* 63.5 (1990), pp. 1241–1261.
- [213] Piergiorgio Strata. “The emotional cerebellum”. In: *Cerebellum* 14.5 (2015), pp. 570–577. ISSN: 1473-4230.
- [214] Isabelle Straub et al. “Gradients in the mammalian cerebellar cortex enable Fourier-like transformation and improve storing capacity”. In: *eLife* 9 (2020). Ed. by Sacha B Nelson, Barbara G Shinn-Cunningham, and Sacha B Nelson, e51771. ISSN: 2050-084X.
- [215] Aparna Suvrathan, Hannah L. Payne, and Jennifer L. Raymond. “Timing Rules for Synaptic Plasticity Matched to Behavioral Function”. In: *Neuron* 92.5 (2016), pp. 959–967. ISSN: 0896-6273.
- [216] Jun Takato et al. “The whisking oscillator circuit”. In: *Nature* 609.7927 (2022), pp. 560–568. ISSN: 1476-4687.
- [217] Hirokazu Tanaka, Takahiro Ishikawa, and Shinji Kakei. “Neural evidence of the cerebellum as a state predictor”. In: *Cerebellum* 18.3 (2019), pp. 349–371. ISSN: 1473-4230.
- [218] Hirokazu Tanaka et al. “The cerebro-cerebellum as a locus of forward model: A review”. In: *Frontiers in Systems Neuroscience* 14 (2020). ISSN: 1662-5137.
- [219] W T Thach. “Somatosensory receptive fields of single units in cat cerebellar cortex.” In: *Journal of Neurophysiology* 30.4 (1967). PMID: 6035687, pp. 675–696.
- [220] Amanda S Therrien and Amy J Bastian. “Cerebellar damage impairs internal predictions for sensory and motor function”. In: *Current Opinion in Neurobiology* 33 (2015), pp. 127–133.
- [221] R.F. Thompson and J.E. Steinmetz. “The role of the cerebellum in classical conditioning of discrete behavioral responses”. In: *Neuroscience* 162.3 (2009). New Insights in Cerebellar Function, pp. 732–755. ISSN: 0306-4522.



- [222] Ya-Weng Tseng et al. “Sensory prediction errors drive cerebellum-dependent adaptation of reaching”. en. In: *Journal of Neurophysiology* 98.1 (2007), pp. 54–62.
- [223] Omer Tsur, Yana Khrapunsky, and Rony Azouz. “Sensorimotor integration in the whisker somatosensory brain stem trigeminal loop”. In: *Journal of Neurophysiology* 122.5 (2019). PMID: 31533013, pp. 2061–2075.
- [224] Shinichiro Tsutsumi et al. “Purkinje Cell Activity Determines the Timing of Sensory-Evoked Motor Initiation”. In: *Cell Reports* 33.12 (2020), p. 108537. ISSN: 2211-1247.
- [225] Koen Vervaeke et al. “Rapid Desynchronization of an Electrically Coupled Interneuron Network with Sparse Excitatory Synaptic Input”. In: *Neuron* 67.3 (2010), pp. 435–451.
- [226] Bart P. Vos et al. “Parallel Fibers Synchronize Spontaneous Activity in Cerebellar Golgi Cells”. In: *Journal of Neuroscience* 19.11 (1999), RC6–RC6. ISSN: 0270-6474.
- [227] Mark J. Wagner and Liquan Luo. “Neocortex-cerebellum circuits for cognitive processing”. In: *Trends in Neurosciences* 43.1 (2020), pp. 42–54.
- [228] Mark J. Wagner et al. “Cerebellar granule cells encode the expectation of reward”. In: *Nature* 544.7648 (2017), pp. 96–100.
- [229] Mark J. Wagner et al. “Shared cortex-cerebellum dynamics in the execution and learning of a motor task”. In: *Cell* 177.3 (2019), 669–682.e24. ISSN: 0092-8674.
- [230] Mark J. Wall and Maria M. Usowicz. “Development of Action Potential-dependent and Independent Spontaneous GABA<sub>A</sub> Receptor-mediated Currents in Granule Cells of Post-natal Rat Cerebellum”. In: *European Journal of Neuroscience* 9.3 (1997), pp. 533–548.
- [231] Danhong Wang, Randy L. Buckner, and Hesheng Liu. “Cerebellar asymmetry and its relation to cerebral asymmetry estimated by intrinsic functional connectivity”. In: *Journal of Neurophysiology* 109.1 (2013). PMID: 23076113, pp. 46–57.
- [232] Richard A Warren et al. “A rapid whisker-based decision underlying skilled locomotion in mice”. In: *eLife* 10 (2021). Ed. by Jesse H Goldberg, Ronald L Calabrese, and Jesse H Goldberg, e63596. ISSN: 2050-084X.

- [233] Dai Watanabe et al. “Ablation of Cerebellar Golgi Cells Disrupts Synaptic Integration Involving GABA Inhibition and NMDA Receptor Activation in Motor Coordination”. In: *Cell* 95.1 (1998), pp. 17–27. ISSN: 0092-8674.
- [234] Michael Wehr and Anthony M. Zador. “Balanced inhibition underlies tuning and sharpens spike timing in auditory cortex”. In: *Nature* 426.6965 (2003), pp. 442–446.
- [235] Ingrid van Welie et al. “Conditional spike transmission mediated by electrical coupling ensures millisecond precision-correlated activity among interneurons in vivo”. In: *Neuron* 90.4 (2016), pp. 810–823. ISSN: 0896-6273.
- [236] Tobias Wiestler, David J McGonigle, and Jörn Diedrichsen. “Integration of sensory and motor representations of single fingers in the human cerebellum”. en. In: *J Neurophysiol* 105.6 (2011), pp. 3042–3053.
- [237] Laurens Witter et al. “Purkinje cell collaterals enable output signals from the cerebellar cortex to feed back to Purkinje cells and interneurons”. In: *Neuron* 91.2 (2016), pp. 312–319.
- [238] Jason Wolfe, Carolin Mende, and Michael Brecht. “Social facial touch in rats”. en. In: *Behav Neurosci* 125.6 (2011), pp. 900–910.
- [239] Daniel M Wolpert, R.chris Miall, and Mitsuo Kawato. “Internal models in the cerebellum”. In: *Trends in Cognitive Sciences* 2.9 (1998), pp. 338–347.
- [240] Thomas A. Woolsey and Hendrik Van der Loos. “The structural organization of layer IV in the somatosensory region (S I) of mouse cerebral cortex: The description of a cortical field composed of discrete cytoarchitectonic units”. In: *Brain Research* 17.2 (1970), pp. 205–242. ISSN: 0006-8993.
- [241] Tadashi Yamazaki and Shigeru Tanaka. “The cerebellum as a liquid state machine”. In: *Neural Networks* 20.3 (2007), pp. 290–297.
- [242] Yan Yang and Stephen G Lisberger. “Interaction of plasticity and circuit organization during the acquisition of cerebellum-dependent motor learning”. In: *eLife* 2 (2013). Ed. by Dora Angelaki, e01574. ISSN: 2050-084X.

- [243] Yan Yang and Stephen G Lisberger. “Modulation of Complex-Spike Duration and Probability during Cerebellar Motor Learning in Visually Guided Smooth-Pursuit Eye Movements of Monkeys”. en. In: *eNeuro* 4.3 (2017).